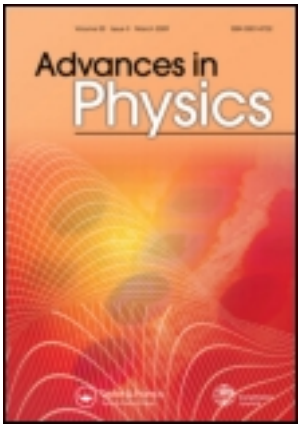

Advances in Physics
Publication details, including instructions for authors and subscription information:
http://www.tandfonline.com/loi/tadp20

Rapidly rotating atomic gases

N.R. Cooper [a b]

[a] T.C.M. Group, Cavendish Laboratory, University of Cambridge, J. J. Thomson Avenue, Cambridge CB3 0HE, UK

[b] L.P.T.M.S., Université Paris-Sud, 91405 Orsay, France

Available online: 11 Dec 2008

To cite this article: N.R. Cooper (2008): Rapidly rotating atomic gases, Advances in Physics, 57:6, 539-616

To link to this article: http://dx.doi.org/10.1080/00018730802564122

Advances in Physics
Vol. 57, No. 6, November–December 2008, 539–616

Rapidly rotating atomic gases

N.R. Cooper*

T.C.M. Group, Cavendish Laboratory, University of Cambridge, J. J. Thomson Avenue, Cambridge CB3 0HE, UK; L.P.T.M.S., Université Paris-Sud, 91405 Orsay, France

(*Received 17 October 2008; final version received 17 October 2008*)

In this article, we review developments in the theory of rapidly rotating degenerate atomic gases. The main focus is on the equilibrium properties of a single-component atomic Bose gas, which (at least at rest) forms a Bose–Einstein condensate. Rotation leads to the formation of quantized vortices which order into a vortex array, in close analogy with the behaviour of superfluid helium. Under conditions of rapid rotation, when the vortex density becomes large, atomic Bose gases offer the possibility to explore the physics of quantized vortices in novel parameter regimes. First, there is an interesting regime in which the vortices become sufficiently dense that their cores, as set by the healing length, start to overlap. In this regime, the theoretical description simplifies, allowing a reduction to single-particle states in the lowest Landau level. Second, one can envisage entering a regime of very high vortex density, when the number of vortices becomes comparable to the number of particles in the gas. In this regime, theory predicts the appearance of a series of strongly correlated phases, which can be viewed as *bosonic* versions of fractional quantum Hall states. In this article, we describe the equilibrium properties of rapidly rotating atomic Bose gases in both the mean-field and the strongly correlated regimes, and related theoretical developments for Bose gases in lattices, for multi-component Bose gases and for atomic Fermi gases. The current experimental situation and outlook for the future are discussed in light of these theoretical developments.

Keywords: Bose–Einstein condensation; superfluidity; quantized vortices; fractional quantum Hall effect

Contents

*Email: nrc25@cam.ac.uk

ISSN 0001–8732 print/ISSN 1460–6976 online

DOI: 10.1080/00018730802564122
http://www.informaworld.com

1. Introduction

One of the most remarkable characteristics of a Bose–Einstein condensate (BEC) is its response to rotation. As was first understood in the context of superfluid helium-4 [1], a Bose–Einstein condensate does not rotate in the manner of a conventional fluid, which undergoes rigid body rotation. Rather, the rotation of superfluid helium leads to the formation of an array of quantized vortex lines. Quantized vortices also appear in the superfluid states of helium-3 and in type-II superconductors under an applied magnetic field[1], which may be viewed as condensates of pairs of fermionic atoms or electrons.

The experimental achievement of Bose–Einstein condensation in ultra-cold atomic gases, formed either from the condensation of atomic bosons [2,3], or of pairs of atomic fermions [4], opens up a wide range of new features in the physics of quantized vortices and vortex arrays, allowing access to parameter regimes that are inaccessible in the helium superfluids or type-II superconductors. This can lead to novel properties of the rotating groundstates, including the possibility of exotic strongly correlated phases. In recent years, there have been advances in experimental capabilities and in the theoretical understanding of rotating ultra-cold atomic gases in these unconventional regimes. The aim of this article is to review the theoretical developments. It focuses mainly on situations in which there are large vortex arrays in a regime of rapid rotation, and on the theoretical predictions of the novel phases that can appear in this regime.

We start with a brief introduction to the properties of BECs and to the physics of quantized vortices.

1.1. *Atomic BECs*

Consider an ideal (non-interacting) gas in three dimensions, of identical particles of mass M, at number density $\bar{n}$ and in equilibrium at a temperature T. The temperature sets the thermal de Broglie wavelength, λ_T, via $\hbar^2/M\lambda_T^2 \sim k_B T$, and the density sets the mean particle spacing $\bar{a} \sim \bar{n}^{-1/3}$. At low temperatures, when $\lambda_T \gtrsim \bar{a}$ the gas must be described by quantum theory, and its properties depend strongly on the statistics of the particles. For bosons there is a phase transition when $\lambda_T \sim \bar{a}$, at a critical temperature

$$T_c = \frac{2\pi\hbar^2}{Mk_B}\left(\frac{\bar{n}}{\zeta(3/2)}\right)^{2/3}. \quad (1)$$

For $T < T_c$ the gas is a BEC, characterized by a non-zero fraction of the particles occupying the same quantum state.

Until recently there was only one experimental realization of an atomic BEC. The transition of helium-4 into a superfluid state below $T_c = 2.17\,\mathrm{K}$ is known to be associated with Bose–Einstein condensation[2], albeit in a system in which the inter-particle interactions are relatively large. However, in recent years, Bose–Einstein condensation has been achieved in a wide variety of atomic species. These are prepared as metastable

low-density gases, $\bar{n} \sim 10^{12}$–$10^{15}\,\mathrm{cm}^{-3}$, confined in magnetic or optical traps. At such low densities, the BEC transition temperature is extremely small, $T_c \simeq 100\,\mathrm{nK}$. Nevertheless, by a combination of laser and evaporative cooling these low temperatures can be routinely achieved.

At the low temperatures involved, the thermal de Broglie wavelength, $\lambda_T \gtrsim \bar{a} \simeq$ 0.1–1 μm, is much larger than the typical range of the inter-atomic potential. The two-particle scattering is therefore dominated by *s*-wave scattering, with a scattering length a_s that is typically of order a few nanometres (for ^{87}Rb, $a_s \simeq 5\,\mathrm{nm}$). A typical atomic gas of bosons is weakly interacting, in the sense that $\bar{n}a_s^3 \ll 1$. Consequently, it can be well described as an ideal Bose gas with very small condensate depletion. (This is in contrast to superfluid helium, for which the strong interactions cause significant condensate depletion.) That said, inter-atomic interactions are still present and are important for many physical properties. Non-zero repulsive interactions will cause the gas to behave as a superfluid, with non-zero critical velocity [6]. This, in turn, leads to the appearance of quantized vortices when the superfluid is forced to rotate.

1.2. *Quantized vortices*

1.2.1. *Quantized vortex line*

It was noted by Onsager and Feynman that superfluid helium cannot rotate as a conventional fluid [1]. A conventional fluid rotating at angular frequency $\boldsymbol{\Omega}$ has the velocity field of rigid body rotation

$$\boldsymbol{v} = \boldsymbol{\Omega} \times \boldsymbol{r} \tag{2}$$

for which the 'vorticity' of the flow, $\nabla \times \boldsymbol{v}$, is uniform

$$\nabla \times \boldsymbol{v} = 2\boldsymbol{\Omega}. \tag{3}$$

If, as is believed to be the case, the superfluid is described by a superfluid wavefunction $\psi_s = \sqrt{n_s}e^{i\phi(\boldsymbol{r})}$ then the superfluid velocity is

$$\boldsymbol{v}_s = \frac{\hbar}{M}\nabla\phi. \tag{4}$$

Hence, the fluid vorticity apparently vanishes:

$$\nabla \times \boldsymbol{v}_s = \frac{\hbar}{M}\nabla \times \nabla\phi = 0. \tag{5}$$

The last equality relies on ϕ being a smooth function of position and overlooks the possibility that the phase ϕ might have line-like singularities (point-like in two dimensions) around which ϕ changes by an integer multiple of 2π. These are the *quantized vortex lines* [1]. Integrating the vorticity over a two-dimensional surface containing such a singularity gives

$$\int \nabla \times \boldsymbol{v}_s \cdot \mathrm{d}\boldsymbol{S} = \oint \boldsymbol{v}_s \cdot \mathrm{d}\boldsymbol{l} = \frac{h}{M} \times \text{integer} \tag{6}$$

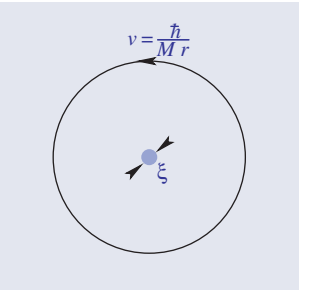

Figure 1. Schematic diagram of the velocity field around a quantized vortex line with one quantum of circulation, $\kappa = h/M$. The superfluid density falls to zero within the vortex core, which has a scale set by the healing length ξ.

indicating a delta-function contribution to the fluid vorticity on the vortex line. The 'circulation' of the vortex, defined as

$$\kappa \equiv \oint \boldsymbol{v_s} \cdot \mathrm{d}\boldsymbol{l} = \frac{h}{M} \times \text{integer} \tag{7}$$

is therefore quantized in units of h/M. This leads to a characteristic velocity profile, with an azimuthal velocity $|\boldsymbol{v}_s|$ which diverges as $r \to 0$, see Figure 1. In order to avoid the infinite kinetic energy associated with this divergent velocity, in the core of the vortex the superfluid density n_s tends to zero, over a lengthscale of the *healing length*, ξ.

The healing length is an important characteristic of a superfluid. Within the Gross–Pitaevskii mean-field theory [6] for a homogeneous interacting Bose condensate the energy is

$$E - \mu N = \int \left[\frac{\hbar^2}{2M} |\nabla \psi|^2 + \frac{1}{2} g |\psi|^4 - \mu |\psi|^2 \right] d^3\boldsymbol{r} \tag{8}$$

where ψ is the condensate wavefunction. This is written for an atomic Bose gas with s-wave interactions, with the contact interaction strength, $g = 4\pi\hbar^2 a_s/M$, chosen to reproduce the s-wave scattering length a_s (see (14)). In many situations, (8) is an accurate microscopic description of an atomic BEC, owing to the small condensate depletion $\bar{n} a_s^3 \ll 1$. For a uniform fluid, minimization with respect to $|\psi|^2$ gives $\mu = g|\psi|^2$. There is therefore one characteristic lengthscale of the equilibrium fluid, the healing length, set by

$$\frac{\hbar^2}{2M\xi^2} = g|\psi|^2 = \mu \quad \Rightarrow \quad \xi \equiv \sqrt{\frac{\hbar^2}{2M\mu}} = \frac{1}{\sqrt{8\pi\bar{n}a_s}}. \tag{9}$$

For an atomic gas, the healing length is typically of the order of $\xi \simeq 0.5\,\mu\mathrm{m}$ and is large compared with the typical particle separation, $\xi/\bar{a} \sim \sqrt{\bar{a}/a_s} \gtrsim 1$. In the case of superfluid helium, for which interactions are strong, the healing length is very short, $\xi \sim 0.8\,\text{Å}$; the vortex cores therefore have a size of the order of the inter-particle spacing.

1.2.2. *Vortex lattice*

If superfluid helium is forced to rotate, for example by cooling liquid helium in a rotating vessel from above the superfluid transition (where the conventional fluid rotates as

a rigid body) into the superfluid phase [7], the superfluid establishes an array of singly quantized vortex lines oriented along the rotation axis.

For dilute vortices, spaced by a distance $a_v \gg \xi$, the arrangement of vortices is dominated by the influence of the kinetic energy of the superfluid flow. Minimizing the kinetic energy of the superfluid flow in the rotating frame leads to the following conclusions [8].

(i) The mean vortex density in the plane perpendicular to the rotation axis is set by the condition that the mean superfluid flow (averaged over a lengthscale large compared with the vortex spacing) mimics rigid body rotation. The integral of the vorticity of a uniformly rotating body (3) over an area A is $2A\Omega$; setting this equal to the circulation of a superfluid containing N_v vortices in this area, $N_v h/m$, leads to Feynman's result for the mean vortex density [1]

$$n_v \equiv \frac{N_v}{A} = \frac{2M\Omega}{h}. \tag{10}$$

(ii) The vortices experience pairwise logarithmic repulsive interactions, with an interaction energy per unit length of

$$\text{constant} - n_s \frac{h^2}{2\pi M^2} \sum_{\langle i,j \rangle} \ln\left(|\boldsymbol{R}_i - \boldsymbol{R}_j|/\xi\right) \tag{11}$$

where n_s is the superfluid density and $\boldsymbol{R}_i = (X_i, Y_i)$ is the position of the ith vortex in the plane perpendicular to the rotation axis. The groundstate configuration of a set of classical particles interacting with logarithmic repulsion is a triangular lattice. One therefore expects the vortices to arrange in a triangular lattice at low temperature [9].

The direct observation of vortex arrays in rotating superfluid helium poses a very significant challenge: it requires the measurement of a set of very small vortex cores, of size $\xi \sim 0.8\,\text{Å}$, spaced by the much larger lengthscale $a_v \simeq 1/\sqrt{n_v} \sim 1\text{mm}$ (at the achievable rotation rates of superfluid helium). Images of the positions of quantized vortices emerging from the surface of rotating helium have been obtained in very remarkable experiments [10,11], showing arrays of small numbers of vortices.

1.3. *Rotating atomic gases*

Vortex lattices may be generated in atomic BECs by confining the gas in a magnetic trap of cylindrical symmetry, and stirring the gas with a rotating deformation [12–14]. The formation of vortices is driven by dynamical instability of the surface modes [15–18] followed by a period of turbulent flow before steady state is reached.

We focus on the equilibrium states that can be achieved, assuming that the system reaches a steady state at a rotation rate Ω. Under typical conditions, the rotation rates are $\Omega \simeq 2\pi \times 100\,\text{Hz}$, setting a mean inter-vortex spacing of $a_v \sim 2\,\mu\text{m}$. This is small compared with the condensate size, allowing large numbers of vortices to be created in the condensate (observations of up to 160 vortices were reported in [13]). The gases are typically in the regime $\xi \lesssim a_v$ for which the vortex lattice structure is determined by the kinetic energy of superfluid flow (11) and one expects a triangular lattice ordering at low temperatures.

Indeed, images of the particle density, taken following expansion of the cloud, show large numbers of vortices ordered in a triangular lattice arrangement [12–14,19,20].

There are many reasons why cold atomic gases are very interesting systems in which to study the properties of superfluid vortices and vortex arrays. The aspects that we focus on in this review are as follows.

- *High vortex density*. In atomic BECs, the inter-vortex spacing $a_v \simeq 2\,\mu$m is comparable to the vortex core size, as set by the healing length which is typically $\xi \simeq 0.5\,\mu$m. One can therefore envisage [21] entering a novel regime in which the rotation frequency is sufficiently high that the separation between the vortices a_v becomes less than the healing length ξ. Indeed, this new regime has been achieved for a Rb condensate, by using an ingenious technique to achieve very high rotation rate and low density [20]. In superfluid helium, where the zero temperature healing length is $\xi \simeq 0.8\,$Å, achieving this regime would require $\Omega \gtrsim 10^{13}$ rad^{-1}. It is of interest to understand the properties of vortex lattices in the regime, $a_v \ll \xi$, which differ markedly from those of superfluid helium for which $\xi \ll a_v$.
- *Strongly correlated phases*. One can envisage entering a regime of even higher vortex density, when the number of vortices is comparable to the number of particles [22]. In this case, theory predicts the formation of strongly correlated phases. These can be understood as *bosonic* analogues of the strongly correlated phases that are responsible for the fractional quantum Hall effect (FQHE) of electrons in semiconductors [23,24]. These states have many interesting and novel properties.
- *Tunable interactions*. There is the possibility to tune the inter-particle interactions: both the strength and the qualitative form of the interaction, by use of a Feshbach resonance and/or dipolar interactions. The groundstate of a rapidly rotating Bose gas is sensitive to the nature of the interaction.
- *Lattice potentials*. The imposition of a rotating optical lattice [25,26], or the use of 'artificial gauge fields' [27–29], allows studies of the interplay of vortex lattices with external lattice potentials. This raises interesting issues involving the effects of commensurability of the two lattice periods. Similar systems may also help to stabilize strongly correlated phases in experiment [26,29–31].
- *Multi-component* (*spinor*) *gases*. The trapping and rotation of Bose condensates with multiple components is possible. This can give rise to more complex forms of vortex lattice order, including topological spin textures, and raises the possibility of novel strongly correlated phases.
- *Fermi gases*. Atomic Fermi gases can have interesting and unusual responses to rotation. In particular, strongly interacting Fermi gases in the BEC to Bardeen–Cooper–Schrieffer (BCS) regime behave as superfluids. Rotation leads to the formation of quantized vortices. Rapid rotation raises the possibility of interesting strongly correlated phases involving the interplay of the physics of superconductivity with the physics of the FQHE.

As is clear from the above list of topics, in this review we focus mainly on one aspect of the physics of rapidly rotating gases: the possibility of the appearance of strongly correlated equilibrium phases in novel parameter regimes accessible in experiments. Recent progress in this field has involved many other interesting developments. These include the

non-equilibrium properties of rotating gases, dynamical excitations, the effects of confinement and trap geometry, and the many experimental developments. In the present article, these subjects are either omitted or only touched upon briefly. The reader is referred to [4,32] for excellent recent reviews that cover these topics in more detail.

2. Rapidly rotating atomic Bose gases

The possibility of achieving high vortex density, and entering a regime where the mean vortex spacing a_v is small compared with the healing length ξ (see [21]), is one of the most striking differences between the physics of atomic BECs and that of rotating helium. We now describe the theoretical description of atomic gases in this rapid rotation regime. This discussion forms the basis for many of the theoretical results described in this review.

2.1. *Rapid rotation limit*

The Hamiltonian describing an interacting atomic gas in an axisymmetric harmonic trap is

$$H = \sum_{i=1}^{N}\left[\frac{|\boldsymbol{p}_i|^2}{2M} + \frac{1}{2}M\omega_\perp^2(x_i^2 + y_i^2) + \frac{1}{2}M\omega_\parallel^2 z_i^2\right] + \sum_{i<j} V(\boldsymbol{r}_i - \boldsymbol{r}_j). \tag{12}$$

Most commonly, the interaction between ultra-cold atoms can be represented by a contact interaction [6]

$$V(\boldsymbol{r}) = g\delta^{(3)}(\boldsymbol{r}) \tag{13}$$

with the interaction strength chosen as

$$g = \frac{4\pi\hbar^2 a_s}{M} \tag{14}$$

to reproduce the *s*-wave scattering length. However, in later sections we also consider situations involving dipolar interactions or a Feshbach resonance in the interaction.

The Hamiltonian (12) describes N identical particles which are confined in a harmonic trap, with natural frequencies $\omega_\perp$ and $\omega_\parallel$. Note that the potential is axisymmetric about the $\hat{z}$-axis. We therefore (for now) neglect the influence of any deformation that is required to stir the gas. One can imagine that the system has been stirred, such that it has picked up a large angular momentum about the $\hat{z}$-axis, but this stirring potential has been removed. Owing to the axial symmetry, the angular momentum will be conserved. The question we address is: What is the groundstate of a Bose gas that has been prepared in this way? Equivalently: what is the lowest energy state of (12) as a function of the angular momentum about the $\hat{z}$-axis?

For much of this review, we consider the situation in which the interactions are relatively weak. In this limit, the relevant single-particle states simplify. To motivate the form of the single-particle states it is convenient to work not in terms of fixed angular momentum L, but in terms of its conjugate thermodynamic variable which is the rotation rate Ω.

2.1.1. *Rotating frame of reference*

In a frame of reference rotating about the $\hat{z}$-axis with angular momentum $\boldsymbol{\Omega} = \Omega\hat{z}$, the Hamiltonian is [33]

$$H_\Omega = H - \boldsymbol{\Omega} \cdot \boldsymbol{L}. \tag{15}$$

In this frame, the one-body terms can be written in a suggestive way

$$\begin{aligned} H_\Omega^{(1)} &= \frac{|\boldsymbol{p}|^2}{2M} + \frac{1}{2}M\omega_\perp^2(x^2+y^2) + \frac{1}{2}M\omega_\parallel^2 z^2 - \boldsymbol{\Omega}\cdot\boldsymbol{r}\times\boldsymbol{p} \\ &= \frac{|\boldsymbol{p} - M\boldsymbol{\Omega}\times\boldsymbol{r}|^2}{2M} + \frac{1}{2}M(\omega_\perp^2 - \Omega^2)(x^2+y^2) + \frac{1}{2}M\omega_\parallel^2 z^2. \end{aligned} \tag{16}$$

The kinetic term in this Hamiltonian is equivalent to that of a particle of charge q^* experiencing a magnetic field $\boldsymbol{B}^*$ with

$$q^*\boldsymbol{B}^* = 2M\boldsymbol{\Omega}. \tag{17}$$

This connection shows that the Coriolis force in the rotating frame plays the same role as the Lorentz force on a charged particle in a uniform magnetic field [34]. Much use is made of the equivalence of these two effects in this review. Indeed, we frequently refer to 'rotation' or 'magnetic field' interchangeably, assuming that the connection is clear.

One difference arises from the centrifugal force of the rotation, which has no analogue for a charged particle in a magnetic field. The centrifugal force acts to reduce the harmonic confinement potential. Stability of a harmonically trapped gas requires that the confinement is retained in (16), which requires that the rotation rate is below the 'centrifugal limit'

$$\Omega \le \omega_\perp. \tag{18}$$

Analogies with the properties of a charged particle in a uniform magnetic field are most evident in the limit of a large number of vortices, $N_v \gg 1$. In this case, very general considerations lead to the conclusion that $\Omega \simeq \omega_\perp$ (see Section 2.5 and Equation (92)). Essentially, one can then neglect any residual confinement and set $\Omega = \omega_\perp$, viewing the system as being uniform in the plane perpendicular to the rotation axis. (The analogy holds also for finite N_v with $\Omega < \omega_\perp$, but involves the Fock–Darwin spectrum for a charged particle in a magnetic field with harmonic confinement [35,36], which makes the present discussion somewhat less clear. This case is covered in the following section.) For $\Omega = \omega_\perp$, the Hamiltonian (16) describes a quasi-two-dimensional system of particles in a uniform magnetic field. The energy spectrum takes the form familiar from studies of the quantum Hall effect [23]

$$E_{n,m,n_\parallel}^{\omega_\perp} = 2\hbar\omega_\perp\left(n + \frac{1}{2}\right) + \hbar\omega_\parallel\left(n_\parallel + \frac{1}{2}\right) \tag{19}$$

where $n = 0, 1, 2, \ldots$ is the Landau level index, $m = -n, -n+1, -n+2, \ldots$ the angular momentum quantum number about the rotation axis, and $n_\parallel = 0, 1, 2, \ldots$ is the subband index for motion along the rotation axis. The spectrum is highly degenerate, with the single-particle states of different angular momentum m having the same energy. The effective 'cyclotron frequency' is $q^*B^*/M = 2\omega_\perp$.

The weak interaction limit occurs when the chemical potential $\mu \sim g\bar{n}$ is small compared to the single-particle level spacings[3]

$$\mu \ll \hbar\omega_{\parallel}, 2\hbar\omega_{\perp}. \tag{20}$$

These conditions are equivalent to the conditions that the healing length is large compared to the inter-vortex spacing, $\xi \gg a_{\rm v}$, and to the subband thickness in the z-direction, $\xi \gg a_{\parallel}$. Although (20) is typically not satisfied for a non-rotating gas, for a rapidly rotating gas the centrifugal forces spread the cloud out, the density falls and the system tends towards this weakly interacting regime [20].

Under these conditions[4] (20), to a good approximation the single-particle states are restricted to (quasi) two dimensions ($n_{\parallel} = 0$) and to the LLL ($n = 0$). The single-particle wavefunctions are [21]

$$\psi_m(\boldsymbol{r}) \propto (x + iy)^m e^{-(x^2+y^2)/2a_{\perp}^2} e^{-z^2/2a_{\parallel}^2} \tag{21}$$

where

$$a_{\perp,\parallel} \equiv \sqrt{\frac{\hbar}{M\omega_{\perp,\parallel}}} \tag{22}$$

are the trap lengths in the radial and axial directions. We refer to this regime (20) as the 'two-dimensional LLL regime'.

To make connections to the quantum Hall effect as clear as possible, we introduce the complex representation

$$\zeta \equiv \frac{x + iy}{\ell} \tag{23}$$

where ℓ is the conventional magnetic length associated with $q^*B^* = 2M\omega_{\perp}$

$$\ell \equiv \sqrt{\frac{\hbar}{2M\omega_{\perp}}} = \frac{a_{\perp}}{\sqrt{2}}. \tag{24}$$

The (normalized) two-dimensional LLL basis states are then

$$\psi_m(\zeta, z) = \frac{1}{\sqrt{2\pi 2^m m!}} \zeta^m \times \left[\frac{e^{-|\zeta|^2/4}}{\ell} \frac{1}{(\pi a_{\parallel}^2)^{1/4}} e^{-z^2/2a_{\parallel}^2} \right]. \tag{25}$$

For simplicity, in the following when writing wavefunctions in the two-dimensional LLL, we omit the ubiquitous [bracketed] exponential terms, focusing only on the prefactors that are polynomial in ζ.

2.1.2. *Laboratory frame of reference*

An alternative way to understand the restriction to the two-dimensional LLL is to work in the laboratory frame, and consider the total angular momentum as the control parameter [21]. This approach makes the appearance of Landau-level wavefunctions somewhat less evident, but it has the advantage of clarifying that $N_{\rm v} \gg 1$ is not required for the restriction to the states (21) in the two-dimensional LLL regime (20).

For the harmonically trapped gas (12) the single-particle energy spectrum is

$$E = \hbar\omega_\perp(2n_\perp + |m| + 1) + \hbar\omega_\parallel(n_\parallel + 1/2) \tag{26}$$

where $m = 0, \pm1, \pm2, \ldots$ is the angular momentum quantum number (about the z-axis) and $n_\perp, n_\parallel = 0, 1, 2, \ldots$ are the radial and axial quantum numbers. For a set of particles $i = 1, N$ occupying these states, the total angular momentum (in units of $\hbar$) is

$$L = \sum_{i=1}^{N} m_i \tag{27}$$

where m_i is the angular momentum of particle i.

For weak interactions (20), to determine the groundstate at fixed total angular momentum L, we must first minimize the total kinetic and potential energies. Clearly, from (26), the particles then must only occupy single-particle states with $n_\perp = n_\parallel = 0$. In addition, one can show that at fixed L (and assuming $L \geq 0$ without loss of generality) particles must only occupy states with $m_i \geq 0$ (see [21]). The resulting set of single particle states, those states with $n_\perp = n_\parallel = 0$ and $m_i \geq 0$, is precisely the set of two-dimensional LLL states (21) and (25).

To see why one requires $m_i \geq 0$, let us first write down the energy for a collection of N particles with total angular momentum (27) restricted to the two-dimensional LLL ($n_\perp = n_\parallel = 0, m_i \geq 0$). The total single-particle energy is

$$E = \sum_{i=1}^{N}\left[\hbar\omega_\perp(m_i + 1) + \hbar\omega_\parallel/2\right] = \left(\hbar\omega_\perp + \frac{1}{2}\hbar\omega_\parallel\right)N + \hbar\omega_\perp L. \tag{28}$$

Now, consider moving one particle, $i = 1$, from its state $m_1 \geq 0$ to a new state m_1', which may have $m_1' < 0$ and then be outside of the two-dimensional LLL. To conserve the total angular momentum L, we, in addition, need to add $m_1 - m_1'$ units of angular momentum to the other particles. Keeping these particles in states with $m \geq 0$ leads to an overall change in energy

$$\Delta E = \hbar\omega_\perp\left[(-|m_1| + |m_1'|) + (m_1 - m_1')\right] = \hbar\omega_\perp\left[|m_1'| - m_1'\right] \tag{29}$$

which is an energy *increase* if $m_1' < 0$. Hence, at fixed $L \geq 0$ the lowest-energy states must have $m_i \geq 0$.

2.1.3. *Effects of weak interactions*

The inclusion of weak interactions poses a theoretical problem that is very closely related to that for electrons in the FQHE [23,24]. For a system of N particles with a given total angular momentum, L, one must distribute the particles within the two-dimensional LLL orbitals such that the angular momentum (27) is fixed. The single-particle (kinetic + potential) energy of all of these states (28) is the same, leading to a very high degeneracy at the single-particle level. The groundstate is determined by the action of the interactions within this degenerate space. This is a fundamentally non-perturbative problem, as in the FQHE. The differences are firstly in the nature of the inter-particle forces, and secondly – and most importantly – that here we are studying bosons, not fermions. We are interested in the nature of the phases that can emerge for rotating

bosons, for the specific forms of interactions that are physically relevant in ultra-cold atomic gases.

For the most part, we focus on the case of contact interactions (13) between bosons. The interaction between particles is fully specified by the Haldane pseudo-potentials (see Appendix A), which for contact interactions reduce to the single parameter

$$V_0 = \sqrt{\frac{2}{\pi}} \frac{\hbar^2 a_s}{M a_\perp^2 a_\parallel}. \tag{30}$$

This parameter sets the energy scale of the rotating bosons in the two-dimensional LLL.

For a set of N particles at total angular momentum L, we write the interaction energy of the groundstate of the contact interactions as $E_I(L,N) \equiv V_0 \epsilon_I(L,N)$ where $\epsilon_I(L,N)$ is a dimensionless function. The total energy (single particle and interaction), is then, using (28)

$$E(L,N) = \left(\hbar\omega_\perp + \frac{1}{2}\hbar\omega_\parallel\right)N + \hbar\omega_\perp L + V_0\epsilon_I(L,N). \tag{31}$$

In the rotating frame of reference, the energy is

$$E_\Omega(L,N) = \left(\hbar\omega_\perp + \frac{1}{2}\hbar\omega_\parallel\right)N + \hbar(\omega_\perp - \Omega)L + V_0\epsilon_I(L,N). \tag{32}$$

At given Ω, the groundstate angular momentum $L(\Omega)$ is obtained by minimizing (32) over the allowed integer values of L. Thus, in the rotating frame of reference, the groundstate angular momentum is a function of the dimensionless control parameter $\hbar(\omega_\perp - \Omega)/V_0$. From the viewpoint of the laboratory frame, in which the control parameter is angular momentum, the rotation frequency is a derived quantity, set by

$$\Omega = \frac{V_0}{\hbar}\frac{\partial \epsilon_I}{\partial L}. \tag{33}$$

This is a standard thermodynamic relation stating that Ω is the conjugate thermodynamic variable to L (expressed at zero temperature and in terms of the parameters we have defined).

For a highly anisotropic trap, with $\omega_\parallel \ll \omega_\perp$, there is the possibility to explore a related regime [38]

$$\hbar\omega_\parallel \ll \mu \ll 2\hbar\omega_\perp. \tag{34}$$

The interactions are then small compared with the cyclotron splitting $2\hbar\omega_\perp$, so the motion perpendicular to the rotation axis is still described by the LLL. However, since the interactions are large compared with the subband spacing, many subbands of the axial confinement are relevant. We refer to this regime (34) as the 'three-dimensional LLL limit'. Following the approach proposed in [38], within mean-field theory in the three-dimensional LLL regime, one can expect the density distribution along the rotation axis to adopt a Thomas–Fermi profile, with overall length $2W_z$. As described in Appendix A

the properties are then the same as in the two-dimensional LLL, but with an overall change in interaction constant (A5), to

$$V_0^{\mathrm{TF}} = \frac{6}{5}\frac{\hbar^2 a_{\mathrm{s}}}{M a_\perp^2 W_z}.$$

(See Section 2.6 for a discussion of the validity of mean-field theory in the three-dimensional LLL regime.)

In the above we have discussed the rapid rotation limit of atomic bosons. The same considerations apply equally well to rotating fermions, leading to two-dimensional LLL and three-dimensional LLL limits at sufficiently low density and weak interactions that (20) or (34) apply. In Section 5 we describe the properties of rapidly rotating fermions in the LLL.

2.2. *Gross–Pitaevskii mean-field theory*

The Gross–Pitaevskii mean-field theory for an interacting Bose gas amounts to the assumption that the many-body state is a pure condensate, in which all particles occupy the same single-particle state $\psi(\boldsymbol{r})$

$$\Psi(\{\boldsymbol{r}_i\}) = \prod_{i=1}^{N} \psi(\boldsymbol{r}_i). \tag{35}$$

As an approximation to the groundstate, the (normalized) condensate wavefunction ψ is chosen to minimize the expectation value of the Hamiltonian. (We discuss the limits of applicability of this ansatz in Section 2.3.)

For a rapidly rotating Bose gas the single-particle orbitals consist only of the states (21). Thus, the condensate wavefunction can be expanded in terms of these states

$$\psi(\zeta, z) = \sum_{m\geq 0} c_m \psi_m \tag{36}$$

with $\sum_m |c_m|^2 = 1$. The mean-field groundstate is obtained by choosing the coefficients c_m to minimize the expectation value of the interaction energy, which for contact interactions (13), is

$$E_I^{\mathrm{GP}}(L, N) = \frac{1}{2} g N^2 \int |\psi(\boldsymbol{r})|^4 \, d^3\boldsymbol{r} \tag{37}$$

with a constraint on the (average) angular momentum,

$$L = N \sum_m m |c_m|^2. \tag{38}$$

The mean-field groundstate therefore depends only on L/N. The determination of the condensed LLL state that minimizes the interaction energy at fixed L/N constitutes the LLL mean-field theory. The application of Gross–Pitaevskii mean-field theory within the two-dimensional LLL regime (20), or the three-dimensional LLL regime with Thomas–Fermi profile (34), is sometimes referred to as the 'mean-field quantum Hall' regime in the literature. We avoid use of this terminology, preferring the term 'mean-field LLL' regime.

As discussed below, the physics of the mean-field LLL regime is in close analogy with that of the Abrikosov lattice in type-II superconductors (predating quantum Hall effects significantly). We reserve the term 'quantum Hall regime' for the regime of strong correlations, described in Section 2.4, where there are close analogies with the FQHE.

Note that, in general, (36) is not an eigenstate of angular momentum, while the Hamiltonian conserves total angular momentum. The fact that the condensate wavefunction does not preserve the rotational symmetry of the Hamiltonian should not necessarily be viewed as a deficiency. Rather this wavefunction correctly captures the fact that the system spontaneously breaks rotational symmetry, in the limit $N \to \infty$ with L/N fixed. This is discussed further in Section 2.3.2.

Noting that the condensate wavefunction (36) is a polynomial in ζ, it may be expressed in terms of its zeros [39] as

$$\psi(\zeta, z) = A \prod_{\alpha=1}^{m_{\max}} (\zeta - \zeta_\alpha) \tag{39}$$

where $m_{\max}$ is introduced as a cut-off in the degree of the polynomial (36), and A is a normalization factor. These zeros are the complex positions of the quantized vortices. Thus the LLL Gross–Pitaevskii wavefunction is fully described by the positions of the vortices. The process of choosing the $m_{\max}+1$ complex coefficients c_m (with normalization) is equivalent to the choice of the locations of $m_{\max}$ vortices.

The minimization for contact interactions has been implemented numerically by several authors [40–42]. A simple result is for the state at $L/N = 1$, for which the lowest energy condensate wavefunction is found to be

$$\psi(\zeta, z) = A\zeta \tag{40}$$

in which all particles are condensed into the $m = 1$ orbital. For other values of L/N the system spontaneously breaks rotational symmetry. For large L/N the number of vortices grows, as $N_v \simeq 3L/N$, and forms a triangular vortex lattice that is weakly distorted by the confinement, see Figure 2. Although small, the distortions of the triangular lattice are crucial to obtain the correct density distribution in the trap. Fixing the positions of the vortices on the triangular lattice leads to a density distribution that, when averaged over a lengthscale larger than the vortex spacing, is Gaussian [38]. The true averaged density distribution is Thomas–Fermi like (i.e. an inverted parabola) [43] as is found from numerical studies [41]. The density distribution in this regime is discussed further in Section 2.5.

The appearance of this triangular vortex lattice is very closely related to the appearance of a triangular lattice of flux lines in type-II superconductors close to the upper critical field. In that case, the order parameter is determined by minimizing the Ginzburg–Landau energy functional (per unit length L along the field direction)

$$\frac{F - F_n}{L} \sim \int \left[\frac{1}{2M} |(-i\hbar\nabla + 2e\boldsymbol{A})\psi_s|^2 + \alpha|\psi_s|^2 + \frac{\beta}{2}|\psi_s|^4 \right] d^2\boldsymbol{r}. \tag{41}$$

Close to H_{c2} the order parameter is small, so to a first approximation one can neglect the quartic term and minimize the quadratic terms. These describe electron pairs (hence charge $-2e$) in a uniform magnetic field: the lowest-energy states are the (degenerate)

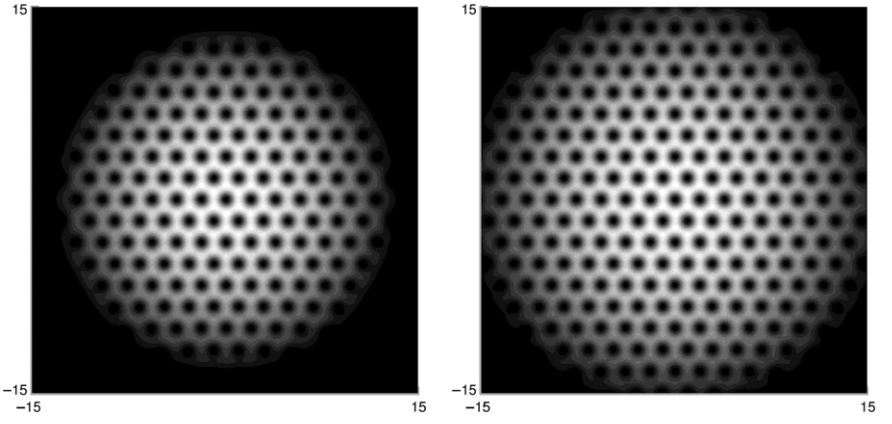

Figure 2. Numerical results for the particle density of an atomic BEC in the weak interaction limit (two-dimensional LLL), for two values of the angular momentum per particle $L/N = 60$ and 90 (see [41]). The lattice structure is determined only by the interactions, which are here chosen to be contact interactions (13). Close to the centre of the trap, the vortices form a regular triangular lattice. Reproduced with permission from [41]. Copyright © 2004 by the American Physical Society.

LLL orbitals. As explained by Abrikosov [44] the groundstate is selected as the linear combination of the LLL orbitals that minimizes the quartic term. The solution is that the groundstate is a *triangular* lattice [45], and is characterized by the parameter

$$\beta_A \equiv \frac{\langle |\psi_s|^4 \rangle_{\rm av}}{\langle |\psi_s| \rangle_{\rm av}^2} \simeq 1.1596, \tag{42}$$

where $\langle \ldots \rangle_{\rm av}$ denotes the (spatial) average over the unit cell of the lattice. This is mathematically equivalent to the LLL mean-field theory for rotating bosons, at least in the uniform case (i.e. close to the centre of a trap containing many vortices). The interaction energy (37) is

$$E_I^{\rm GP} = \frac{1}{2} g_{\rm 2d} N^2 \int |\psi(x,y)|^4 \, d^2\boldsymbol{r}, \tag{43}$$

where $g_{\rm 2d} \equiv g/(\sqrt{2\pi} a_\parallel)$ is the two-dimensional coupling constant, and $\psi(x,y)$ is the two-dimensional component of the condensate wavefunction, which is restricted to states in the LLL. Using the above result (42), one concludes that the groundstate is a triangular lattice, and its energy (for a system of N particles in a total area A) is

$$E_I^{\rm GP} = \frac{1}{2} g_{\rm 2d} \beta_A \frac{N^2}{A} = \beta_A V_0 \frac{N^2}{N_{\rm v}}. \tag{44}$$

In the last equality, we have replaced the area A by the number of vortices $N_{\rm v} = A/(\pi a_\perp^2)$.

2.2.1. *Landau-level mixing*

The limit of weak interactions (20) where the LLL regime is applicable, corresponds to the case of dense vortices, $\xi \gg a_\perp$. For dilute vortices, $\xi \ll a_\perp$, interactions lead to contributions from higher Landau levels to the condensate wavefunction. It was

explained above that for both $\xi \ll a_\perp$ (dilute vortices) and $\xi \gg a_\perp$ (dense vortices) the mean-field groundstate is a triangular vortex lattice. As $\xi/a_\perp$ varies between these two limits, there is a smooth crossover [46,47]. This crossover has been observed in experiments of Eric Cornell's group, which have achieved a chemical potential $\mu \sim g\bar{n}$ that is less than the effective cyclotron splitting $2\hbar\omega_\perp$. In these experiments, μ remains of the order of $1.5\hbar\omega_\parallel$, so it is approaching the quasi-two-dimensional limit. Experimental evidence for the crossover into the LLL regime has been found in the apparent core size of the vortices [48], which shows the variation expected within calculations in the LLL [46,47]. The frequencies of the collective modes were predicted to show a reduction on entry into the LLL regime [49,50]. The experimental results appear to confirm the expected variation [51], but this conclusion has been queried in a subsequent theoretical study that reassesses the expected shear modulus [52] and indicates that in the experiments of [51] the collective mode frequencies have not reached the limiting values expected in the LLL regime.

Very different physics controls the energetics in the two limits: for strong interactions $\xi \lesssim a_\perp$ the vortex lattice is determined by the kinetic energy, for weak interactions in the LLL regime $\xi \gtrsim a_\perp$ the vortex lattice is determined entirely by the interactions. One should therefore view the smooth crossover in the properties as somewhat of a coincidence. As discussed in Section 2.2.3, changing the form of the interaction potential can lead to large changes in the vortex lattice structure in the LLL regime, $\xi \gtrsim a_\perp$.

2.2.2. *Anisotropic traps*

In order to model the process of stirring the trapped atomic BEC, one should include a potential that breaks the rotational symmetry of the Hamiltonian (12). A simple form is to introduce an elliptical perturbation of the transverse confinement, which is at rest in the rotating frame of reference. This gives two (slightly) different oscillator frequencies ω_x, ω_y in place of the single $\omega_\perp$.

For this model, there exists a generalization of the LLL description for a weakly interacting gas [53]. The centrifugal limit (18) is now set by the condition that $\Omega \leq \min(\omega_x, \omega_y)$. Close to this limit, the gas elongates in one of the directions transverse to the rotation axis leading to a quasi-one-dimensional geometry [54–57] for rapid rotation.

2.2.3. *Dipolar interactions*

Under certain circumstances, it has been proposed that the atoms (or molecules) in a cold trapped gas may carry an electric or magnetic dipole moment [58]. One should then add to the usual contact interaction the long-range dipole–dipole interaction. For two dipolar atoms with aligned dipole moments the effective interaction is

$$V(\boldsymbol{r}) = \frac{4\pi\hbar^2 a_s}{M}\delta^3(\boldsymbol{r}) + C_d \frac{1 - 3\cos^2\theta}{r^3}, \tag{45}$$

where θ is the angle between the dipole moment and the line separating the atoms, see Figure 3.

A BEC of atoms with significant dipolar interactions has been realized by condensing chromium-52 (see [59]), which is an atom with a very large magnetic dipole moment,

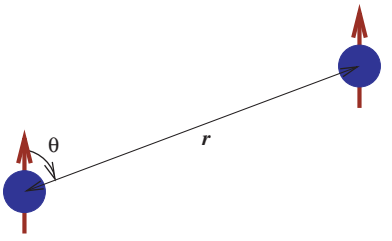

Figure 3. Geometry of two atoms with aligned dipole moments, as discussed in the text.

$\mu = 6\mu_B$, such that $C_d = \mu_0\mu^2/4\pi$. The relative size of dipolar and contact interactions is parameterized by the dimensionless ratio

$$\epsilon_{dd} \equiv \frac{C_d M}{3\hbar^2 a_s}, \tag{46}$$

which is $\epsilon_{dd} \simeq 0.16$ for native conditions in ^{52}Cr, and has been further increased to $\epsilon_{dd} \simeq 1$ by using a Feshbach resonance to reduce a_s (see [60]). Very recently, there has been the exciting achievement of the condensation of hetero-nuclear molecules in their ground rovibrational state [61]. Such systems can have large *electric* dipole moments, leading to very strong electric dipole interactions [58].

Consider a rapidly rotating atomic gas (in the two-dimensional LLL limit), and for simplicity let us choose the dipole moments to be directed parallel to the rotation axis [62]. The mean-field theory requires one to minimize the expectation value of the interaction energy

$$\frac{1}{2}\int\int |\psi(\boldsymbol{r})|^2 V(\boldsymbol{r}-\boldsymbol{r}')|\psi(\boldsymbol{r}')|^2 \, d^3\boldsymbol{r}\, d^3\boldsymbol{r}' \tag{47}$$

for $\psi(\boldsymbol{r})$ in the LLL and for the interaction potential (45). Although this is a simple generalization of the Abrikosov problem, it is one that does not naturally appear in that context, where the microscopic physics determining the superconductivity acts on scales much less than the vortex lattice period.

The mean-field groundstates have been found for the case of a translationally invariant vortex lattice [62,63]. The results [62] are shown in Figure 4, as a function of

$$\alpha \equiv \frac{V_2}{V_0}, \tag{48}$$

where [62]

$$V_0 = \sqrt{\frac{2}{\pi}}\frac{\hbar^2 a_s}{M a_\perp^2 a_\parallel} + \sqrt{\frac{2}{\pi}}\frac{C_d}{a_\perp^2 a_\parallel} - \sqrt{\frac{\pi}{2}}\frac{C_d}{a_\perp^3} \tag{49}$$

$$V_{m>0} = \sqrt{\frac{\pi}{2}}\frac{(2m-3)!!}{m!2^m}\frac{C_d}{a_\perp^3} \tag{50}$$

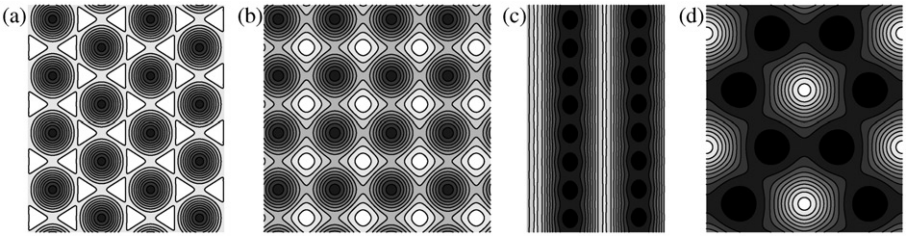

Figure 4. Mean-field groundstates of a rotating BEC in the two-dimensional LLL, for particles interacting by both contact and dipolar interactions. The relative size of these is controlled by $\alpha = V_2/V_0$. The structure of the vortex lattice varies from (a) triangular ($0 \leq \alpha \leq 0.20$) to (b) square ($0.20 \leq \alpha \leq 0.24$) to (c) 'stripe crystal', with simple rectangular unit cell ($0.24 \leq \alpha \leq 0.60$), to 'bubble crystal' phases ($\alpha \geq 0.60$) the simplest of which is shown in (d). Reproduced with permission from [62]. Copyright © 2005 by the American Physical Society.

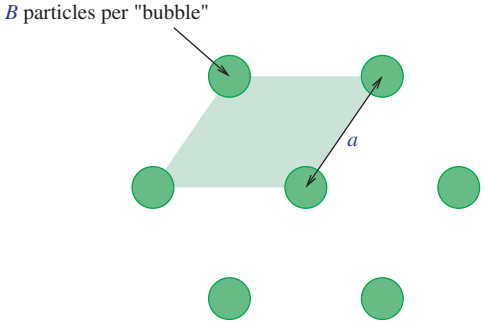

Figure 5. Schematic diagram of the bubble crystal phase.

are the Haldane pseudo-potentials for the dipolar interaction (45) in the limit $a_\parallel/a_\perp \ll 1$. (See Appendix A for definitions of the Haldane pseudo-potentials.)

The results show that the mean-field groundstate is very sensitive to long-range repulsion, passing through a series of vortex lattice phases as α increases. The contact interaction aims to make $|\psi(\boldsymbol{r})|^2$ as uniform as possible, while the long-range repulsion causes $|\psi(\boldsymbol{r})|^2$ to cluster, leading to crystalline phases of clusters of particles at large α. These are referred to as 'bubble crystal' phases [62], in analogy with the terminology used for structures of similar symmetry in two-dimensional electron gases in high Landau levels [64,65]. There is a sequence of bubble crystal phases as α increases, which are parameterized by the number of vortices per bubble, q. For two-dimensional particle density $n_{2\mathrm{d}}$ the number of particles per bubble is $B = n_{2\mathrm{d}}(\sqrt{3}/2)a^2$, where a is the lattice constant of the bubble crystal, assumed triangular (see Figure 5). For $B \gg 1$, the energy per particle is

$$\frac{E}{N} = \frac{1}{2}V_0 B + \frac{1}{2}K\frac{C_{\mathrm{d}}}{a^3}B = \frac{\sqrt{3}}{4}n_{2\mathrm{d}}\left[V_0 a^2 + \frac{KC_{\mathrm{d}}}{a}\right] \tag{51}$$

where $K = 11.034$ is the Madelung constant for dipolar interactions on the triangular lattice [66]. The energy is minimized for $a_{\min} = (\frac{KC_d}{2V_0})^{1/3}$, such that the number of vortices per bubble is

$$q \equiv n_v \frac{\sqrt{3}}{2} a_{\min}^2 = \frac{1}{\pi a_\perp^2} \frac{\sqrt{3}}{2} \left(\frac{KC_d}{2V_0}\right)^{2/3} = \sqrt{3} \left(\frac{2K}{\pi^2}\right)^{2/3} \left(\frac{V_2}{V_0}\right)^{2/3}. \tag{52}$$

Vortex lattices have not, as yet, been created in experiments on the dipolar condensates. If these condensates can be made to enter the regime of rapid rotation that has been achieved in rubidium [51] one expects not just to see a crossover in the physical properties, but a true phase transition into a vortex lattice of different symmetry that depends on the ratio of short- to long-range interactions (48). The dependence of the mean-field phases on the degree of Landau level mixing, as quantified by $\mu/\hbar\omega_\perp$, has been studied in [67].

2.3. *Beyond mean-field theory*

We now turn to describe the properties of rapidly rotating atomic BECs beyond the Gross–Pitaevskii mean-field approach. Much of our understanding has been derived from numerical exact diagonalization studies. These numerical techniques are described in Appendix B.

In the remainder of this section we describe some of the results for rotating bosons in a harmonic trap (12) in the weak interaction limit (20), and concentrate on the case of contact repulsive interactions (13).

2.3.1. *Low angular momentum $L \leq N$*

For small values of the total angular momentum L the exact groundstates of a rapidly rotating Bose gas are known analytically. The following states (53), (54), (56) have been shown to be exact eigenstates of the contact repulsion by both analytical [68] and numerical [69] studies, and to be the groundstates for a class of repulsive interactions [70,71] that includes contact repulsion (13).

- For $L = 0$ there is only one state in the two-dimensional LLL: the pure condensate in the $m = 0$ orbital

$$\Psi_{L=0}(\{\zeta_i\}) \propto 1. \tag{53}$$

- For $L = 1$ the groundstate is the centre-of-mass excitation of the $L = 0$ state

$$\Psi_{L=1}(\{\zeta_i\}) \propto \zeta_c \tag{54}$$

$$\zeta_c \equiv \frac{1}{N} \sum_{i=1}^{N} \zeta_i \tag{55}$$

for which the interaction energy is the same as for the $L = 0$ groundstate, $\epsilon_I(1, N) = \epsilon_I(0, N)$.

- For $2 \leq L \leq N$ the groundstates are the elementary symmetric polynomials in the variables $(\zeta_i - \zeta_c)$

$$\Psi_L(\{\zeta_i\}) \propto \sum_{p_1 < p_2 < p_L} (\zeta_{p_1} - \zeta_c)(\zeta_{p_2} - \zeta_c) \cdots (\zeta_{p_L} - \zeta_c). \tag{56}$$

For contact interactions, the energies of the states with $L \leq N$ ($L \neq 1$) are [68,69,72]

$$E_I(L, N) = V_0 \epsilon_I(L, N) = \frac{1}{2} V_0 N(N - 1 - L/2), \tag{57}$$

A close connection of these exact states for finite N to the condensed wavefunctions of the Gross–Pitaevskii theory can be made by considering the limit $N \to \infty$. Consider first the case $L = N$, for which

$$\Psi_{L=N}(\{\zeta_i\}) \propto \prod_i (\zeta_i - \zeta_c). \tag{58}$$

If the coordinate ζ_c were simply a number this would be the wavefunction of a pure condensate with a vortex at complex position ζ_c, Equation (39). The fact that ζ_c is the centre-of-mass coordinate (55), and therefore a function of the particle coordinates, means that this state is not fully condensed. Nevertheless, the fluctuations of the centre-of-mass from its average value $\langle \zeta_c \rangle = 0$, computed for the state $\Psi_{L=N}$, are

$$\langle \zeta_c^2 \rangle \sim 1/N. \tag{59}$$

Thus, in the limit $N \to \infty$,

$$\Psi_L(\{\zeta_i\}) \overset{N \to \infty}{\longrightarrow} \prod_i \zeta_i \tag{60}$$

which is the fully condensed state with a single vortex at the origin, (40). This observation, that one recovers a fully condensed state in the limit $N \to \infty$, keeping $L/N = 1$ fixed and staying within the two-dimensional LLL ($g\bar{n} \ll \hbar\omega_\perp, \hbar\omega_\parallel$), is a specific example of the result that Gross–Pitaevskii theory is exact [73] in the limit $N \to \infty$ with $g\bar{n}$ and L/N finite. One may generalize this to cases with $L \leq N$. To this end, we note that in the large N limit of (53), (54), (56), obtained by setting $\zeta_c \to 0$, the wavefunctions (53), (54), (56) are the set of all $N+1$ symmetric polynomials of $\{\zeta_i\}$. These polynomials can be generated by the condensate wavefunction

$$\Psi_Z(\{\zeta_i\}) = \prod_i (\zeta_i - Z) \tag{61}$$

where Z is a complex coordinate which may be viewed as the location of a single vortex. Thus, we conclude that, in the two-dimensional LLL, the lowest energy condensate wavefunction for $L/N \leq 1$ is precisely described as a *single* vortex state. For $|Z|$ finite and non-zero, the condensed state contains a single vortex located away from the origin, so it breaks rotational symmetry.

The relation between the exact spectra and the condensed states has been studied in detail for $L = 2N$ in [74].

2.3.2. *Spontaneous symmetry breaking*

It is a general feature of the Gross–Pitaevskii theory for a rotating gas in an axisymmetric trap that the lowest-energy condensed state spontaneously breaks the rotation symmetry of the Hamiltonian. For example, for (12) the general mean-field state is not rotationally invariant about the z-axis [40], but shows small clusters of vortices with local crystalline order.

Rotational symmetry breaking may be seen in the properties of the exact energy spectrum in the limit $N \to \infty$ with $N_v \sim L/N$ constant. Specifically, in this limit, the exact energy per particle (32) of the groundstate tends to the form

$$\frac{E_\Omega(L,N)}{N} \overset{N\to\infty}{\longrightarrow} \text{constant} + V_0 N f(L/N) + \hbar(\omega_\perp - \Omega)(L/N) \tag{62}$$

for a certain subset of angular momentum states L, discussed further below. In this equation, V_0 is the energy scale (30) and $f(L/N) \equiv \lim_{N\to\infty} \epsilon_I(L,N)/N^2$ is a dimensionless function which is set by the form of the interactions. In the thermodynamic limit, we require that the energy per particle (and, hence, the chemical potential) remains finite. For example, to remain within the two-dimensional LLL (20) requires the chemical potential to remain finite, $\mu \lesssim \hbar\omega_\perp$, $\hbar\omega_\parallel$. Since $\mu \sim V_0 N/N_v$, this requirement sets the condition that $V_0 N \to$ constant. Under this condition, the function f has an overall scale of the order of one.

At a general value of Ω, the exact groundstate angular momentum L^* is found by minimizing the energy per particle (62) over the allowed integer values of L. Provided that $f(L/N)$ is a (locally) smooth function with a simple minimum at L^*, which is found to be the generic case, all states which have L that is within of order $\sqrt{N}$ of the optimal value L^* have an excitation energy per particle that is of order V_0, and so vanishes in the appropriate thermodynamic limit, $N \to \infty$ with $V_0 N \to$ constant. That is, in the thermodynamic limit there is a degeneracy between of order $\sqrt{N}$ states of angular momentum close the optimal value L^*. The emergence of a degeneracy between a large number of states of different angular momenta is a signature of spontaneous rotational symmetry breaking in the thermodynamic limit [75].

Evidence for the appearance of rotational symmetry breaking can be found in the exact spectra at $L > N$, computed numerically for small numbers of particles.

Figure 6 shows the exact groundstate energy as a function of total angular momentum L for $N = 25$ particles, at a value of Ω chosen such that the mean-field state is a pair of vortices, with a two-fold rotational symmetry. A notable feature is that the groundstate degeneracies occur between states which differ in angular momentum by multiples of $\Delta L = 2$. This feature is an indication that in the thermodynamic limit the groundstate does not break rotational symmetry completely, but retains a two-fold symmetry. This is consistent with the mean-field state (see [40] at $L/N = 1.75$). For a state that retains a two-fold rotation symmetry, the values of L for which the limiting expression (62) applies are those that are spaced by $\Delta L = 2$ from the true groundstate value L^*; the function $f(L/N)$ describes the smooth envelope of the dependence of the energies of the states at these angular momenta.

The appearance of the quasi-degeneracies with increasing N is conveniently analysed by constructing scaling plots of $[E(L+1) + E(L-1) - 2E(L)]$, as a function of the scaled angular momentum, L/N, see Figure 7. This plot shows regions with

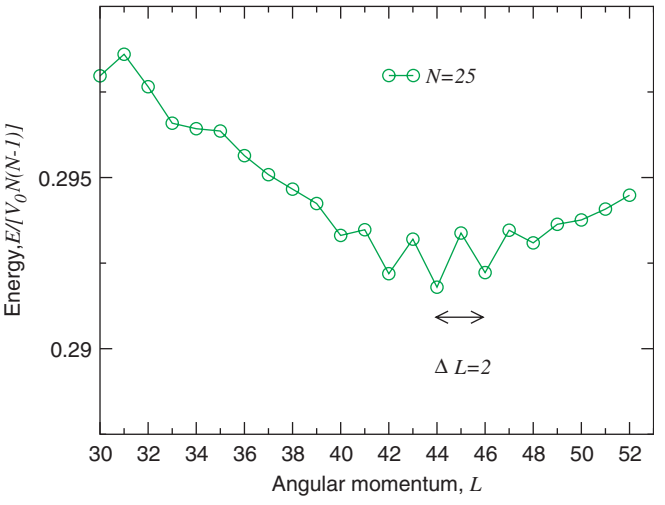

Figure 6. Groundstate energy as a function of the angular momentum, computed from exact diagonalization studies of rotating bosons in the two-dimensional LLL with contact repulsion (13), at rotation frequency Ω set to a value for which the mean-field groundstate shows two vortices. The groundstate is at $L^* = 44$, the spectrum shows the appearance of low-lying excited states at angular momenta that differ from this by multiples of two. In the thermodynamic limit, $N \to \infty$, the exact spectrum shows the appearance of quasi-degeneracies between states spaced in angular momentum by $\Delta L = 2$. This is a signature that in the thermodynamic limit the groundstate breaks rotational symmetry partially, leaving a two-fold symmetry axis [76].

quasi-degeneracies spaced by $\Delta L = 2$ ($1.5 \lesssim L/N \lesssim 2$) and by $\Delta L = 3$ ($2 \lesssim L/N \lesssim 2.5$), which indicate rotational symmetry breaking to states with residual two-fold and three-fold rotation axes. Analysis of the second derivatives $[E(L+\Delta L) - E(L-\Delta L) - 2E(L)]$ for $\Delta L = 2, 3$ in these regions (see Figure 7 for the case $\Delta L = 2$) allows the construction of scaling plots that confirm the above behaviour of the function $f(L/N)$ at large N.

For $L/N < 1$, rotational symmetry breaking can be deduced directly from considerations of the exact analytic wavefunctions of Section 2.3.1. For $L \leq N$, the exact energy spectrum for contact interactions (57) leads to $f(x) = x/4$. Since the function $f(x)$ has vanishing second derivative, this case is special from the point of view of rotational symmetry breaking. At one special value of the rotation frequency, $1 - \Omega/\omega_\perp = V_0 N/(4\hbar\omega_\perp)$, *all* states with $L \leq N$ are degenerate in the thermodynamic limit. There are therefore approximately N degenerate states, rather than approximately $\sqrt{N}$. This enhanced degeneracy reflects the fact that, at this rotation frequency, the mean-field state (61) is itself degenerate with respect to the position of the vortex, that is with respect to all possible angular momenta $0 \leq L/N \leq 1$.

Evidence of rotational symmetry breaking can also be found in the exact spectrum of the excitations above the lowest energy state at a given L. The relationship of the exact spectrum to the expected properties of Bogoliubov excitations of the mean-field groundstate has been discussed for $L \leq N$ in [77].

The condensate fractions and condensed wavefunctions for small numbers of rotating bosons have been investigated in [78]. These are deduced from the exact groundstates, allowing for rotational symmetry breaking. The positions of the vortices in the

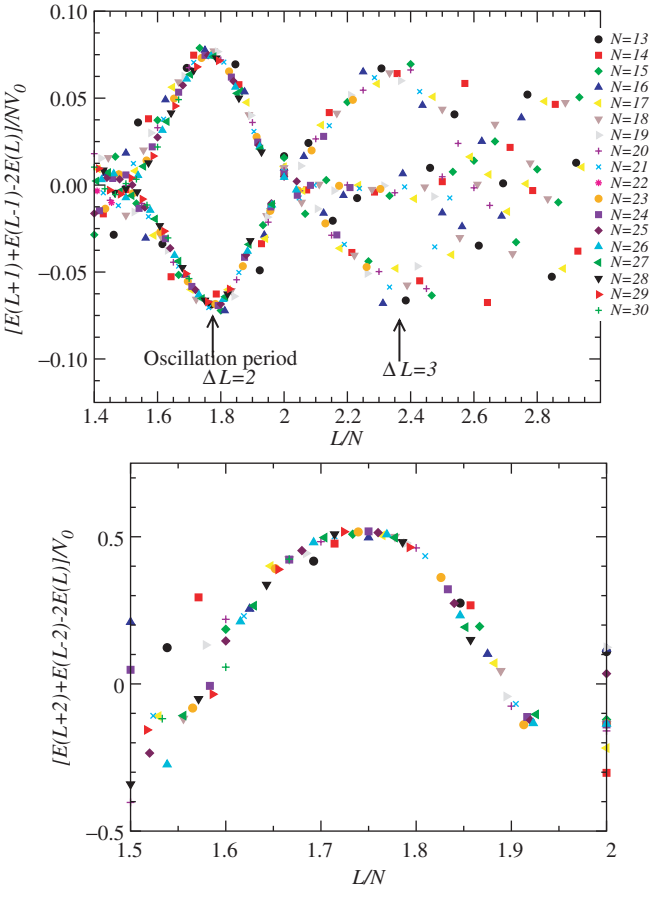

Figure 7. Scaling plots of the (numerical second derivatives of) the groundstate energy as a function of the angular momentum, computed from exact diagonalization studies of rotating bosons in the two-dimensional LLL with contact repulsion (13). The data collapse indicates that the large N asymptotic behaviour has been reached. These plots determine the scaling of the energies with N discussed in the text, which lead to the prediction of spontaneous rotational symmetry breaking in the thermodynamic limit $N \to \infty$, $V_0 N \to$ constant. There are regions which show clear two-fold and three-fold periods, corresponding to mean-field groundstates that break rotational symmetry partially to retain two-fold and three-fold symmetry axes, respectively [76].

condensate wavefunction (39) thus obtained show patterns similar to those from mean-field theory [40]. The condensate fraction is large for a single vortex ($L = N$) for $N \gtrsim 9$. For the system size studied ($N = 6$) the condensate fraction falls quickly to small values as the angular momentum is increased beyond the case of a single vortex ($L > N$) [78].

Anisotropic traps. For a rotating trap with a quadrupolar deformation [53–57], which can represent the stirred atomic BEC, angular momentum is not conserved. However, the wavefunction *parity* is preserved: the deformation does not couple states with odd and even L. Close to the rotation frequency at which the first vortex enters the system, the exact spectra show close degeneracy of levels of opposite parity for large numbers of

particles [79]. This quasi-degeneracy of the levels of the exact spectrum is an indication that the mean-field state spontaneously breaks the reflection symmetry of the trap: for $N \to \infty$ there are two degenerate condensed states in which a vortex sits either on one side or on the other side of the trap (in the reflection symmetry related position). The lifting of the degeneracy of these two states, at finite N, has been explained in terms of the rate of tunnelling of the vortex between these two locations [79].

Restoration of rotational symmetry. Noting that the Gross–Pitaevskii theory breaks rotational symmetry, an improved mean-field theory for rotating Bose gases has been proposed and analysed in [80]. In this theory the Gross–Pitaevskii wavefunction is projected onto an eigenstate of angular momentum. This restores the property that the exact groundstate for a finite N must have definite angular momentum. The resulting 'rotating vortex cluster' state has a lower energy than the Gross–Pitaevskii state, which may be important in situations when N is sufficiently small.

2.3.3. *Signatures of strong correlations*

From the first studies of rapidly rotating atomic Bose gases [21] it has been recognized that the groundstates include strongly correlated phases. In particular, the exact groundstate of N bosons in the two-dimensional LLL at high angular momentum, $L = N(N-1)$ (see [21]), is the bosonic Laughlin state [81]. This state (78) and its properties are described in detail in Section 2.4. For now we simply note that this is a strongly correlated liquid phase of the bosons. It has a vanishing condensate fraction, and does not have any long-range crystalline order (in either the particle or vortex density).

Evidence for other strongly correlated states was found in exact diagonalization studies of small numbers of particles [82]. As the rotation frequency is swept from $\Omega = 0$ to the centrifugal limit $\Omega = \omega_\perp$, the groundstate undergoes a series of transitions, between states with different values of angular momentum, L. The angular momentum L does not increase uniformly, but undergoes steps between certain 'magic angular momenta' in a sequence that depends on the total number of particles N. The states at these magic angular momenta were shown to be strongly correlated, in the sense of small condensate fraction. Furthermore, these states were shown to include the Moore–Read, or Pfaffian, state at $L = N(N-2)/2$ (see Section 2.4), and a set of other uncondensed states could be accounted for in terms of condensates of 'composite bosons' rather than of the underlying bosons [82].

An alternative description of the rotating groundstates was introduced in [83]. This work proposed a generalization of the 'composite fermion' construction used in the FQHE [24,84,85] to the case of rotating bosons. See Section 2.4 for a definition and discussion of these states. In this theory, one parameterizes the N-boson wavefunction in terms of a Slater determinant of N single-particle wavefunctions, which represents a set of N non-interacting composite fermions (80). For a composite fermion state with total angular momentum $L_{\rm CF}$ the resulting boson wavefunction has angular momentum [83] $L = L_{\rm CF} + N(N-1)/2$. Treating the composite fermions simply as non-interacting particles, with a Landau level spectrum, leads to the prediction of a set of special values of the angular momentum $L^*_{\rm CF}$ at which one expects the non-interacting composite fermions to have stable groundstates. These so-called 'compact states' [83,86] identify a set of special values of the angular momentum for the bosons $L^* = L^*_{\rm CF} + N(N-1)/2$

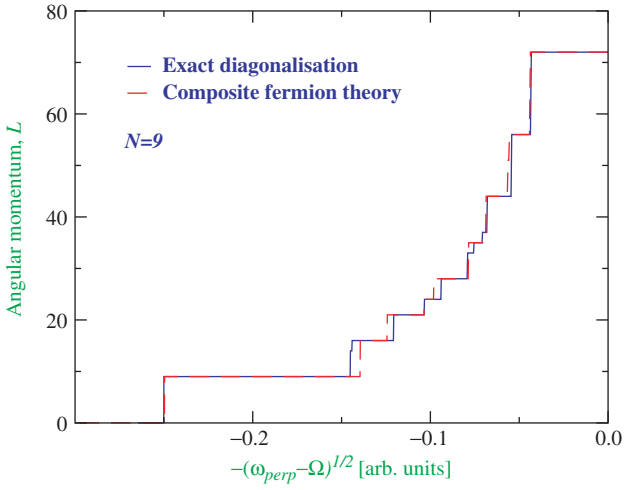

Figure 8. Groundstate angular momentum as a function of rotation rate Ω for $N=9$ bosons in the two-dimensional LLL with repulsive contact interactions. The solid line shows the results of exact diagonalization studies, with plateaus at the 'magic angular momenta'. The dashed line is the parameter-free prediction from the composite fermion theory [83]. This is obtained by finding the groundstate angular momentum using just the set of 'compact states' of the composite fermions. These compact states account for all of the magic angular momenta that appear in the exact spectrum; discrepancies arise only in the positions and widths of the plateaus, which depend very sensitively on small energy differences.

and provide a parameter-free trial many-boson wavefunction at each angular momentum. The theory is very successful at describing the exact groundstates of rotating bosons for the systems sizes that were studied (up to $N=10$): the values L^* deduced from the composite fermion theory account for almost all of the magic angular found in the exact studies; the overlaps of the trial composite fermion wavefunctions with the exact groundstates are very large [83]. An example of the accuracy of the composite fermion theory is shown in Figure 8.

Barberán *et al.* [87] investigated the pair correlations of the exact groundstates for small numbers of bosons. These results show evidence for local crystalline order. These crystalline correlations appear even for the Laughlin state for the system sizes studied ($N \leq 8$). Since the Laughlin state is the exact groundstate for all N, and it is not crystalline in the thermodynamic limit, these crystalline correlations are interpreted as a feature of the states of small numbers of particles [87].

The exact groundstates of small numbers of particles have been related to 'rotating boson molecule' states [88], in studies of up to $N=11$ particles [89]. These studies are based on the idea of an underlying crystalline order, combined with the projection of these cluster states onto states of definite angular momentum, leading to angular averaging of the particle density. This interpretation provides an alternative viewpoint on the magic angular momenta. It can account for the values of the magic angular momenta in terms of the shell structure of ordered crystalline arrangements of the bosons, most clearly for $N=6$ and $N=9$. It would be of interest to see the results of calculations of the overlaps of the variational rotating boson molecule wavefunctions with the exact groundstates.

For small numbers of particles it is perhaps moot to discuss which of a set of approximate theories should be used to describe the system[5]. Descriptions that are apparently very different (liquids of composite fermions, rotating vortex clusters or rotating boson molecules) could, in principle, all capture aspects of the groundstate and each could give useful physical insight. The relative merits can only be judged in their quantitative successes. However, qualitative distinctions between different descriptions can arise in the thermodynamic limit $N \to \infty$.

2.4. *Strongly correlated phases*

2.4.1. *The filling factor*

In order to make sharp statements about *phases of matter*, one must consider the thermodynamic limit, $N \to \infty$. There are different ways in which to take this limit for a rotating gas of bosons, depending on how one chooses to scale the angular momentum L with the number of particles N.

The simplest situation to consider is $N \to \infty$ keeping the number of vortices fixed. Since $N_v \sim L/N$ this requires $L \to \infty$ such that $L/N \to$ constant. The particle density then grows as $\bar{n} \propto N$, so for the mean-field interaction $g\bar{n}$ to remain finite (for example, to stay in the two-dimensional LLL regime), one should take $gN \to$ constant. With this set of scalings, the Gross–Pitaevskii theory has been shown to be exact [73]: the groundstate is a pure condensate in this thermodynamic limit. We have shown explicit examples of how this limit emerges from the exact spectra at finite N in Section 2.3.2.

Although this limit is appropriate for the description of atomic BECs in many experimental situations, from the perspective of many-body physics it is not the most interesting limit, leading as it does to states that are fully condensed. A much more interesting limit can be found by exploiting analogies with the FQHE. This regime may be of importance in future experiments at high vortex density.

The FQHE refers to a set of strongly correlated quantum phases of electrons in the two-dimensional LLL states [23,24]. These states are characterized by the electron *filling factor*

$$\nu_e \equiv n_e \frac{h}{eB}, \tag{63}$$

where n_e is the two-dimensional number density of electrons. From the above mapping of the rotating atomic gas (17), the analogous quantity is [22]

$$\nu \equiv n_{2d} \frac{h}{q^* B^*} = n_{2d} \frac{h}{2M\Omega} \tag{64}$$

where the two-dimensional density n_{2d} is related to the three-dimensional density by the integral along the rotation axis, $n_{2d} \equiv \int n(\boldsymbol{r}) \mathrm{d}z$. From (10), the filling factor can be written in terms of the vortex density as

$$\nu = \frac{n_{2d}}{n_v}. \tag{65}$$

In an inhomogeneous trap, Equation (65) should be interpreted as a local relation, defined on lengthscales larger than the mean vortex spacing. Considering the uniform limit, in

which the particles are uniformly distributed (on average) over an area containing N_v vortices, the relation takes the simple form

$$\nu = \frac{N}{N_v}. \tag{66}$$

Note that, for a system with a large number of vortices N_v, which shall be the focus of the studies described below, the rotation frequency is $\Omega \simeq \omega_\perp$ (92), and so $n_v \simeq 1/(\pi a_\perp^2)$ in (65).

It is interesting to study the nature of the groundstate of a rotating atomic gas for $N \to \infty$, $N_v \to \infty$ such that $\nu \to$ constant. A sharp question can be formulated in this thermodynamic limit: what is the phase diagram of a rapidly rotating atomic gas as a function of the filling factor ν? This is the question that was first raised in [22], and that we address in the remainder of the section.

Note that for *bosons* in the two-dimensional LLL, the filling factor can take any value, including values larger than one. (This contrasts with the case of fermions where the Pauli exclusion principle limits the occupation.) The only limitation to the theory as presented is that, for the single-particle states to remain in the two-dimensional LLL we require that interactions (and, hence, chemical potential) remain sufficiently small (20). Since $\mu \sim \nu V_0$, if V_0 is small compared with the trap level spacings ($\hbar\omega_\perp, \hbar\omega_\parallel$) the filling factor can be very large and the system still be in the two-dimensional LLL. This is the situation in the experiments of [90], where the LLL condition is achieved $\mu \lesssim 2\hbar\omega_\perp$ with a large filling factor $\nu \simeq 500$.

It has been argued in [22,49,50] that for a filling factor above a critical value ν_c the groundstate is a triangular vortex lattice, so the Gross–Pitaevskii mean-field theory is at least qualitatively accurate. Indeed, as described above, the Gross–Pitaevskii theory is exact in the limit $\nu \to \infty$ (this follows from the thermodynamic limit in which $N \to \infty$ with N_v finite). However, for small values of ν, corrections to mean-field theory are large. These corrections cause mean-field theory to fail qualitatively for $\nu < \nu_c$, and the groundstate is replaced by strongly correlated phases very different from the vortex lattice [22]. A very instructive way in which to understand the importance of the filling factor on the mean-field groundstate is to evaluate the *quantum fluctuations* of the vortices.

Quantum fluctuations of vortices. Consider the dynamics of a single vortex line in a two-dimensional fluid (i.e. a straight vortex line). We describe the quantum dynamics of the vortex line using a canonical quantization approach, but the results agree with those found in other ways [91,92]. The classical dynamics of a two-dimensional vortex, at a position X and Y in an external potential $V(X, Y)$, follows from the standard Magnus force dynamics of a vortex line in a classical fluid

$$-\rho_s \kappa \dot{Y} + F_X^{\text{ext}} = 0, \tag{67}$$

$$+\rho_s \kappa \dot{X} + F_Y^{\text{ext}} = 0, \tag{68}$$

where ρ_s is the mass density (per unit area) of the fluid and κ the circulation of the vortex. The only amendment for a quantized vortex in a superfluid is that the circulation is quantized, $\kappa = h/M$, so we may write

$$\rho_s \kappa = (n_{2d} M)\frac{h}{M} = n_{2d} h. \tag{69}$$

A Lagrangian that reproduces this classical dynamics is[6]

$$L = n_{2\mathrm{d}} h \dot{X} Y - V(X, Y), \quad [\vec{F}^{\mathrm{ext}} = -\vec{\nabla} V]. \tag{70}$$

Constructing the momentum conjugate to the particle coordinate X and applying canonical quantization, leads to

$$\Pi_X \equiv \frac{\partial L}{\partial \dot{X}} = n_{2\mathrm{d}} h\, Y \tag{71}$$

$$[\hat{X}, \hat{\Pi}_X] = i\hbar \Rightarrow [\hat{X}, \hat{Y}] = \frac{i}{2\pi n_{2\mathrm{d}}}. \tag{72}$$

The X and Y coordinates are conjugate[7], so obey the generalized uncertainty relation

$$\Delta X \Delta Y \geq \frac{1}{4\pi n_{2\mathrm{d}}}, \tag{73}$$

which implies

$$\Delta X^2 + \Delta Y^2 \geq \frac{1}{2\pi n_{2\mathrm{d}}}. \tag{74}$$

The result (74) makes physical sense: one cannot locate the vortex line to a distance less than the mean two-dimensional separation between the particles. It is interesting to note that this result has an entirely classically interpretation, but emerges from a quantum calculation owing to the cancellation of Planck's constant in the circulation with Planck's constant in the commutator. Furthermore, the result (74) is consistent with the calculation of fluctuations of the vortex (59) for the exact one-vortex wavefunction (58). Equation (59) implies $\Delta X^2 + \Delta Y^2 \sim \ell^2/N \sim 1/n_{2\mathrm{d}}$, where we take the typical particle density $n_{2\mathrm{d}} \sim N/\ell^2$ noting that the N particles are within an area of $\sim \ell^2$ in this inhomogeneous state (58).

The importance of the filling factor for the properties of a large vortex lattice becomes clear if one applies a form of Lindemann criterion and asserts that the vortex lattice will become unstable if the (rms) quantum fluctuations in vortex position are larger than some multiple α_L of the vortex spacing

$$\sqrt{\Delta X^2 + \Delta Y^2} = \frac{1}{\sqrt{2\pi n_{2\mathrm{d}}}} \geq \alpha_L \times a_{\mathrm{v}} = \alpha_L \sqrt{\frac{2}{\sqrt{3} n_{\mathrm{v}}}} \tag{75}$$

$$\nu \equiv \frac{n_{2\mathrm{d}}}{n_{\mathrm{v}}} \geq \nu_{\mathrm{c}} = \frac{\sqrt{3}}{4\pi \alpha_L^2}. \tag{76}$$

Putting in a typical value for the Lindemann parameter, $\alpha_L^2 \simeq 0.02$ (see [93]), one finds $\nu_{\mathrm{c}} \simeq 7$.

The theory described above for a single vortex neglects the kinetic energy of the vortex. It amounts to the evaluation of the quantum fluctuations of only the guiding centre coordinate. Including the inertia of the vortex leads, in addition, to a zero-point cyclotron

motion of the vortex position. Combining the quantum fluctuations of the zero-point cyclotron motion with the quantum fluctuations of the guiding centre, one finds

$$\Delta X^2 + \Delta Y^2 \geq \frac{1}{\pi n_{2d}} \tag{77}$$

that is, *twice* the value (74) from the guiding centre fluctuations alone. Using this expression (77) in the Lindemann analysis, leads to a critical filling factor that is twice as large, $\nu_c = \sqrt{3}/(2\pi\alpha_L^2)$, which eva;uates to $\nu_c \simeq 14$ using the same value for the Lindemann parameter as above is used. This is the estimate that was given in [22,93].

A more controlled calculation of the quantum fluctuations of a vortex lattice involves the consideration of the collective modes of the entire array, rather than just the motion of a single vortex. This calculation has been performed for a uniform vortex lattice array, by determining the low-frequency 'Tkachenko' modes [94–96] and evaluating their contributions to the quantum fluctuations of an individual vortex [49]. Applying the same Lindemann criterion as above, leads to a critical filling factor of $\nu_c \sim 8$. A more complete calculation that includes, in addition to the Tkachenko modes, the gapped 'inertial modes' of the vortex lattice [50] leads to a critical filling factor of $\nu_c \sim 17$. The difference between these two results, of roughly a factor of two, is again due to the neglect or inclusion of the inertial contributions to the fluctuations of the vortices [50]. That the results of calculations based on the collective modes are so close to those found from single-vortex calculations is an indication that these fluctuations are dominated by the short-wavelength modes.

2.4.2. *Numerical evidence for crystalline phases*

While instructive, considerations based on the Lindemann criterion are hardly predictive, depending very sensitively on α_L which, itself, is estimated [93] from the thermal melting of three-dimensional crystals. For this reason it is useful to have a direct determination of the transition.

The transition to the vortex lattice phase at large ν has been studied in large scale exact diagonalization studies [22,97]. The strategy is to work on a geometry with periodic boundary conditions (the torus geometry, Section B.3), which is consistent with the formation of a vortex lattice. The signal of crystallization is the collapse to very low energies (above the groundstate energy) of a set of excitations at momenta that are reciprocal lattice vectors of the vortex lattice. (This is directly analogous to the signal of rotational symmetry breaking in a trap, leading to quasi-degeneracies of energy levels at angular momenta spaced by ΔL, which was discussed in Section 2.3.2.) By looking for the emergence of broken translational symmetry, it was estimated that the transition to the triangular vortex lattice occurs at $\nu_c \simeq 6$ (see [22]). Numerical evidence for the appearance of a triangular vortex lattice is shown in Figure 9. At $\nu = 6$ the largest system that could be studied by exact diagonalization was $N = 48$, $N_v = 8$. Since the lattice contains only eight vortices, there are surely significant finite size effects in the estimate of the location of the phase transition.

More recent work [97] focusing on $\nu = 2$ has shed more light on this issue. In the regime $\nu = 2 \rightarrow 6$ the numerical results were shown to be consistent with the existence of a competing crystalline phase with 'smectic' order, that is, a stripe state with broken translational order in only one direction. This can be viewed as a phase in which the vortex

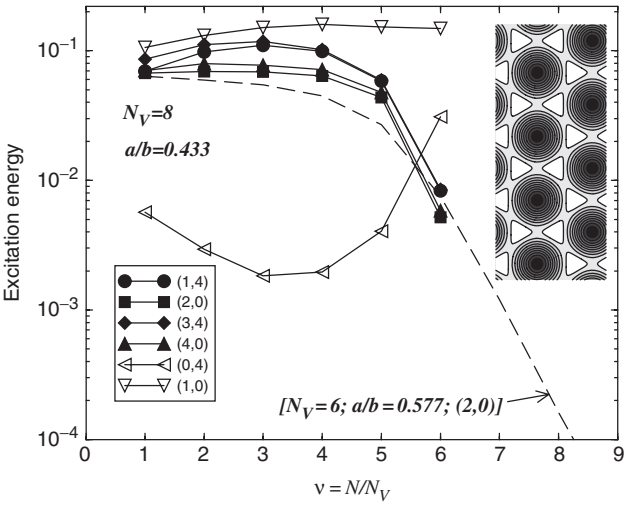

Figure 9. Numerical evidence for the development of short-range crystalline order at filling factor $\nu = N/N_\nu \gtrsim 6$ (see [22]), for bosons in the two-dimensional LLL on the torus geometry with aspect ratio chosen to be commensurate with the triangular vortex lattice. The graph shows the excitation energies at a set of different points (K_x, K_y) in the Brillouin zone as a function filling factor ν. For $\nu \gtrsim 6$ the excitations at reciprocal lattice vectors of the triangular vortex lattice (filled symbols) become very small. This is a signal, in the finite-size system, of a tendency to translational symmetry breaking. (For $\nu \lesssim 6$ there is a low-energy excitation which is located at a position in the Brillouin zone that is consistent both with the Read–Rezayi states and with the 'smectic' phase.) Reproduced with permission from [22]. Copyright © 2001 by the American Physical Society.

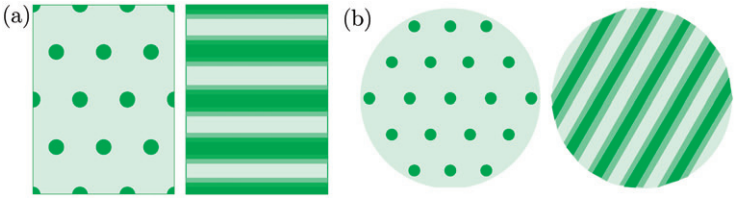

Figure 10. Schematic diagrams of the 'smectic' phase that appears in exact diagonalization studies on the torus (a), and its possible effect in disordering the vortex lattice in a trapped gas (b). The vortex lattice is quantum-disordered along lines of the vortices, giving a phase with broken translational symmetry in just one direction [97].

lattice is quantum melted owing to fluctuations of vortices along lines, leading to averaged density patterns of the form shown in Figure 10. While this state appears to describe the groundstate in the system sizes that can be studied numerically ($N_\nu \leq 12$), it is possible that finite-size effects may favour this over competing phases. Estimates suggest that the finite-size effects in experiments on cold gases will mean that the smectic phases are likely to be important in practice [97]. The first indications of quantum disordering of vortex lattices as filling factor is reduced is likely to be the appearance of (local) stripe ordering, perhaps as in Figure 10.

In the range of filling factor $2 \lesssim \nu \lesssim 6$ close to the appearance of the short-range vortex-lattice ordering at $\nu \gtrsim 6$, the usefulness of exact diagonalization studies becomes

limited with respect to determining the groundstates in the thermodynamic limit, owing to the influence of finite-size effects. This is apparent from the strong dependence of the numerical spectrum on the boundary conditions (aspect ratio of the torus), which shows there to be competition between different phases: the vortex lattice, Read–Rezayi states and the smectic state. Understanding the nature of the groundstates in this regime is a very difficult theoretical challenge, involving a strongly interacting many-body system close to a quantum phase transition. This would be a particularly interesting regime to explore experimentally.

2.4.3. *Incompressible liquid phases*

For $\nu < \nu_c$ the vortex lattice phase (a triangular vortex lattice) is unstable to quantum fluctuations, and is replaced by a series of strongly correlated phases. These phases are best understood at small filling factors, far from the transition to the vortex lattice phase. As the filling factor approaches this transition, our understanding becomes much poorer (see the discussion in Section 2.4.2).

Laughlin state. The strongly correlated phase that is best understood is the bosonic Laughlin state [81], at $\nu = 1/2$. The wavefunction describing this state is

$$\Psi_{\text{Laughlin}}(\{\zeta_i\}) \propto \prod_{i<j}^{N} (\zeta_i - \zeta_j)^2. \tag{78}$$

This is the *exact* groundstate for contact repulsion (13) at total angular momentum $L = N(N-1)$ (see [21]). This may be noted from the fact that this is the unique symmetric polynomial function of N variables that has the property that it vanishes when any two coordinates coincide: it is therefore the unique zero-energy eigenstate of the contact interaction (13) in the two-dimensional LLL.

The state has the property that its average density is uniform [81], up to a radius of around $2\sqrt{N}\ell$ beyond which the density falls to zero. Although the particle density of this state is uniform, there are still vortices in the system. However, unlike the vortex lattice phase (39), these vortices are not localized in space (translational symmetry is not broken). Rather, the vortices can be viewed as being *bound to the particles* [98,99]. This can be seen by noting that the wavefunction (78) changes phase by $2 \times 2\pi$ each time the position ζ_i of any particle i encircles the position of any other particle $\zeta_{j\neq i}$. Each particle, therefore, experiences two vortices bound to the position of every other particle, so the total number of vortices experienced by any one particle is $N_v = 2(N-1)$. Thus, (78) describes a phase that has filling factor $\nu = N/N_v = 1/2$ in the thermodynamic limit[8].

The Laughlin state for bosons shows all of the characteristics familiar from the conventional FQHE [23,24]: it is an incompressible fluid, with gapped collective excitations in the bulk, and gapless edge modes; the particle-like excitations have fractional particle number and fractional statistics (they are 'abelian anyons') [23].

Incompressibility of the bosonic Laughlin state for rotating bosons is evident from exact diagonalization studies of the collective excitation spectrum. The spectrum shows the characteristics of an incompressible liquid (see Figure 11) in which the excitations are gapped at all momenta rather than having the linear sound mode of a compressible liquid.

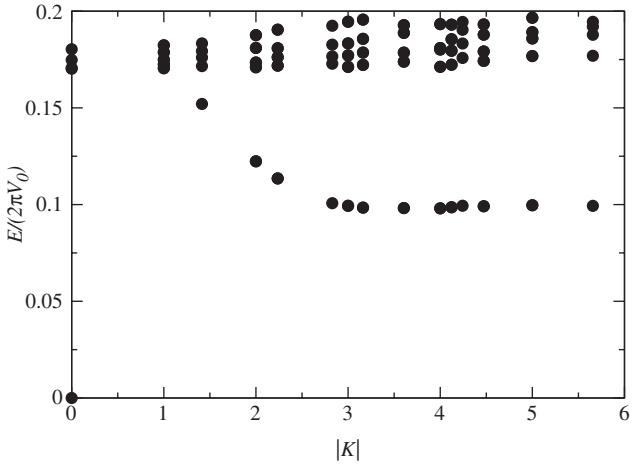

Figure 11. Excitation spectrum of the Laughlin state at $\nu = 1/2$, for bosons interacting with contact interactions, obtained by exact diagonalization studies for $N = 8$ and $N_v = 16$ on a torus with square geometry, $a/b = 1$. The states are labelled by the magnitude of the conserved wavevector in units of $2\pi/a$ (see Section B.3). The zero-energy state at $|\boldsymbol{K}| = 0$ is the Laughlin groundstate; the excitations are gapped at all wavevectors, characteristic of an incompressible liquid.

Calculations of the energy gap on finite size systems, show convergence to the thermodynamic limit, with a collective mode gap of $0.095(5) \times (2\pi V_0)$ [100,101].

Note 2.1: The numerical results in [100,101] are stated to be in units of $\sqrt{32\pi}\hbar\omega_\perp a_s/a_\parallel = 4\pi V_0$. For consistency with the numerical calculations of [22] and here, we assume that the results of [100,101] are, in fact, in units of $2\pi V_0$.

For $L > N(N-1)$, the groundstate of the contact interaction becomes degenerate, with a subspace spanned by quasi-hole excitations of (78) [102]. These states may be written

$$\Psi(\{\zeta_i\}, \{w_\alpha\}) \propto \prod_{i=1}^{N} \prod_{\alpha=1}^{N_{\rm qh}} (\zeta_i - w_\alpha) \times \Psi_{\rm Laughlin}, \tag{79}$$

where w_α are the coordinates of $N_{\rm qh}$ quasiholes[9]. From the general properties of the Laughlin states [23], these quasiholes have a fractional particle number, giving rise to a density depletion the integral of which is exactly 1/2 of an atom; they behave under adiabatic exchange as particles with fractional exchange statistics [103] ('anyons') with statistics parameter 1/2, corresponding to "semion" statistics.

Incompressibility implies that the chemical potential has a discontinuity: the chemical potential for adding particles to a bulk system, μ_+, is not the same as the chemical potential for removing particles, μ_-. Since the chemical potential for a bulk system is the derivative of the energy density with respect to the number density, this implies that the energy density has a cusp for an incompressible state. One can relate these thermodynamic quantities to the creation energies of quasiparticles, $\Delta_{\rm qp}$, and quasiholes, $\Delta_{\rm qh}$, in the incompressible state. For the $\nu = 1/2$ Laughlin state, quasiparticle and quasihole excitations have a fractional particle number of 1/2. Thus, adding a single particle to the bulk of the system involves the creation of two quasiparticles, and an energy increase

of $\mu_+ = 2\Delta_{qp}$; removing a particle involves the creation of two quasiholes, and an energy increase of $-\mu_- = 2\Delta_{qh}$. Hence, the discontinuity in chemical potential is $\mu_+ - \mu_- = 2(\Delta_{qp} + \Delta_{qh})$. For the Laughlin state with contact interactions, the energy to create a quasihole vanishes, $\Delta_{qh} = 0$. The quasiparticle creation energy is non-zero, and is available only from numerical studies [22,100,101]. The numerical results are consistent with the expectation that the quasiparticle energy is equal to the collective mode gap [100,101]. (The large wavevector collective mode can be viewed as a widely separated quasiparticle–quasihole pair, so is a measure of $(\Delta_{qp} + \Delta_{qh})$. From Figure 11, this is $\Delta_{qp} + \Delta_{qh} = \Delta_{qp} \simeq 0.1\ (2\pi V_0)$.)

Composite fermion states. At certain higher filling factors, $\nu > 1/2$, there appear strongly correlated phases that are accurately described in terms of non-interacting 'composite fermions' [83,100,101,104]. As described in Section 2.3.3, the states formed from non-interacting composite fermions provide an accurate description of the groundstates of small numbers of rotating bosons in a trap. These are the small-system signatures of bulk incompressible liquid phases (in the thermodynamic limit).

Composite fermions are formed from binding vortices to particles. Since the underlying particles are bosons, one can form a composite particle which has Fermi statistics by binding a single vortex to the location of each particle. This may be made explicit within the Jain construction [84], by writing the many-particle wavefunction for the bosons as [83]

$$\Psi(\{\boldsymbol{r}_k\}) = \hat{P}_{\mathrm{LLL}} \prod_{i<j} (\zeta_i - \zeta_j) \psi_{\mathrm{CF}}(\{\boldsymbol{r}_k\}). \tag{80}$$

The Jastrow factor $\prod_{i<j} (\zeta_i - \zeta_j)$ causes any particle i to experience a single vortex at the location of any other particle $j \neq i$. Since this factor is completely antisymmetric under particle exchange, to obtain a bosonic wavefunction the function ψ_{CF} must also be antisymmetric: this is the wavefunction of the composite fermions. In general terms, one can appreciate why this is a useful variational state: the Jastrow factor suppresses the amplitude for two particles to approach each other, as does the composite fermion wavefunction. Taken alone, these two factors would give a bosonic wavefunction that is a zero-energy eigenstate of the contact interactions. However, for $L < N(N-1)$, this construction requires ψ_{CF} to include basis states that are not in the LLL. To recover a bosonic state within the LLL, one must project the single-particle states into these states, as represented by the operator $\hat{P}_{\mathrm{LLL}}$ (see [84]). For $L < N(N-1)$ the projected wavefunction does not vanish as two particles approach each other, so it is a state with a non-zero contact interaction energy.

Since one vortex is bound to each particle, in a large (uniform) system the composite fermions experience

$$n_{\mathrm{v}}^{\mathrm{CF}} = n_{\mathrm{v}} - n_{2\mathrm{d}} \tag{81}$$

vortices per unit area, so have a filling factor (64)

$$\nu^{\mathrm{CF}} = \frac{n_{2\mathrm{d}}}{n_{\mathrm{v}}^{\mathrm{CF}}}. \tag{82}$$

Treating the composite fermions as *non-interacting* particles which completely fill p Landau levels, i.e. $\nu^{\mathrm{CF}} = \pm p$, one is led to the bosonic version of the 'Jain' sequence

$$\nu = \frac{p}{p \pm 1}. \tag{83}$$

At these filling factors, the composite fermion theory predicts the appearance of an incompressible liquid state of the bosons, and provides a trial wavefunction (80).

The states constructed in this way have been shown to successfully describe the results of exact diagonalization studies in a variety of ways.

For trapped systems (in the disc geometry) these include:

(i) the prediction of the 'magic angular momentum' for states of small numbers of rotating clusters [83];
(ii) large overlaps of the ground state wavefunctions with the composite fermion wavefunctions [83];
(iii) the form of the edge excitation spectrum for a bulk incompressible liquid of this kind is known [105,106]; the edge modes found in exact diagonalization studies are consistent with these expectations for bulk regions at $\nu = 1/2$, 2/3, 3/4 [107].

For uniform systems, the evidence for composite fermion states at $\nu = 1/2$, 2/3 and 3/4 includes the following.

(i) The existence of a sequence of states for different particle numbers N at the expected 'shift' on the sphere (see (B4)), which have a uniform groundstate charge density and an energy gap (i.e. consistent with incompressible liquids) [100,101].
(ii) The prediction of the quantum numbers of the low-lying excited states [101].
(iii) Large overlaps of the exact groundstate and of the low-lying excited states with the parameter-free wavefunctions formed from the above composite fermion wavefunctions [104].

Extrapolation of the energy gap at $\nu = 2/3$ shows a value of about $0.05 \times (2\pi V_0)$ in the thermodynamic limit [101][10]; a similar extrapolation for $\nu = 3/4$ is unreliable owing to the small number of system sizes available.

Moore–Read and Read–Rezayi states. One of the most interesting aspects of the physics of rapidly rotating Bose gases is the prediction [21,22,97,108,109] of the appearance of *non-abelian* phases: incompressible liquid phases whose quasiparticle excitations obey 'non-abelian exchange statistics'.

Non-abelian phases of matter are currently attracting intense theoretical and experimental interest in the condensed matter physics community [110]. In part, this is due to the possibility to explore experimentally this most exotic consequence of quantum many-body theory. In part, these studies are motivated by the possibility ultimately to build a 'topological quantum computer', which makes use of the properties of a non-abelian phase to form a quantum register which has topological protection against decoherence. Experimental work is largely centred on studies of the $\nu = 5/2$ fractional quantum Hall state of electrons in semiconductors. This state is thought likely to be a non-abelian phase of matter described by the Moore–Read, or Pfaffian, state [111] or a close relative thereof. Experiments are working towards the detection of the expected unconventional exchange statistics of the quasiparticle excitations of this state. Unfortunately, the creation of a universal topological quantum computer would not be possible with the Moore–Read state, as its properties do not allow arbitrary unitary transformations of the quantum register. Other non-abelian phases, known as the Read–Rezayi states [112], would allow universal topological quantum computation. There is

some theoretical evidence that these states might appear in semiconductor systems, but this is still very preliminary [113].

With this background, it is striking that theoretical studies have shown very convincing evidence for the appearance of the Moore–Read state [111] and the Read–Rezayi states [112] for rotating Bose gases with realistic two-body interactions. One of the major goals of the creation of rapidly rotating atomic gases would be to allow (possibly the first) measurements of non-abelian phases of matter.

The construction of Moore–Read and Read–Rezayi states for bosons may be viewed as a generalization of the bosonic Laughlin state. The Laughlin state for bosons is the densest exact zero-energy eigenstate of the two-body contact interaction (13) within the two-dimensional LLL. Similarly, the Moore–Read and Read–Rezayi states are the densest exact zero-energy eigenstates of a $k+1$-body contact interaction

$$\sum_{i_1<i_2<\cdots<i_{k+1}=1}^{N} \delta(\boldsymbol{r}_{i_1}-\boldsymbol{r}_{i_2})\delta(\boldsymbol{r}_{i_2}-\boldsymbol{r}_{i_3})\cdots\delta(\boldsymbol{r}_{i_k}-\boldsymbol{r}_{i_{k+1}}). \tag{84}$$

For N divisible by k, the groundstate wavefunctions of (84) may be written in a simple way

$$\Psi^{(k)}_{\mathrm{RR}}(\{\zeta_i\}) \propto \mathcal{S}\Big[\prod_{i<j\in A}^{N/k}(\zeta_i-\zeta_j)^2 \prod_{l<m\in B}^{N/k}(\zeta_l-\zeta_m)^2\cdots\Big], \tag{85}$$

where $\mathcal{S}$ symmetrizes over all possible ways of dividing the N particles into the k groups $(A, B\ldots)$ of N/k particles each [114]. It is straightforward to convince oneself that (85) vanishes when the positions of $k+1$ particles coincide, as required. By counting the degree of the polynomial $L=N(N/k-1)$, or the number of vortices $N_{\mathrm{v}}=2(N/k-1)$ experienced by each particle, one sees that these states describe bosons at filling factor

$$\nu^{(k)}=\frac{k}{2}. \tag{86}$$

Here $k=1$ is the Laughlin state; $k=2$ is the Moore–Read state; $k\geq 3$ are the Read–Rezayi states. Although these states have a similar structure, it should be remembered that the properties of these phases are very different, with quasiparticle excitations that obey abelian ($k=1$) or non-abelian ($k\geq 2$) exchange statistics.

Numerical evidence for the Moore–Read state ($k=2$) for bosons interacting with contact interactions has been reported on the disc [115], torus [22] and spherical [100,104] geometries. Large overlaps of the exact wavefunctions with the model states (85) are found. While a large wavefunction overlap is encouraging, this is not necessarily the best way to characterize a phase of matter. In the thermodynamic limit, owing to the exponential increase in the size of the Hilbert space, the wavefunction overlap with any trial state will surely vanish, even if the two wavefunctions describe the same topological phase. A robust characterization of the topological phase is provided by the groundstate degeneracy on the torus [116]; this degeneracy is expected to survive (and even improve) in the thermodynamic limit, provided the wavefunction is in the same topological phase as the trial state (85). For the Moore–Read state, this degeneracy appears clearly in the spectrum for the system sizes that can be studied numerically [22,117], see Figure 12.

Evidence for the appearance of phases of matter that are described by the Read–Rezayi states ($k\geq 3$) at $\nu=k/2$ for contact repulsion (13) has been found on the torus geometry [22].

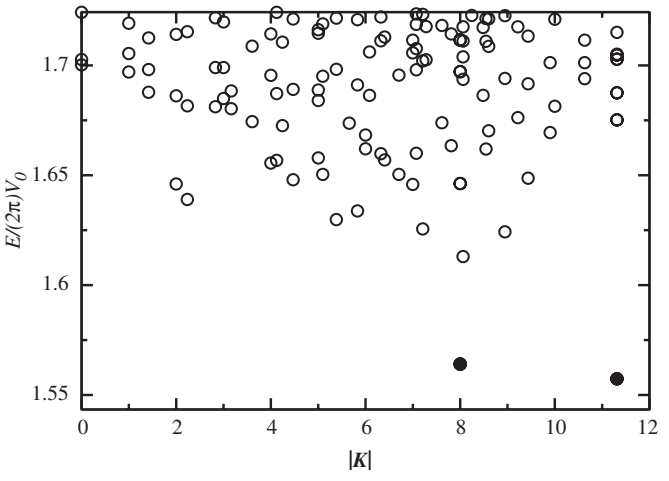

Figure 12. Low-energy spectrum for the $\nu = 1$ state with contact interactions, obtained by exact diagonalization studies on a torus with square geometry for $N = 16$ and $N_v = 16$. The states are labelled by the magnitude of the conserved wavevector on this periodic geometry. The appearance of low-energy states (shown as filled circles) at $\boldsymbol{K} = (8, 8)$, $\boldsymbol{K} = (8, 0)$ and $\boldsymbol{K} = (0, 8)$ (the last two are indistinguishable in this plot by symmetry) is consistent with the expected three-fold degeneracy of the Moore–Read state. (Here $\boldsymbol{K}$ is measured in units of $2\pi/a$ where a is the side of the (square) torus.)

While wavefunction overlaps are large, at least for k that is not too large, the expected groundstate degeneracy is less clearly resolved than for the Moore–Read state ($k = 2$) [108]. Studies of the groundstates in the spherical geometry at $\nu = 3/2, 2$, at the shifts (see (B4)) appropriate for the $k = 3$ and $k = 4$ Read–Rezayi states, were determined to be inconclusive [100,118] with no clear sign that the thermodynamic limit had been reached. It thus appears that, for contact interactions, the correlation lengths of the groundstates at $\nu = 3/2$ and $\nu = 2$ are somewhat larger than the available system sizes. (The origin of this lack of convergence is related to the competing "smectic" state at intermediate filling factors [97]; see Section 2.4.2.) However, it has been found that by changing the inter-particle interactions to introduce an additional small non-local repulsion, the spectra at $\nu = 3/2$ and 2 smoothly evolve into spectra with very clear groundstate degeneracies which show excellent evidence of being in phases described by the $k = 3$ and $k = 4$ Read–Rezayi states [97,108,109]. It appears that the small non-local interaction makes the correlation lengths smaller than the system sizes available. These results are described further in Section 2.4.5.

2.4.4. *Feshbach resonance*

For a model of rotating bosons interacting by a Feshbach resonance, it can be shown that (for certain parameters) the *exact* groundstates are the Moore–Read and Read–Rezayi states [8,119]. The hybridization of atoms into molecules leads to a suppression of the repulsive inter-atomic interactions. Tuning the resonance to the point where the net two-body repulsion vanishes leads to an effective theory for dressed atoms (which are resonating into molecules) in the two-dimensional LLL which involves effective three- and

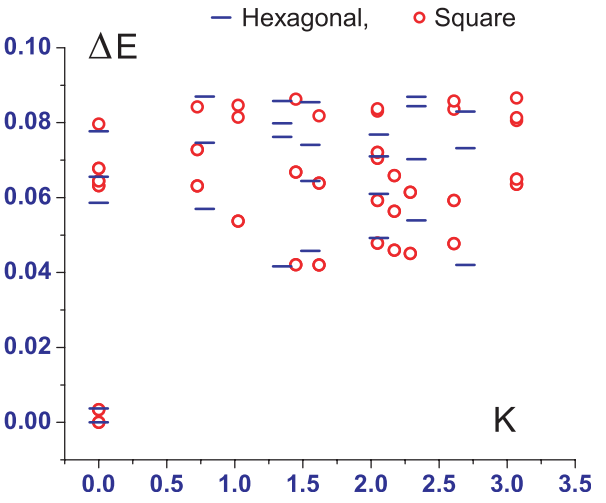

Figure 13. Numerical evidence for the appearance of the $k=3$ Read–Rezayi state for bosons at $\nu=3/2$. (Here $N=18$, $N_v=12$ on a torus with two different units cells, for contact interactions with a small amount of dipolar interaction, $\alpha=V_2/V_0=0.380$.) The spectrum depends weakly on the unit cell, so the results are representative of the thermodynamic limit. There is a very clear two-fold degeneracy of the groundstate, exactly as expected for the $k=3$ Read–Rezayi state. (The overall four-fold degeneracy is recovered by the additional two-fold centre-of-mass degeneracy owing to the half-integer filling factor.) Reproduced with permission from [108]. Copyright © 2005 by the American Physical Society.

four-body contact interactions. These arise from processes in which two atoms hybridize into a molecule which then collides with an atom, or another molecule.

2.4.5. *Dipolar interactions*

The effects of dipolar interactions on the strongly correlated phases of rotating bosons have been investigated in [62,97,108,117,120]. Qualitatively similar effects are found from studies of a model interaction in which a non-zero V_2 Haldane pseudo-potential is introduced [109,120,121] in addition to the contact V_0. In this section we focus on the case of dipolar interactions, with pseudo-potentials (45).

The strength of the dipolar interaction relative to the contact interaction is characterized by the ratio $\alpha=V_2/V_0$ (48). One expects the nature of the groundstates to vary with α.

For small positive values of α the nature of the groundstate does not change significantly. However, it has been shown that this can lead to improvements in the overlaps of the groundstates (as computed in exact diagonalization studies) with the Moore–Read state at $\nu=1$ and the Read–Rezayi states at $\nu=3/2$ and 2 (see [97,108,117,120]). It appears that the effect of a small amount of additional long-range repulsion is to reduce the correlation length of the groundstate sufficiently that it is less than the available system sizes. Numerical results then show convergence to the thermodynamic limit. Evidence for the $k=3$ Read–Rezayi state at $\nu=3/2$ is shown in Figure 13. Currently, these results provide by far the most convincing theoretical evidence for the existence of a Read–Rezayi topological phase in a system with realistic two-body interactions.

For larger values of the non-local interaction, the nature of the groundstate changes character.

The change in the nature of the groundstate at $\nu = 1/2$ was described in [62], based on the results of exact diagonalization studies on the torus. For $\alpha = 0$ the exact groundstate is the Laughlin state. For $\alpha \gtrsim 0.5$ the groundstate changes character abruptly (the overlap with the Laughlin state becomes very small). The states for $\alpha \gtrsim 0.5$ were found to be compressible crystalline phases. Numerical evidence was given for a stripe phase at $\alpha = 0.528$, and for the $q = 4$ bubble crystal phase at $\alpha = 0.758$. These results are consistent with expectations of mean-field theory, Figure 4, which indicates stripe and bubble crystal phases at these values of α. Mean-field theory is expected to be reliable only for sufficiently large ν. Why does it work so well even for $\nu = 1/2$ in this regime of $\alpha \gtrsim 0.5$? The answer can be found by noting that the mean-field phases at these values of α involve clustering of particles, so the quantum fluctuations are reduced. For example, the $q = 4$ bubble crystal phase at $\alpha = 0.758$ has $\nu q = 2$ particles per bubble, so can be viewed as a crystal of pairs of particles. A calculation of the Lindemann criterion for quantum melting of the $q = 4$ bubble crystal phase leads to a critical filling factor of $\nu_c^{q=4} \simeq 0.4$, using a Lindemann criterion that gives $\nu_c \simeq 6$ for the critical filling factor at which the triangular vortex lattice is unstable to quantum fluctuations [62]. This estimate is consistent with the observation of crystalline order even down to $\nu = 1/2$.

The collapse of the incompressible states for large values of α has been reported at filling factors $\nu = 1$ (see [117,120]), $\nu = 3/2$ (see [108]) and $\nu = 2$ (see [97]). In all cases the transition is into compressible states. At $\nu = 1$ the Moore–Read state is destroyed for $\alpha \gtrsim 0.4$, and evidence has been given for the appearance first of a stripe phase [117,120] and then of bubble crystal phases [120]. These results are consistent with the increased stability of the stripe and bubble crystal phases at $\nu = 1/2$ as the filling factor is increased. (The $q = 4$ bubble crystal phase is a crystal of clusters of $\nu q = 4$ or 6 particles for $\nu = 1$ or 3/2, respectively.)

As compared with the case of contact interactions, one qualitatively new effect of small non-zero value of α is that it allows the emergence of other strongly correlated phases for $\nu < 1/2$. At $\nu = 1/3$ numerical evidence has been given [117] for the appearance of the composite fermion liquid [120] state. One further anticipates the appearance of other incompressible states (e.g. the Laughlin states at $\nu = 1/m$ with $m \geq 4$) and the transition, at sufficiently small ν, to a Wigner crystal phase of the individual atoms, analogous to that for electrons in FQHE systems or dipolar interacting fermions [123]. The properties of rotating dipolar bosons in this regime remain to be studied in detail.

2.5. *Density distribution in a trap*

In much of the above, we have treated the rapidly rotating gas in the uniform limit. This applies when $\Omega = \omega_\perp$ and the residual transverse trapping potential in the rotating frame

$$V_\Omega^\perp(r_\perp) = \frac{1}{2} M\left(\omega_\perp^2 - \Omega^2\right) r_\perp^2 \tag{87}$$

vanishes. In this formula $r_\perp \equiv \sqrt{x^2 + y^2}$ is the radial distance from the rotation axis. Clearly $\Omega = \omega_\perp$ requires the numbers of vortices N_v and of particles N to be infinite.

In any finite system one has $\Omega < \omega_\perp$ so there will remain a weak harmonic trapping potential. This trapping leads to inhomogeneity of the density, which we now discuss.

The first corrections to the particle density at large but finite N_v can be found by using the local density approximation (LDA). This amounts to the assumption that at each point in space there is a locally defined chemical potential

$$\mu(r_\perp) = \mu - V_\Omega^\perp(r_\perp). \tag{88}$$

Then, the two-dimensional particle density is found from the local chemical potential, as

$$n_{2d}(r_\perp) = n_{2d}[\mu(r_\perp)], \tag{89}$$

where $n_{2d}[\mu]$ is the two-dimensional density of a *uniform system* at chemical potential μ. Within a reasonable assumption of locality in the physics determining the equation of state, one expects the LDA to be accurate provided the particle density varies slowly on a lengthscale of the correlation length of the relevant phases; for the situations we have been discussing this correlation length is of the order of the mean vortex spacing $a_v \simeq a_\perp$.

Through (89), the spatial density profile $n_{2d}(r_\perp)$ depends on the equation of state, $n_{2d}[\mu]$. The profile therefore takes different forms in the vortex-lattice ($\nu > \nu_c$) and strongly correlated ($\nu < \nu_c$) regimes.

A useful general result exists. For a Bose gas with repulsive interactions, the density falls to zero for $\mu < 0$. Therefore, the edge of the cloud is at a radius

$$R_\perp = \sqrt{\frac{2\mu(0)}{M(\omega_\perp^2 - \Omega^2)}} \tag{90}$$

where $\mu(0)$ is the chemical potential at the centre of the cloud. Since the average vortex density is $n_v = 2M\Omega/h$, the total number of vortices within the Thomas–Fermi radius $R_\perp$ is

$$N_v = \pi R_\perp^2 n_v = \frac{2\pi M\Omega}{h}\frac{2\mu(0)}{M(\omega_\perp^2 - \Omega^2)}. \tag{91}$$

Inverting this relation, and taking the limit $N_v \gg 1$ in which the LDA is valid, shows that the rotation frequency is

$$\frac{\Omega}{\omega_\perp} \simeq 1 - \frac{\mu(0)}{\hbar\omega_\perp}\frac{1}{N_v} + \mathcal{O}(1/N_v^2). \tag{92}$$

Thus, for N_v sufficiently large (larger than $\hbar\omega_\perp/\mu(0)$), the rotation frequency is close to the trap frequency $\omega_\perp$.

Deep in the vortex lattice phase $\nu \gg 1$, the equation of state can be found from mean-field theory, (44), giving $\mu = 2\beta_A \nu V_0$ where ν is the local filling factor (65). The LDA therefore predicts a density distribution of the form [43]

$$n_{2d}(r_\perp) = \nu(r_\perp) n_v = \frac{\mu(0)}{2\beta_A V_0} n_v \left(1 - \frac{r_\perp^2}{R_\perp^2}\right). \tag{93}$$

This is the inverted parabola familiar from the Thomas–Fermi approximation for a trapped BEC. This been shown to provide an excellent description of the vortex lattice phase ($\nu \gg 1$) within the two-dimensional LLL [41,43], showing that the LDA is accurate

in this regime. Further applications of the LDA allow one to relate $\mu(0)$ to the total number of particles N, and Ω to the angular momentum L (see [41,43]). This leads to the result that the number of vortices inside the Thomas–Fermi radius scales as

$$N_{\rm v} \simeq 3\frac{L}{N} \tag{94}$$

for large $N_{\rm v}$. Detailed theoretical studies of the particle density and vortex distributions of finite vortex lattices in the mean-field LLL regime have been reported in [41–43,124]. Among the motivations for these considerations was the observation that if the vortices adopt a uniform triangular array the mean particle density follows a Gaussian profile on average [38], rather than the more conventional Thomas–Fermi profile. The reconciliation of these views led to the conclusion that the vortex lattice distorts slightly towards the edge of the trap [41–43], in such a way that the above Thomas–Fermi profile is achieved. The arrangement of vortices outside the Thomas–Fermi radius has been discussed in [124].

In the strongly correlated regime, the equation of state has a jump in the chemical potential at the density of each incompressible phase. As a consequence, within the LDA the filling factor does not fall smoothly with radius. The density distribution shows a 'wedding cake' structure [125] characteristic of incompressible phases, with regions in which the two-dimensional particle density is pinned to values $\nu^* n_{\rm v}$ where ν^* are filling factors at which the groundstate is incompressible. This is expected to give clear experimental evidence for the appearance of incompressible phases in images of the density distribution following expansion [125].

2.6. *Quantum melting in the three-dimensional LLL regime*

The three-dimensional LLL regime (34) can be relevant for a rapidly rotating Bose gas in an anisotropic trap $\omega_\parallel \ll \omega_\perp$ (see [38]). The regime is also of importance for the situation in which the rotating gas is sliced into many parallel layers by a one-dimensional optical lattice with wavevector parallel to the rotation axis[11] (see Figure 14). The optical lattice leads to an increased effective mass $M_\parallel$ for motion along the rotation axis, $M_\parallel > M$. For a deep lattice in the tight binding limit, with lattice period $d_\parallel$ and single-particle tunnelling amplitude J, the effective mass for motion along the rotation axis is

$$M_\parallel = \frac{\hbar^2}{2Jd_\parallel^2}, \tag{95}$$

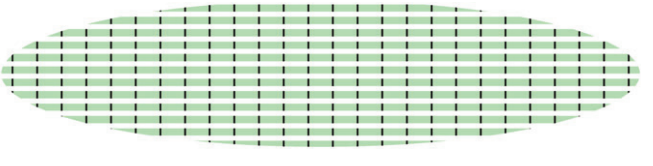

Figure 14. Schematic diagram illustrating the use of an optical lattice, directed along the rotation axis, to slice the rotating condensate into many parallel layers. Each layer has a reduced filling factor, $\nu_{\rm layer} = \nu/N_{\rm L}$, where $N_{\rm L}$ is the number of layers. In addition, the tight axial confinement of each layer ($a_\parallel^{\rm layer} \lesssim d_\parallel$) leads to an increased energy scale for interactions (30).

which diverges as $J \to 0$. Hence, the oscillator energy $\omega_\parallel \propto 1/M_\parallel$ is reduced, leading to an anisotropic confinement $\omega_\parallel \ll \omega_\perp$.

The use of a one-dimensional optical lattice has been suggested as a means of increasing the quantum fluctuations of the vortices and allowing entry into the strongly correlated regime [125–127]. This also has the advantage of increasing the interaction energy scale of the strongly correlated phases (see Section 6.2).

The origin of the enhanced quantum fluctuations of the vortices is simple to understand in the limit of a very deep lattice in which the layers become decoupled. Then, the relevant quantity controlling the quantum fluctuations is the filling factor *per layer*

$$\nu_{\text{layer}} \simeq \frac{N}{N_{\text{v}} N_{\text{L}}} = \frac{\nu}{N_{\text{L}}} \tag{96}$$

where $N_L \simeq a_\parallel / d_\parallel$ is the number of layers that the optical lattice forms, which could be of the order of $N_{\text{layer}} \sim 50$–100. The vortex lattice in each layer will disorder owing to quantum fluctuations for $\nu_{\text{layer}} < \nu_{\text{c}}$ (where $\nu_{\text{c}} \sim 6$ is the two-dimensional result [22,49,50]), leading to quantum melting at a very high *total* filling factor $\nu < \nu_{\text{c}} N_{\text{L}}$.

The quantum fluctuations of a uniform vortex lattice (N_{v} large) in the three-dimensional LLL regime of a layered geometry have been investigated theoretically in [125]. The critical filling factor for a uniform system was estimated as a function of the coupling between the layers both by applying the Lindemann criterion based on the quantum fluctuations of the vortices, and by evaluating the condensate depletion. The degree of interlayer coupling is controlled by the dimensionless ratio of the interlayer tunnelling energy J and the mean interaction energy in a single layer, $V_0 \nu_{\text{layer}}$ with V_0 (30) evaluated for the subband thickness $a_\parallel^{\text{layer}} < d_\parallel$ of each individual layer. The results show the crossover from the regime of strongly coupled layers $J \gg V_0 \nu_{\text{layer}}$ where the two-dimensional LLL regime is valid and quantum melting occurs for $\nu \lesssim \nu_{\text{c}}$, to the regime of decoupled layers for $J \ll V_0 \nu_{\text{layer}}$ and quantum melting requires only $\nu \lesssim \nu_{\text{c}} N_{\text{L}}$.

The criterion for quantum melting in the intermediate three-dimensional regime can be understood in simple geometric terms. In this three-dimensional geometry, the vortices do not simply fluctuate as straight lines. Quantum fluctuations involve also bending of the vortex lines: the Kelvin modes of the vortices [128]. The relevant Kelvin modes are those with wavelengths longer than a certain minimum wavelength, which one can think of as the lengthscale over which the vortices remain straight. This minimum wavelength is set by the healing length (9) along the rotation axis [125]

$$\xi_\parallel \simeq \sqrt{\frac{\hbar^2}{2 M_\parallel \mu}}, \tag{97}$$

or, if the healing length becomes less than the lattice period $\xi_\parallel < d_\parallel$, then one should use $d_\parallel$ as the minimum wavelength. Note that, for a system in the three-dimensional LLL (34), the healing length satisfies $\xi_\parallel \ll a_\parallel$, so the vortex fluctuations do involve flexural motion.

Applying a Lindemann criterion [125] to these fluctuations of the vortex lines leads to the conclusion that quantum melting of the three-dimensional vortex lattice occurs when the filling factor in a slab of thickness $\xi_\parallel$ is less than a critical value of the order of one. We take this critical value to be $\nu_{\text{c}} \sim 6$ for consistency with the two-dimensional

studies [22,49,50]. Then the condition for quantum melting of the three-dimensional vortex lattice is

$$\frac{\bar{n}\xi_{\parallel}}{n_{\rm v}} < \nu_{\rm c}, \tag{98}$$

where $\bar{n}$ is the three-dimensional particle density. With this criterion in mind, and using (97), the condition for validity of mean-field theory in the three-dimensional LLL regime (34) is

$$\bar{n} \gg a_{\rm s} n_{\rm v}^4 \sim \frac{a_{\rm s}}{a_{\perp}^4}. \tag{99}$$

It is only in this limit (99) that one can model the three-dimensional LLL regime by a Thomas–Fermi profile for the particle density (A4) along the rotation axis.

The quantum fluctuations of a confined vortex lattice ($N_{\rm v}$ finite) in a layered geometry have been studied in [126,127]. These works provide a detailed study of the Tkachenko modes for the finite-size vortex lattice. The quantum melting of clusters of vortices is found to be inhomogeneous, owing to the inhomogeneous particle density. Melting can lead to a fluid of vortices, or to a shell structure in which shells of vortices can decouple from their neighbours but maintain inter-vortex correlations within a shell. A critical comparison is made with the expected location of the vortex lattice/vortex liquid boundary in the inhomogeneous system as predicted by the local density approximation. For small vortex arrays ($N_{\rm v}$ small) in the limit of weak interlayer coupling, one expects a transition to quantum Hall 'Mott' phases in which number fluctuations between layers are suppressed [128].

3. Atomic Bose gases in rotating optical lattices

The effects of a periodic pinning array on vortices in superconducting materials is a matter of significant experimental and theoretical interest [129–132]. At low temperatures, the vortex lattice can undergo a transition from the triangular Abrikosov lattice (in the absence of pinning) into phases that are pinned to the lattice, with a series of different ordered structures. The nature of the groundstate involves the interplay between the vortex density $n_{\rm v}$ and the density of periodic pinning sites $n_{\rm site}$, and can involve rich and interesting commensurability effects [130] as a function of the ratio

$$f \equiv \frac{n_{\rm v}}{n_{\rm site}}, \tag{100}$$

the mean number of vortices per pinning site.

The interplay between vortex–vortex interactions and a vortex pinning potential can be conveniently studied in rotating atomic BECs. Regular arrays of pinning sites can be imposed by a rotating optical lattice potential [130], and allow detailed investigations of the vortex lattice structure and the dynamics. Furthermore, the extension of experimental studies into the strongly interacting regime, where the optical lattice is strong and the (non-rotating) Bose gas is close to the Mott insulating regime, will allow the study of vortex-commensurability effects in a regime of strong correlations.

3.1. *Rotating optical lattices*

Conceptually, the simplest way to investigate the physics of vortices in a static periodic potential is to impose a rotating optical lattice on a trapped BEC in an otherwise cylindrically symmetric potential well. The optical lattice is at rest in the rotating frame. In the steady state, the gas will come to equilibrium in this frame of reference.

The coupling of a BEC to rotating lattices has been explored in experiments in which a rotating mask imposes a rotating optical lattice of square or triangular symmetry [133]. Owing to the small angle of the light passing through the mask relative to the rotation axis, the periods of these lattices (about 8 μm) are large compared with the optical wavelength. An alternative geometry has been proposed that could allow rotating optical lattices with smaller lattice constants, of the order of half the optical wavelength [26].

For a strong optical lattice, in which atoms are restricted to a single Wannier orbital at each site [134,135], schemes have been proposed by which to imprint the required Peierls phases to simulate the motion of a charged particle in a uniform magnetic field. The uniform magnetic field has the same effect as the Coriolis forces of uniform rotation; we therefore use 'rotation' and 'magnetic field' interchangeably, assuming that a harmonic confinement potential is applied to cancel the centrifugal effects of rotation. One class of method makes use of optically induced transitions to other hyperfine levels of the atom to imprint geometric potentials on the tunnelling matrix elements [28,136]. In another proposal, time-dependent potentials are imposed to modulate the lattice potentials and tunnelling amplitudes in register. Provided that this modulation is sufficiently fast compared with the timescales relevant for the physics of the cold atomic gas, these have the effect of imprinting the necessary phase modulations to simulate a uniform magnetic field [29].

The results of these studies [28,29,136] are proposals for generating systems that are well described by the Bose–Hubbard model in a uniform magnetic field

$$\hat{H} = -J \sum_{\langle i,j \rangle} \left[\hat{a}_i^\dagger \hat{a}_j e^{iA_{ij}} + \hat{a}_j^\dagger \hat{a}_i e^{iA_{ji}} \right] + \frac{1}{2} U \sum_i \hat{n}_i (\hat{n}_i - 1) - \mu \sum_i \hat{n}_i, \tag{101}$$

where $\hat{a}_i^{(\dagger)}$ are the field operators for boson creation/destruction at the lattice site i, and $\hat{n}_i = \hat{a}_i^\dagger \hat{a}_i$ is the number operator. Here J is the tunnelling energy and U is the on-site boson interaction. The ratio size of J/U can be varied by changing the strength of the optical lattice [134,135]. The sites i are defined on a two-dimensional lattice, which, for convenience, we consider to be a Bravais lattice (all sites are equivalent, with one site per unit cell). To simulate a uniform magnetic field (or uniform rotation), the link phases $A_{ij} = -A_{ji}$ must have the gauge-independent property that their sum around any unit cell of the lattice (the discrete version of the line integral $\oint \boldsymbol{A} \cdot \mathrm{d}\boldsymbol{r}$) is a constant

$$\sum_{\text{unit-cell}} A_{ij} = 2\pi f, \tag{102}$$

where $0 \leq f < 1$ is the mean number of vortices (flux quanta) per unit cell of the lattice.

A related scheme has been proposed in which 'non-abelian' gauge fields can be generated in optical lattice systems [137]. We restrict attention to the physics of the above model with an abelian gauge field (101).

3.2. *Weakly interacting regime: vortex pinning*

For a weakly interacting Bose gas, and in the regime where the two-dimensional density of particles is sufficiently large, $n_{2d} \gg n_v$, n_{site}, it is appropriate to treat the system within mean-field theory.

This was first discussed for a uniform system, within an effective model for the vortex interactions in the presence of a square lattice pinning potential [138]. The maxima of the potential act as pinning centres for the vortices, owing to the particle depletion at the vortex cores. At a vortex density of $f = 1$ it was found that there exist three phases: the unpinned triangular Abrikosov lattice; the strongly pinned square lattice with one vortex per lattice site; and an intermediate phase in which half of the vortices are pinned. The phase diagram is a function of the strength and period of the pinning potential relative to, respectively, the chemical potential and the healing length of the BEC. Extensions to other vortex densities $f < 1$ and calculations of the collective mode dynamics are reported in [139].

A study of a rotating square lattice over a wide range of vortex fillings in a harmonically trapped atomic BEC is reported in [140]. A direct numerical solution of the Gross–Pitaevskii equation in a trap containing around 100 lattice sites was performed. A very rich range of configurations was found, including states with doubly quantized vortices pinned to certain lattice sites, and the appearance of domain walls between regions of (locally) different order. Owing to the many competing phases, the inhomogeneity of a trapped gas leads to a very much more complex situation than the uniform case.

The experiments reported in [133] studied the effects of rotating triangular [141] and square lattices. The locking of a BEC (initially rotating at a different rate to the optical lattice) to a rotating triangular lattice was investigated. No clear enhancement in the locking was found at the commensurability point $f = 1$. For a rotating square lattice, the structural phase transition was observed from the triangular vortex lattice (at weak pinning) to a square lattice (strong pinning), at a pinning strength in rough agreement with the predictions of [138,140]. Incommensuration effects were found to be difficult to observe in experiment [133], as the finite number of vortices can compress or expand to stay close to commensurate conditions.

Another approach to the physics of this mean-field regime is applicable in the case of a very strong optical lattice, for which the Bose–Hubbard model (101) can be used. Under conditions of weak interactions $U \ll J$ and when the mean number of particles per lattice site is large [142,143], one can replace the Hamiltonian (101) by the phase representation

$$\hat{H} = -\sum_{\langle i,j \rangle} \tilde{J}_{ij} \cos\left(\theta_i - \theta_j + A_{ij}\right) - \frac{U}{2} \sum_j \frac{\partial^2}{\partial \theta_j^2}, \tag{103}$$

where $\tilde{J}_{i,j} = 2\sqrt{n_i n_j} J$ with n_i the mean particle number per site. This model is familiar from studies of 'frustrated Josephson junction arrays'. In the limit $U \ll \tilde{J}$ it reduces to the classical uniformly frustrated XY model, the groundstates of which have been found for infinite uniform lattices at certain rational values of the vortex density f (see [144–146]). The groundstate at $f = 1/2$ is two-fold degenerate. A Gutzwiller mean-field study [31] of the Bose–Hubbard model in this regime $J \ll U \ll \tilde{J}$ for f close to $1/2$ shows the appearance of two competing groundstates. In [143] the influence on the classical groundstates of the inhomogeneity in $\tilde{J}$ owing to the harmonic trap has been studied.

3.3. *Strongly interacting regime*

Understanding the nature of the groundstate of the Bose–Hubbard model in a magnetic field (101) poses a very difficult theoretical problem. It involves the interplay of several very interesting and complex aspects of physics.

- As discussed above for weak interactions, there is the interplay of commensurability of the vortex density n_v with the lattice site density n_{site}, controlled by $f = n_v/n_{site}$. This same commensurability is responsible for a complex form of the energy spectrum of a single particle [147], which has a fractal structure referred to as the 'Hofstadter butterfly' [148].
- In the continuum limit (in the absence of any pinning potential), there can appear strongly correlated phases related to FQH states when the two-dimensional particle density n_{2d} is comparable to the vortex density n_v, controlled by the filling factor $\nu = n_{2d}/n_v$. (See Section 2.4.3.)
- In the absence of rotation, $f = 0$, the interplay between interactions U and kinetic energy J leads to the physics of the Mott–Hubbard transition for bosons [134,135].

The relevant dimensionless parameters controlling the properties of the system are the vortex filling factor f, the particle filling factor n, and the ratio U/J of particle interactions to the bandwidth. In addition, the properties can depend on the geometry of the lattice on which the system is defined. (Unless stated otherwise, it is assumed that the lattice is square.)

3.3.1. *Mean-field theory*

The groundstates of the Hamiltonian (101) have been studied within mean-field theory by several authors, focusing on different aspects of the very rich physics that can arise.

The nature of the vortices and vortex lattices close to the Mott-insulating states (n is integer) were studied in [149]. It was found that the vortex cores tend to have a local particle density that is equal to that of the nearest Mott state, which can be larger or smaller than the average background density.

In [142] a mean-field treatment of the quantum phase model (103) has been used to study the transition at $f = 1/2$ into the Mott insulating phase. The boundary of the Mott phase has been studied in detail in [150] as a function of the vortex filling f. It was shown to follow a dependence that is set by the extremal energy of the corresponding one-particle state in the Hofstadter spectrum. That the phase boundary of a strongly interacting phase (the Mott insulator) can be described in terms of a single-particle property is a surprise; the connection arises from the fact that the boundary is determined by the appearance of dilute particles, the properties of which are governed by the single-particle spectrum [151].

Goldbaum and Mueller [151] have studied the vortex lattice structures close to the Mott-insulating state in detail. They have shown that, in contrast to the case of *weakly* interacting Bose gases [138,140], the vortex cores do not necessarily get pinned to the maxima of the potential (i.e. the plaquettes of the lattice); vortex lattices are found in which the vortices are pinned to the minima of the potential (the sites of the lattice). This is related to the presence of Mott phases at vortex cores [149], which can act to increase the particle density at the vortex core as compared with the average particle density, making it energetically favourable to locate the core in the potential minima.

3.3.2. *Strongly correlated phases*

Going beyond mean-field theory involves considerations of the effects of quantum fluctuations of the vortices.

The quantum fluctuations of a single vortex have been described in [152], for $\tilde{J} \gg U$, when the interaction term in (103) is small. Fluctuations lead to a finite vortex mass, which is predicted to have experimental consequences in Bragg spectroscopy measurements.

For a dense array of vortices forming a vortex lattice, one can expect that, if sufficiently strong, quantum fluctuations will disorder the vortex lattice. A novel form of disordered vortex phase was proposed for the 'dice' lattice, at vortex density $f = 1/3$ (see [153]). It is argued that in this situation, the first effect of quantum fluctuations of the vortices is to lead to a so-called 'vortex Peierls' phase: in this phase the vortices are partially delocalized, tunnelling between pairs of nearest-neighbour sites, while retaining the broken translational symmetry expected for a conventional vortex lattice.

For very strong quantum fluctuations, one expects the vortex lattice states to disorder completely and form strongly correlated liquid states, analogous to the incompressible liquid states discussed for rotating Bose gas in the continuum, see Section 2.4.3. Indeed, the Bose–Hubbard model in a magnetic field (101) contains all of the physics of the continuum (as discussed in Section 2) in the corner of parameter space where both vortex filling and particle filling are small $n, f \ll 1$: in this continuum limit, the groundstate depends only on the filling factor $\nu \equiv n/f$ and includes the correlated phases described in Section 2.4.3.

The influence of a lattice potential on the bosonic Laughlin state (78) has been studied in large-scale exact diagonalization studies on periodic lattice geometries [26,29], intended to represent the bulk region of a system with a large number of lattice sites. Fixing the filling factor (64) to $\nu \equiv n/f = 1/2$, the influence of the lattice was varied by increasing the vortex density f from small values (when a continuum approximation is valid), to large values (when the lattice structure is important). It is found that the groundstate is well described by the Laughlin state for sufficiently small f. Calculations of the wavefunction overlap indicate that the (continuum) Laughlin wavefunction accurately describes the exact groundstate for $f \lesssim 0.25$ (see [29,154]); a computation of the Chern number associated with the topological order show that this takes the value expected for the $\nu = 1/2$ Laughlin phase for $f \lesssim 0.4$ (see [26,154]). The excitation gap of the Laughlin state is estimated from the numerics as a function of f and U/J. In the hard-core limit $U \gg J$, the gap above the $\nu = 1/2$ Laughlin state is found to be as large as $\simeq 0.25J$ at $f \simeq 0.11$ (see [26]).

Exact diagonalization studies have been performed to investigate the properties of small clusters of sites with open boundaries, corresponding to rotating lattices in a bounded trap geometry [155–157]. As a function of the rotation rate, the groundstate shows transitions between states of differing 'quasi-angular momentum': the conserved quantum number associated with the point-group symmetry of the lattice in the rotating frame. These transitions represent the entry of vortices into the system [156].

Numerical constraints for the Bose–Hubbard model limit exact diagonalization studies to very small system sizes (typically the number of particles is $N \leq 5$ in [26,29,155–157]). This makes the investigation of possible strongly correlated phases of bosons on rotating lattices very challenging. An analytic proposal for strongly correlated quantum Hall states

of bosons has been given in [30,31]. The construction is based on the observation that the single-particle energy spectrum close to rational fractions $f = l/q + \delta$ (l, q integer, $\delta \ll 1$) appears to form a set of q states (which differ strongly on the scale of the lattice constant a), but each of which is modulated by the same Landau level wavefunctions over a large lengthscale of order $\sqrt{1/\delta}$ times the lattice constant. For δ sufficiently small, one can treat the system within a continuum theory, but now for q species of bosons. The interspecies interactions are determined by the microscopic wavefunctions. At $f = 1/2 + \delta$ it is argued that in the continuum limit ($n, \delta \ll 1$) one can construct exact groundstates of the model with on-site interaction (101); these are formed from the '(221)' quantum Hall state [158] (see (109)) at the effective filling factor $\nu' \equiv n/\delta = 2/3$.

The physics of strongly interacting bosons in rotating lattices is a very rich and interesting topic, with the potential for exotic strongly correlated phases. Much of the phase diagram remains to be explored. It is an area where experiment is likely to raise surprises.

4. Rotating multi-component Bose gases

The physics of ultra-cold atomic gases is very much enriched by the possibility to trap and cool more than one atomic species. Mixtures of degenerate atomic gases offer a vast array of different situations and parameter regimes in which new and interesting phenomena can emerge.

Consistent with this wide range of parameters, there have been many theoretical studies of vortices and vortex lattices in multi-component Bose gases. Here, we describe only those studies that are most closely related to the topics discussed in Section 2 for the one-component Bose gas. Specifically, we focus on results in the two-dimensional LLL regime (20) appropriate for conditions of rapid rotation, and limit attention to the two-component Bose gas and the spin-one Bose gas.

4.1. *Two-component Bose gases*

The bulk properties of an ultra-cold two-component Bose gas, with the components labelled by $i = 1, 2$, are characterized by the two masses M_i and the set of all mutual two-body s-wave scattering lengths, a_{ij} (see [159]). A two-component BEC is described by the condensate wavefunction

$$\begin{pmatrix} \psi_1(\boldsymbol{r}) \\ \psi_2(\boldsymbol{r}) \end{pmatrix}, \tag{104}$$

and the mean-field interaction energy is

$$E_I^{\mathrm{GP}} = \frac{1}{2} \int \sum_{i,j=1}^{2} g_{ij} |\psi_i|^2 |\psi_j|^2 \, d^3\boldsymbol{r}, \tag{105}$$

where $g_{ij} \equiv 2\pi\hbar^2 a_{ij}/\mu_{ij}$ with $\mu_{ij} \equiv M_i M_j/(M_i + M_j)$ the reduced mass [160].

For the case of equal interactions $g_{ij} = g$ there is an exact symmetry of the interaction energy under SU(2) rotations of the condensate wavefunction (104). It is then convenient

to parameterize the condensate wavefunction in a manner that makes this invariance manifest, writing

$$\begin{pmatrix} \psi_1(\boldsymbol{r}) \\ \psi_2(\boldsymbol{r}) \end{pmatrix} = \sqrt{n} e^{i\chi} \begin{pmatrix} \sin(\theta/2)\, e^{i\phi/2} \\ \cos(\theta/2)\, e^{-i\phi/2} \end{pmatrix}, \tag{106}$$

where n is the particle density, χ a global phase, and θ and ϕ parameterize the spinor coordinates by the polar and azimuthal angles on the surface of the sphere. For SU(2) invariant interactions, $g_{ij} = g$, the interaction energy is invariant under rotations of θ, ϕ, as well as of the global phase χ. For experimentally relevant situations, the interaction parameters can be close to the SU(2) invariant condition (see Note 4.1 below). Departures from the SU(2) lead to weak anisotropies in the energy as a function of θ and ϕ (see [161]).

Note 4.1: For the $|F=1, m_F=-1\rangle$ and $|F=2, m_F=1\rangle$ states of ^{87}Rb, the ratios are $g_{11} : g_{22} : g_{12} = 1.024 : 0.973 : 1.0$ (see [162,163]). For the $|F=1, m_F=0\rangle$ and $|F=1, m_F=1\rangle$ states of ^{23}Na these are $g_{11} : g_{22} : g_{12} = 1 : 1.035 : 1.035$ [see 189].

For a uniform three-dimensional system, stability of the individual condensates requires $g_{11}, g_{22} \geq 0$. Within this stable regime, depending on the interactions the two components can be miscible or immiscible. The condition for immiscibility, in which case the BEC phase separates into spatially-separated regions of component-one and component-two, is [159,164]

$$g_{11} g_{22} < g_{12}^2. \tag{107}$$

Two-component BECs have been formed from the trapping of two hyperfine states of the same atomic species (for ^{87}Rb [165] and for ^{23}Na [166]), and from the trapping of mixtures of two different atomic species (for ^{41}K$-^{87}$Rb [167,168] and ^{85}Rb$-^{87}$Rb [169]). Experiments on these two-component condensates show evidence for both miscible and immiscible regimes compatible with (107), and have investigated the transition between these regimes as the scattering lengths are varied [168,169].

When the two components are two hyperfine states of a single atomic species, the masses are identical $M_1 = M_2 \equiv M$; when they correspond to two different atomic species, then $M_1 \neq M_2$. The rotational properties of the two-component gas are very different in these two cases, which we therefore discuss in turn.

4.1.1. *Rotating two-component BEC: equal masses*

Single vortex states. Experimental studies of quantized vortices in atomic BECs were initiated by experiments on a two-component BEC [170]. Coherent excitation of a ^{87}Rb BEC in a single hyperfine state (which could be either one of the two trapped states) was performed in such a way as to convert atoms into the other trapped hyperfine level with one unit of circulation. The imprinted configuration therefore had a single quantized vortex for the particles in the excited component. The phase of the rotating component was directly imaged in an interference technique, to confirm the quantized circulation. The subsequent evolution of the two-component system was studied, showing evidence for differences in the dynamics and stability depending on which of the two hyperfine levels was excited into a circulating state.

The structure of the axisymmetric vortex state created in these experiments is easily written in the two-dimensional LLL regime, for which the condensate wavefunction takes the form [171]

$$\begin{pmatrix} \psi_1 \\ \psi_2 \end{pmatrix} = \begin{pmatrix} a \\ b\zeta \end{pmatrix} \times e^{-|\zeta|^2/4} e^{-z^2/2a_\parallel^2}, \tag{108}$$

where a and b are amplitudes whose ratio determines the relative populations of the two components N_1/N_2. This wavefunction describes a state in which component-two has one unit of angular momentum while component-one is at rest. Note that, despite the density suppression in the core of the vortex of component-two, there remains non-zero particle density for component-one in the core region. This is a general feature of the vortices in two-component BECs with repulsive interspecies interactions $g_{12} > 0$ (see [159,161,171–174]). Since the density does not vanish, one can use the representation (106) to describe this vortex as spin-texture in the variables (θ, ϕ, χ). In terms of this description, the vortex configuration (108) has a non-trivial topological classification. It is referred to as a 'half quantum vortex' [174] or (two-dimensional) 'Skyrmion' [171]. The properties of these spin textures have been investigated in detail for interactions that (weakly) break the SU(2) symmetry [161]. The results show the appearance also of vortex states which break the axial symmetry of the trap.

Beyond mean-field theory, there exist exact results for the case of SU(2) invariant interactions, $g_{ij} = g$, in the two-dimensional LLL limit. For small values of angular momentum, $L \leq \min(N_1, N_2)$, the results of exact diagonalization studies on $N = N_1 + N_2 \leq 8$ particles have been used to motivate a conjecture for the exact (analytic) groundstates [175]. The numerical studies show that the groundstate contains only single-particle states with angular momenta $m \leq 1$; such states can be shown to be exact eigenstates of the SU(2) interactions. Similar conclusions hold also for the rotating spin-one Bose gas with SU(3) invariant interactions [176], discussed in Section 4.2.

Many vortex states. Theoretical studies of lattices of many vortices were performed by Mueller and Ho [177] within the mean-field LLL regime[12]. As for the case of the one-component BEC, in the LLL limit the condensate wavefunction may be expressed in terms of the positions of the vortices. However, for the two-component condensate wavefunction there is a set of vortex locations for each of the two components. For the case $g_{11} = g_{22} \equiv g \neq g_{12}$ studied in [177] the two components are identical, so one expects each to have the same vortex structure up to a relative translation. The groundstates were determined as a function of g_{12}/g for an infinite lattice. A series of vortex lattice phases was found, with structures depicted in Figure 15. These results illustrate the very rich physics that is possible in a rotating two-component BEC. For $g_{12}/g > 1$, corresponding to the regime of phase separation (107) for the non-rotating gas, the groundstate consists of interlaced rectangular arrays of vortices. For large g_{12}/g the vortices become closely spaced along one direction, leading to vortex sheets; the particle density then tends towards an array of parallel stripes in which one component has low density and the other a high density.

The vortex lattice states have been studied beyond the LLL and including the effects of the trap [178,179]. The results show qualitatively similar phases to those described above. Stripe-like states (vortex sheets) appear in the regime of phase separation.

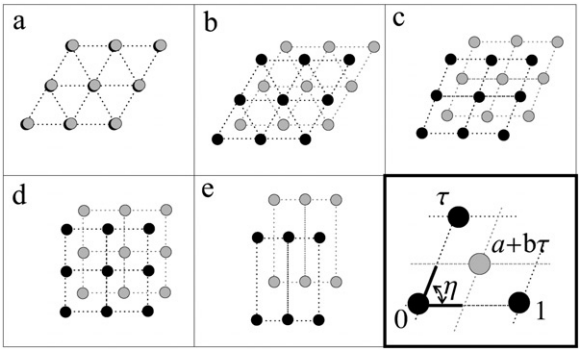

Figure 15. Vortex lattices in the mean-field LLL regime of a two-component BEC for $g_{11} = g_{22} \equiv g$, and at different values of g_{12}/g. The filled and shaded circles show the locations of vortices in each of the components. For $g_{12}/g < 0$ the interspecies interactions are attractive, so the vortex cores of the two lattices attract each other. (a) The vortex lattices of the two components each form a triangular vortex lattice, with coincident vortices. For $g_{12}/g > 0$ the interspecies interactions are repulsive, so the vortex cores repel each other. A series of lattices is found which appear as (b) interlaced triangular lattices; (c) interlaced rhombic lattices; and, finally, (d) interlaced square or (e) rectangular lattices. At the SU(2) point $g_{12}/g = 1$, the interlaced rectangular lattices of the two components can be viewed as a triangular lattice if the differences of the two components is ignored. The final panel illustrates the variational parameters used in the study. Reproduced with permission from [177].

Dynamical modes have been studied in the uniform system in the LLL [180] and beyond the LLL in the trapping geometry [179].

Experimental studies of the vortex lattices in rotating two-component ^{87}Rb BECs have been reported in [181]. The interspecies interactions are repulsive $g_{12} > 0$ so the vortices in the two components repel each other. The interactions are close to the SU(2) invariant values $g_{11} \simeq g_{12} \simeq g_{22}$ (see Note 4.1), but just inside the regime of phase separation (107). The experimental results showed evidence for the appearance of a stable vortex lattice phase with two inter-penetrating lattices of approximate square symmetry, consistent with the phases found in [177,178].

Exact results for the interacting two-component system with many vortices are very limited.

In the two-dimensional LLL regime, the groundstate at high angular momentum can be determined analytically for repulsive contact interactions. Recall that, for spinless bosons with repulsive contact interactions, the exact groundstate at high angular momentum is the Laughlin state (78) with total angular momentum $L = N(N-1)$ corresponding to filling factor $\nu = 1/2$. For the two-component case with $g_{ij} > 0$, and for equal numbers of atoms in the two components $N_1 = N_2 = N/2$, the exact zero-energy groundstate is an incompressible liquid described by the '(221)' bosonic Halperin state [158]

$$\Psi^{(221)}_{\text{Halperin}}(\{\zeta_i\}) \propto \prod_{i<j}(\zeta_i^{(1)} - \zeta_j^{(1)})^2 \prod_{i<j}(\zeta_i^{(2)} - \zeta_j^{(2)})^2 \prod_{i,j}(\zeta_i^{(1)} - \zeta_j^{(2)}), \tag{109}$$

where $\zeta_i^{(1)}$ are the coordinates of the $N/2$ particles in component-one and $\zeta_i^{(2)}$ the coordinates of the $N/2$ particles in component-two. This state can be viewed as a fluid of

pairs of particles forming spin singlets. This function vanishes when the coordinates of any two particles coincide, so it is a zero-energy eigenstate of the contact interaction Hamiltonian; it is the groundstate provided the interactions are repulsive $g_{ij} > 0$. The total angular momentum is $L = 3N^2/4 - 1$; which corresponds to a uniform fluid state with a total filling factor $\nu_1 + \nu_2 = 2/3$, which is therefore denser than the Laughlin state.

A series of non-abelian states that can describe two-component Bose systems in the two-dimensional LLL was proposed in [182]. These 'non-abelian spin-singlet' (NASS) states form a sequence labelled by $k = 1, 2, \ldots$, and are the exact groundstates of the two-component Bose gas for a $k+1$-body contact interaction (84), at filling factors[13] $\nu = 2k/3$. For $k = 1$ the state in this sequence is the above Halperin (221) state; for $k \geq 2$ the NASS states are *non-abelian* phases which are spin-singlet generalizations of the Moore–Read and Read–Rezayi states. Owing to the importance of the Moore–Read and Read–Rezayi phases in describing the phases of rotating spinless bosons with realistic two-body interactions (see Section 2.4), it would be interesting to explore the relevance of NASS states for a two-component Bose gas with realistic two-body interactions.

4.1.2. *Rotating two-component BEC: unequal masses*

The rotational properties of a two-component BEC formed from two atomic species raises additional interesting features. Since the atomic masses differ, $M_1 \neq M_2$, if the two components were to rotate (on average) at the same rotation frequency Ω, then by the Feynman criterion (10) the mean vortex densities in the two components would be unequal

$$\frac{n_{\rm v}^{(1)}}{n_{\rm v}^{(2)}} = \frac{M_1}{M_2}. \tag{110}$$

This imbalance of the average vortex densities competes with an energetic gain from interspecies interactions which is obtained by making the vortex densities equal (or commensurate).

The multi-vortex states of a two-component BEC with unequal masses have been studied theoretically in [183]. The interspecies interaction is assumed to be attractive $g_{12} < 0$, such that the cores of the vortices in the two components attract.

For strong attractive interactions, the vortices pair, and the system forms a locked state in which the average vortex densities are equal. How does one reconcile the equality of the vortex densities in this phase with the above relation (110)? Consider a system that has come to equilibrium at a drive frequency Ω, and that forms a locked vortex lattice of pairs of vortices. The locations of the vortex cores must rotate uniformly at the drive frequency Ω, and they will have some density $n_{\rm v}$ that is determined by the energetics (including the inter-vortex interactions). Since the vortex density is fixed to $n_{\rm v}$, the individual fluid components are flowing with average flow fields that lead to rotation of the two fluids with rates $\Omega_i = hn_{\rm v}/(2M_i)$. Clearly $\Omega_1 \neq \Omega_2$ and, in addition, neither Ω_1 nor Ω_2 need match the drive frequency Ω. Thus, there is a relative motion of the fluids with respect to the vortex cores. This relative motion leads to Magnus forces on the vortices. One reconciles these features by noting that the Magnus forces are exactly balanced by the inter-particle interactions that act to pin the vortices to each other [183], as they must be for consistency with the statement that the vortex lattice is at equilibrium at the drive frequency Ω.

For weak attractive interspecies interactions the vortices separate and the vortex densities are set by those expected for independent condensates, with $n_{\rm v}^{(1)} \neq n_{\rm v}^{(2)}$ (110).

The transition between these two regimes is controlled by the parameter $|g_{12}|\bar{n}/(\hbar\Omega)$ where $\bar{n}$ is the mean particle density. Thus, in a trap geometry, the inhomogeneity of density leads to spatial variation: a region of locked vortex lattice at centre of the trap, and an unlocked region at the outer edge [183].

Related issues arise in models of rotating Bose gases close to a Feshbach resonance [119]. The atoms and molecules (formed from resonant association of pairs of atoms) have unequal masses M and $2M$, leading to different mean vortex densities for the atomic and molecular condensates [184]. It is found that the coherent coupling can lead to the formation of states in which the atomic and molecular vortices form units resembling a carbon dioxide molecule. The arrangement of the orientations of these units within an approximately triangular array leads to many near degenerate configurations and glass-like behaviour. A range of other interesting vortex lattice phases have been identified [184].

4.2. *Spin-one Bose gas*

Spinor atomic gases may be realized by trapping a high spin atom in an optical trap, which does not lift the spin degeneracy. The inter-particle interactions are spin-rotationally invariant, and for spin $S=1$ must take the form [185,186]

$$H_{\rm int} = \sum_{i<j} \delta(\boldsymbol{r}_i - \boldsymbol{r}_j)\big[c_0 + c_2 \boldsymbol{S}_i \cdot \boldsymbol{S}_j\big], \tag{111}$$

where c_0 and c_2 are the only two interaction parameters. In terms of the two s-wave scattering lengths, denoted $a_{\rm s}^0$ and $a_{\rm s}^2$ for scattering in the two scattering channels with total spin $S=0,2$, the coupling constants in (111) are $c_0=(g_0+2g_2)/3$, $c_2=(g_2-g_0)/3$, where[14] $g_S = 4\pi\hbar^2 a_{\rm s}^S/M$.

For $c_2<0$, the system acts to maximize the total spin, which is achieved by aligning all spins; this is referred to as the 'ferromagnetic' state. It is characterized by a non-zero value of the expectation value of the local spin density $\langle\hat{\boldsymbol{S}}\rangle$. The breaking of spin-rotational symmetry leads to a manifold of groundstates related by SO(3) transformations [186]. For $c_2>0$, the system acts to minimize the total spin; this is the 'polar' state. It has vanishing spin density, $\langle\hat{\boldsymbol{S}}\rangle=0$. Still, it breaks spin-rotational invariance, with a groundstate manifold described by $S^1\times S^2/Z_2$ (see [186,187]). Thus, in contrast to the two-component condensate, which is characterized by a global phase and a local spinor direction (106), the topology of the spin-one Bose gas is much richer.

Both ferromagnetic and polar spin-one BECs have been studied experimentally, with ^{87}Rb ($c_2<0$) [188] and with ^{23}Na ($c_2>0$) [166,189,190]. In both of these experimental systems, the spin-dependent interaction is weak, with $|c_2/c_0|\ll 1$. Consequently, in spin-textured configurations such as vortex lattices, it can be energetically favourable for the condensate to have mixed character, with regions in which the local order parameter is of ferromagnetic character (with non-zero average spin) and regions where it is of polar character (with vanishing average spin).

Single vortex states. The resulting textures for single vortices of a spin-one BEC have been studied theoretically within mean-field theory [191–193]. Within the LLL mean-field regime the description of these states is simplified [171,176]. However, a wide range of textures can still appear, with forms that depend on c_2/c_0 and on the total angular momentum.

The angular momentum is carried by spin-textures, which can be of the form of 'skyrmions' of the ferromagnetic order or of 'π-disclinations' of the polar phase.

In the two-dimensional LLL regime, the *exact* groundstates at small angular momentum, $L \leq N$, have been found for the case $c_2 = 0$ in which case the interactions have a full SU(3) symmetry [176]. There exist exact eigenstates of the Hamiltonian for which the only occupied single particle states are those with angular momenta $m \leq 1$ (for $0 < L \leq 2N/3$), or those with $m \leq 2$ (for $2N/3 < L \leq N$). Exact diagonalization studies confirm the states to be the exact groundstates for all system sizes studied.

Many vortex states. The vortex lattices of a uniform $S = 1$ Bose gas have been studied within mean-field theory for the polar regime $c_2 > 0$ (see [194]). A rich series of phases of five different lattices of textured vortices was found, depending on c_2/c_0. The vortex lattices were studied within LLL mean-field theory in [176] for both positive and negative c_2. Eight different symmetries of vortex lattice were found, which are illustrated in Figure 16. The phases involve arrangements of various spin-textures of the spinor order, with lattices of Skyrmions, π-disclinations and conventional vortices [176].

Turning to consider rapidly rotating gases beyond mean-field theory, there exist some interesting exact results. In the two-dimensional LLL regime appropriate for rapid rotation, the groundstate at high rotation rate can again be determined analytically for repulsive contact interactions, g_0, $g_2 > 0$. It is an incompressible liquid state that may be viewed as a generalization of the Halperin (221) state (109). The exact (zero-energy) groundstate can be viewed as a liquid of clusters of triplets of particles in the three spin projections of spin-one [195,196], and is the $\mathrm{SU}(4)|_1$ state in the sequence of [197]. For N divisible by three (such that all particles can form complete clusters) the angular momentum is $L = N(2N/3 - 1)$, which corresponds to a filling factor $\nu = 3/4$. These clustered states may be generalized to an arbitrary number of components n; they form the exact groundstates of repulsive contact interactions at filling factors $\nu = n/(n+1)$ (see [196,197]).

A series of generalized Read–Rezayi states has been proposed for rotating $S = 1$ bosons [197]. The states in this sequence, labelled $\mathrm{SU}(4)|_k$, have the property that their

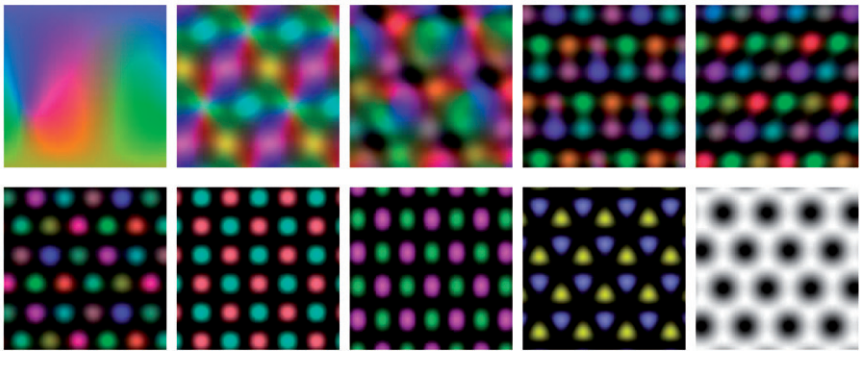

Figure 16. Vortex lattices in the mean-field LLL regime for a spin-1 BEC at different values of c_2/c_0. The first panel shows the Hammer–Aitoff projection of the colours on the spin-sphere, in which the intensity encodes the size of the spin $|\langle \hat{\boldsymbol{S}} \rangle|$. The images are the spatial distributions of the expectation values of the local spin density for the vortex lattices at $c_2/c_0 = -0.1, -0.05, 0.01, 0.016, 0.04, 0.1, 0.54, 0.7, 0.9$. In the last picture, $c_2/c_0 = 0.9$, the spin vanishes, and so the intensity shows the particle density, which forms a triangular Abrikosov lattice. Reproduced with permission from [176].

wavefunctions vanish when the coordinates of $k+1$ particles (in any spin component) coincide; they are therefore exact groundstates of repulsive $k+1$-body contact interactions (84) between the atoms. They describe incompressible liquid phases at[15] $\nu = 3k/4$ involving clusters of $3k$ particles. For $k=1$ this is the clustered state [195–197] described above, which is the exact groundstate for two-body contact repulsion between all particles. For $k > 1$ the phases have quasiparticle excitations which obey *non-abelian* exchange statistics. Although not the exact wavefunctions for two-body interactions, these represent interesting trial wavefunctions for possible quantum Hall phases of rotating spin-one Bose gas at $\nu > 3/4$. In [176,197] the results of numerical studies of the exact groundstates in this regime were reported. A large overlap of the exact groundstate (of the two-body interactions) with the $SU(4)|_2$ state is reported at $\nu = 3/2$, which is evidence of the appearance of this non-abelian phase.

A second generalization of the Read–Rezayi states, labelled $SO(5)|_k$, and describing $S=1$ bosons at filling factor $\nu = k$ is proposed in [197]. These states are exact zero-energy eigenstates of a $k+1$-body contact interaction, for a special choice of c_2/c_0. They involve clustering of groups of $2k$ particles. These phases have the additional interesting feature of involving fractionalization both of atom number or 'charge' (as is common in FQH states) and also of spin, their quasiparticle excitations having atom number 1/2 and spin 1/2.

5. Rapidly rotating Fermi gases

The possibility to cool Fermi gases to quantum degeneracy $T < T_F$ (see [198]) and to achieve regimes of strongly correlated quantum phases of two-component Fermi gases [4], raises interesting questions concerning the properties of degenerate Fermi gases under rotation.

For a one-component Fermi gas s-wave interactions vanish due to the Pauli principle. For an ultra-cold atomic gas (with low relative momentum $\hbar k$ between colliding particles) the dominant interactions are in the p-wave channel. The cross section is typically very small, vanishing as $\sigma_1 \sim V^2 k^4$ as $k \to 0$, where the 'scattering volume' V is set by the inter-atomic forces and therefore typically $V \ll 1/k^3$ for a cold gas. Nevertheless, it is possible to introduce significant interactions between the identical fermions. This can be achieved by using atoms or molecules that have strong dipolar interactions [58]; or by use of a 'Feshbach resonance' to enhance the p-wave interactions [199].

For a two-component Fermi gas, there can be s-wave interactions between the two components. Moreover, by use of a Feshbach resonance, these interactions can be made very large. In this way, experiments have been able to study the evolution between the BCS paired state (for weak attraction between the two species) and the BEC state (of small molecules formed from tightly bound pairs of the atoms), through a regime of strong correlations [4].

In this section we discuss theoretical predictions for the effects of rapid rotation on one- and two-component Fermi gases.

5.0.1. *Non-interacting Fermi gas*

The single-particle states for a fermion in an axisymmetric harmonic trap are the same as those discussed in Section 2.1. However, we now consider states beyond the LLL, so we need to generalize the discussion.

Working in the rotating frame, at angular frequency Ω, the single-particle energies of particle in an axisymmetric harmonic well are

$$E^{\Omega}_{n_\perp,m,n_\parallel} = \hbar\omega_\perp(2n_\perp + |m| + 1) - \hbar\Omega m + \hbar\omega_\parallel(n_\parallel + 1/2), \tag{112}$$

where $n_\perp = 0, 1, 2, \ldots$ and $m = 0, \pm 1, \pm 2$ are the radial and angular momentum quantum numbers for motion in the plane perpendicular to the rotation axis, and $n_\parallel = 0, 1, 2, \ldots$ is the subband index for motion parallel to the rotation axis. If there are additional internal degrees of freedom (hyperfine levels), there is one such orbital state for each level.

In general, one should take account of confinement in all directions, owing to the inhomogeneity of the trapped gas. However, as in the case of bosons, it is useful to consider the limit $\Omega \simeq \omega_\perp$ in which the system becomes locally homogeneous in the plane perpendicular to the rotation axis. The spectrum can then be written

$$E^{\omega_\perp}_{n,m,n_\parallel} = 2\hbar\omega_\perp(n + 1) + \hbar\omega_\parallel(n_\parallel + 1/2), \tag{113}$$

where now $n = 0, 1, \ldots$ is the Landau level index and the angular momentum takes the values $m = -n, -n+1, -n+2$. (The relationship is obtained by noting $n = n_\perp + (|m| - m)/2$.) Note that the states in a single Landau level (labelled by m) are degenerate. The particle density sets the highest occupied Landau level (maximum n) and subband (maximum $n_\parallel$).

The properties of the gas depend on the aspect ratio of the trap, $\omega_\perp/\omega_\parallel$. It is of interest to consider the two limiting cases: the quasi-two-dimensional regime, $\omega_\parallel \gg \omega_\perp$; and the three-dimensional regime, $\omega_\parallel \ll \omega_\perp$.

In the quasi-two-dimensional regime, the particle density is sufficiently small or the axial confinement is sufficiently strong that only $n_\parallel = 0$ is occupied, i.e. $\mu < E^{\omega_\perp}_{0,0,1}$. One can then define the filling factor as before, and as is conventional in the FQHE systems, by

$$\nu \equiv \frac{n_{2\mathrm{d}}}{n_{\mathrm{v}}} = \frac{n_{2\mathrm{d}}h}{2M\omega_\perp}. \tag{114}$$

In this quasi-two-dimensional regime, even a non-interacting Fermi gas shows a series of incompressible states. These arise because of the fact that the spectrum is discrete, with a set of highly degenerate states (over m) at $E_{n,m,0}$. These appear each time ν is an integer and a Landau level is filled. (At this point the chemical potential has a discontinuity equal to the Landau level spacing, $2\hbar\omega_\perp$.) If there are additional internal degrees of freedom these incompressible states occur at those filling factors for which atoms of all species fill an integer number of Landau levels.

The three-dimensional regime (34) is relevant for anisotropic traps $\omega_\parallel \ll \omega_\perp$. Here, for each Landau level state, the motion along the rotation axis can be viewed as a quasi-one-dimensional gas, and the energy is more conveniently written as

$$E^{\omega_\perp}_{n,m,k_\parallel} = 2\hbar\omega_\perp(n + 1) + \frac{\hbar^2 k_\parallel^2}{2M}, \tag{115}$$

where $k_\parallel$ is the wavevector along the rotation axis. In this case, the system does not show incompressibility. However, there is a $1/\sqrt{E}$ divergence in the density of states at the position of each Landau level, associated with the quasi-one-dimensional motion.

The existence of Landau level quantization is predicted to lead to signatures in the density distribution for a trapped Fermi gas, when the rotation frequency is close to the

trap frequency $\Omega \simeq \omega_\perp$ (see [200]). The experimental signatures depend on the aspect ratio of the trap: they are strongest for the quasi-two-dimensional limit, where there is strict incompressibility leading to plateaus in the density distribution; but features survive also in the three-dimensional case owing to the singularities in the density of states [200].

5.1. *One-component Fermi gas*

Under conditions of rapid rotation, and at sufficiently low particle density, the Fermi gas will be in the quasi-two-dimensional LLL regime ($n = n_\parallel = 0$). At the single-particle level, the system is then degenerate when the filling factor is non-integer, $\nu < 1$. The groundstate is determined by minimizing the inter-particle interactions.

In the following we describe the results of studies of the effects of two important forms of inter-particle interactions on the properties of a rapidly rotating one-component Fermi gas.

5.1.1. *Dipolar interactions*

The properties of a Fermi gas in the two-dimensional LLL have been investigated for the case of dipolar interactions. Antisymmetry of the wavefunction requires the relative angular momentum of any two particles to be odd, so the inter-particle interaction is characterized by the Haldane pseudo-potentials (50) at odd m. The relevant energy scale can be large for fermionic molecules with electric dipole interactions [201], leading to the possibility of stable correlated phases in rapidly rotating dipolar Fermi gases.

The possibility to use dipolar interactions to stabilize the $\nu = 1/3$ Laughlin state was described in [201]. The energy gap for creation of a quasi-hole excitation (which contributes to the incompressibility of the state, see Section 2.4.3) was estimated to be $\Delta_{\rm qh} = (0.9271 \pm 0.019) C_d/\ell^3$ for a trap with spherical symmetry ($\omega_\perp = \omega_\parallel$) (see [201]).

The groundstates of small numbers of dipolar-interacting fermions ($N \leq 10$) in the two-dimensional LLL in a harmonic trap have been investigated numerically [202] over a wide range of different rotation rates (angular momenta). The results were analysed within the framework of the composite fermion construction, in which the interacting Fermi system is represented by non-interacting composite fermions [24,84]. This construction works well for analogous studies of harmonically trapped electrons in the FQHE regime (i.e. Coulomb forces instead of dipolar forces) [84]. As described in Section 2.3.3 a generalization of the composite fermion method to treat rotating bosons in harmonic traps also works well [202]. For the case of dipolar interacting fermions, some discrepancies are reported from the apparent predictions of composite fermion theory [201]. However, these appear to arise from an incomplete application of the composite fermion theory for some of the groundstates found in numerics. (Most of the discrepancies reported in [202] arise from the neglect of a set of the 'compact' composite fermion states that account for the physics in other situations [83,86]. Specifically, for $N = 10$, the composite fermion theory predicts a set of compact states at $L = 73, 80, 85, 93, 95$; these values fill out most of the missing entries in Table (4) of [202]. The results reported therefore appear consistent with composite fermion theory describing the high angular momentum states accurately.) To check the accuracy of the composite fermion description of these states, or to determine whether the states are of a different character [202], it

would be useful to compute overlaps of the exact groundstates with the trial composite fermion states [83,86].

The fact that dipolar interactions are long ranged allows the stabilization of a Wigner crystal state at very low filling factor $\nu \ll 1$. The transition from Laughlin states to the Wigner crystal phase is predicted to occur at $\nu < 1/7$ (see [123]), close to the value at which the transition is believed to occur in FQHE systems.

In the case of a quasi-two-dimensional fermionic gas with filling factor larger than one, $\nu > 1$ (i.e. when more than one Landau level is occupied), the nature of the groundstate of the particles in the partially occupied Landau level (let us label this level by n) are determined solely by the interactions. However, now the Haldane pseudo-potentials should be computed in this nth Landau level. Consequently, the groundstate at a filling factor $\nu = n + \nu'$ $(0 \leq \nu' \leq 1)$ can differ from that at $\nu = \nu'$. Studies in the quantum Hall literature show that Hartree–Fock mean-field theory is accurate when $n \gg 1$ (see [65]). For large filling factors, the mean-field states of dipolar atomic Fermi gases are expected [67] to be qualitatively similar to those of electrons in semiconductor systems [64,65]. Depending on the filling of the partially-occupied Landau level, the groundstate will be a 'stripe' or 'bubble' phase [64,65] of similar translational symmetry to the mean-field states discussed for bosons in Section 2.2.3.

5.1.2. *p-wave Feshbach resonance*

Although weak at low collision energy, identical fermions experience non-zero p-wave interactions. These interactions can be resonantly enhanced in the vicinity of a Feshbach resonance, i.e. close to the threshold for formation of a new bound state in the p-wave channel. Such resonances have been studied in ultra-cold gases of ^{40}K [199,203,204] and ^{6}Li [205–207].

Close to a p-wave resonance, at low collision energy (when the wavevector $\max(k_F, 1/\ell)$ is sufficiently small) the p-wave scattering phase shift takes the form

$$\delta_1(\boldsymbol{k}) = (1/3)k^3 a_1^3. \tag{116}$$

This defines the scattering length a_1. The quantity a_1^3 is often referred to as the 'scattering volume' [208], the modulus of which diverges at the position of the resonance.

In the LLL, the interaction may be represented by the pseudo-potentials. For the p-wave interaction, the only non-zero pseudo-potential is in the $m = 1$ channel, with [209]

$$V_1 = \sqrt{\frac{2}{\pi}} \frac{\hbar^2}{M} \frac{a_1^3}{m a_\parallel \ell^4}. \tag{117}$$

This two-body interaction is the special case for which the $\nu = 1/3$ Laughlin state is exact [210]. For $\nu < 1/3$ the groundstate is highly degenerate, and may be viewed as a gas of $1/3$ anyons of the Laughlin state.

Analytic results do not exist[16] for $\nu > 1/3$, or for the excitation spectrum above the $\nu = 1/3$ groundstate. Numerical studies on the sphere [209] have investigated the groundstates and low-energy excitations above the Laughlin $\nu = 1/3$ state and the 'Jain sequence' [84] states at $\nu = 2/5$, $3/7$. These studies show that in the thermodynamic limit $N \to \infty$ the excitation gaps appear to converge to non-zero values, establishing these states as incompressible and determining numerical estimates values for the excitation gaps.

The overall energy scale is set by the V_1 pseudo-potential. Experimental observation of these states will require cooling to temperatures less than around V_1/k_B. The issue of stability of a degenerate one-component Fermi gas close to a p-wave resonance [204,207,211] is an interesting open question, as is the effect of rapid rotation on this stability.

5.2. *Two-component Fermi gas*

5.2.1. *BEC–BCS crossover*

Degenerate gases of two species of fermions may be formed either from two atomic species, or from two hyperfine states of the same fermionic atom [212,213]. We denote the two components as spin-up and spin-down. For simplicity we assume that the two components have equal densities and equal masses M.

Since intra-species s-wave interactions are excluded by the Pauli principle, the dominant interactions at low energy are the inter-species s-wave interactions. By use of a Feshbach resonance, these interactions can be made strong. A Feshbach resonance arises when, close to the energy of the two dissociated atoms, there exists a bound molecular state of the two atoms in some different hyperfine levels. Owing to the different hyperfine structure of the bound state from the dissociated atoms, by varying a magnetic field one can cause the energy of the bound state to cross the energy of the two dissociated atoms. Hybridization of the molecular level with the unbound atoms leads to a Feshbach resonance in the s-wave scattering amplitude.

For a detailed discussion of the physics of the resonant scattering, the reader is referred to [4]. In brief, the consequence of the formation of the bound state is that the s-wave scattering length a_s passes through a divergence,

$$a_s(B) \propto \frac{1}{B_{res} - B}, \tag{118}$$

as illustrated in Figure 17. On approaching the resonance from the side on which the bound state has not formed ($B > B_{res}$), the scattering length becomes large and negative; approaching the resonance from the side on which the bound state has formed ($B < B_{res}$), the scattering length becomes large and positive. For short-range interactions, the properties of the (balanced) two-component Fermi gas close to the Feshbach resonance depend on the parameter $k_F a_s$. (We denote the Fermi energy $\epsilon_F = \hbar^2 k_F^2/(2M)$.)

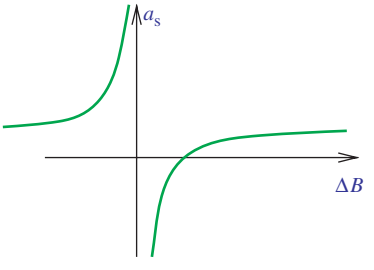

Figure 17. Schematic diagram of the variation of the s-wave scattering length close to a Feshbach resonance as a function of the detuning $\Delta B = (B - B_{res})$.

The nature of the groundstate can be understood in the limiting cases far from the resonance, when $k_F|a_s|$ is small.

When a_s is small and positive, there exists a bound-state even for one pair of atoms. The groundstate of a many particle system consists of tightly bound pairs of atoms of the two species; the resulting small bosonic molecules behave as a weakly-interacting Bose gas and form a BEC at low temperatures. This is the 'BEC side' of the resonance.

When a_s is small and negative, the weak attractive interaction causes a BCS instability of the Fermi surface, leading to a BCS paired superfluid. There is an energy gap that, in this BCS limit of weak interaction, is exponentially small

$$\Delta \sim \epsilon_F \exp\left(-\frac{\pi}{2k_F|a_s|}\right). \tag{119}$$

This is the 'BCS side' of the resonance.

As the resonance is swept, such that $1/k_F a_s$ varies from the BCS to BEC regime, it is believed that the groundstate of the Fermi gas evolves smoothly. This 'BEC–BCS crossover' has been confirmed in recent experimental studies of several groups [4].

Cold atomic gases allow additional novel physics to be studied by imposing an imbalance between the populations of the two components. In conventional superconducting systems, a population imbalance can be achieved by using the Zeeman splitting in a magnetic field. However, a magnetic field also induces orbital effects, precluding a study of the effects of the density imbalance alone. In atomic gases the density imbalance can be achieved without any orbital effects [214,215].

New physics can also emerge in atomic gases in the complementary situation: that is, to study purely the *orbital* effects of a magnetic field, without inducing any population imbalance. This can be achieved by setting the densities of the two hyperfine levels to be equal, and introducing the orbital effects of the magnetic field by rotation. This is the situation that we describe in this section.

The effects of moderate rotation are well understood. At all points across the crossover, the low-energy phase is a condensate, and responds as a superfluid of pairs of fermions. Rotation causes the formation of an array of vortices with density, $2(2M)\Omega/h$, which is the Feynman result (10) with the mass, $2M$, of the pair of particles. The formation of a lattice of quantized vortices has been demonstrated in experiments described in [216]. The results reveal the superfluid nature of the system across the whole range of the crossover regime, and are consistent with vortices having a quantum of circulation of $h/(2M)$ associated with condensation of pairs of fermions.

5.2.2. *Effects of rapid rotation*

One expects that the effects of rapid rotation will be rather different in the BEC and BCS sides of the resonance.

Far on the BEC side, the effects of rapid rotation are similar to those discussed above for rapidly rotating bosons. In the quasi-two-dimensional regime, the mean-field vortex lattice will survive up to vortex densities at which the filling factor (66) is of the order of one, at which point there is a transition to strongly correlated states. In the three-dimensional regime, the transition to the strongly correlated regime occurs at high vortex density according to (98).

Far on the BCS side, the effects of rotation are similar to the orbital effects of a magnetic field on type-II superconductors. For conventional superconductors, the upper critical field is well described by the semi-classical approximation of Gorkov [217,218] (see also [219]). Translating to the quantities of interest to us, this predicts the transition to a normal state when[17]

$$\hbar\Omega \gtrsim 4.24\Delta^2/\epsilon_{\rm F}. \tag{120}$$

One can understand this semi-classical result in terms of a balance of energies. On the one hand the condensation energy per particle on forming the superfluid is of the order of $\Delta^2/\epsilon_{\rm F}$. This should be compared with the kinetic energy of the superfluid flow. Since the superfluid cannot rotate as a rigid body, in the rotating frame of reference the superfluid has a non-zero kinetic energy. To estimate this kinetic energy, note that the vortex spacing $a_{\rm v} \sim (2(2M)\Omega/\hbar)^{-1/2}$ sets a typical velocity $\hbar/Ma_{\rm v}$, so the kinetic energy per pair is $M(\hbar/Ma_{\rm v})^2 \sim \hbar\Omega$. The semi-classical formula states that once this kinetic energy is larger than the condensation energy, it does not pay to form the superfluid, and a rigidly rotating Fermi gas has lower energy.

How the transition between the BEC and BCS regimes occurs in a rapidly rotating gas is an interesting question.

The mean-field theory for a rotating Fermi gas in a harmonic trap has been studied in [220] across the whole crossover regime. This theory gives results on the BCS and BEC sides that match with the above expectations in these limits, and provides a useful way to connect between these two regimes. The approach works explicitly with a trapped gas, and the mean-field theory has the benefit of being accurate in the limit of a 'narrow' Feshbach resonance [221]. The narrow resonance limit has the feature that the molecular bosons that form have vanishing interactions. As a result, for a trapped gas at any $\Omega \neq \omega_\perp$ the molecular gas on the BEC side is confined to the lowest harmonic oscillator state and carries zero angular momentum. This is an unphysical situation for rotating atomic Fermi gases which interact, typically, through 'wide' Feshbach resonances. However, it is unclear under what conditions (if any) this might affect the validity of the predictions for rotating Fermi gases beyond the narrow resonance limit.

BCS regime: upper critical rotation rate. A complementary approach has been described in [222,223]. These works study mean-field theory in a situation in which the trapping potential is weak, so the system is in the uniform three-dimensional regime,

$$\Omega \simeq \omega_\perp \gg \omega_\parallel, \tag{121}$$

with single-particle energy spectrum (115). The linearized BCS mean-field equations were used to determine the critical temperature below which the system is unstable to the formation of a BCS superfluid, as a function of the rotation rate Ω.

In [222], the effects of a trap are introduced within the local density approximation (see Section 2.5). This gives rise to inhomogeneity in the trap, with normal and superfluid regions co-existing at different radii. An upper critical rotation rate is determined as a function of detuning, at which the entire cloud becomes normal for a temperature of $k_{\rm B}T/\hbar\Omega = 10^{-3}$.

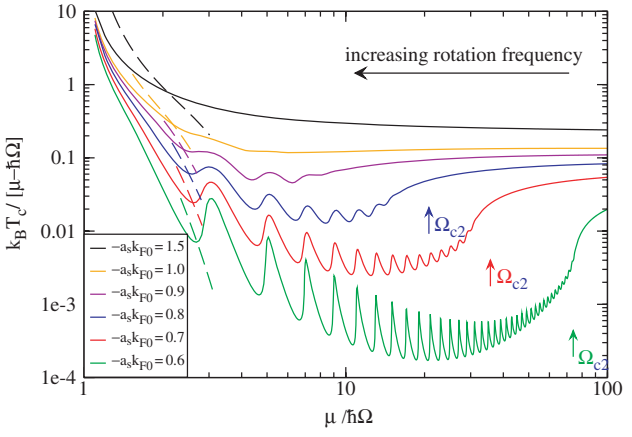

Figure 18. Solid lines: transition temperature for formation of a BCS superfluid state for a rotating Fermi gas in the uniform three-dimensional limit, as a function of rotation rate Ω for different interaction strengths $k_F a_s$. For weak interactions, as the rotation rate increases at fixed chemical potential μ (right to left on the graph), the transition temperature falls abruptly at the semi-classical upper critical rotation rate. However, it remains non-zero and rises as Ω/μ increases. For strong interactions the transition temperature becomes a monotonically increasing function of Ω. Dashed lines: transition temperature for formation of a CDW state. Reproduced with permission from [223].

In [223], similar mean-field equations were studied for the uniform three-dimensional limit (121). These results show that the critical temperature $T_c(\Omega)$ *never* vanishes. In fact, as the rotation rate increases, the transition temperature becomes an *increasing* function of rotation rate, see Figure 18. This is consistent with studies of BCS theory in the solid state setting beyond the semi-classical Gorkov approximation [224]. The increase in transition temperature at high rotation rate is related to the enhancement of the density of states at the Fermi level, owing to the $1/\sqrt{E}$ singularities of the quasi-one-dimensional motion along the rotation axis. These results show that the upper critical rotation rate found in [222] is a function of temperature; as $T \to 0$ the BCS mean-field theory predicts that the system remains superfluid for all $k_F a_s$ and Ω.

That BCS mean-field theory predicts the groundstate to be superfluid for all $k_F a_s$ and Ω is a statement that the BCS state has a lower (free) energy than the normal phase for any attractive interaction. Despite the orbital motion induced by the rotation, the Fermi gas will always undergo a superconducting instability at sufficiently low temperature. This does not rule out the possibility of destruction of the superfluid phase by transition to another state. In [223] it was shown that the BCS phase competes with a charge density wave (CDW) state. The CDW is a state in which the atomic density is spontaneously modulated along the rotation axis with a period such that the atomic filling factor in each layer is $\nu_a = 2$, see Figure 19. This competition was analysed in detail for the case of interacting fermions in the LLL, allowing fluctuations of both the CDW and superconducting state. The calculations show that the dominant instability is towards the CDW state. (The transition temperature into the CDW is plotted as a dashed line in Figure 18.) Thus, an upper critical rotation frequency *does* exist on the BCS side of the transition: it is set by the transition into this CDW [223]. At intermediate Ω it was argued that the CDW and superconducting state can coexist, leading to a novel form of supersolidity.

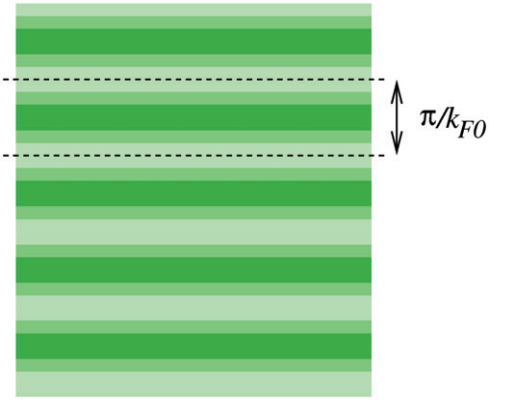

Figure 19. Schematic diagram of the charge density wave state that sets the upper critical rotation rate for destruction of fermionic superfluidity. The wavevector of the density wave lies along the rotation axis. Its period is set by the particle density, and is such that the atomic filling factor of each layer is $\nu_a = n_a/(2\pi\ell^2) = 2$. It is a fully gapped state.

Transition from BEC to BCS. The above considerations are expected to be valid on the BCS side of the transition. Understanding how the results connect to the BEC side is an interesting open problem. One thing that is clear is that, in the rapid rotation limit, in which all fermions (or bosonic molecules) are confined to the LLL, the transition from BCS to BEC side must involve a phase transition[18].

In the quasi-two-dimensional case this can be seen by noting that states on the two sides of the transition are topologically distinct. On the BCS side, where the atoms experience weak attractive interactions, the groundstate is a compact droplet with $\nu_a = 2$ (a full Landau level for both atomic species); this state has two gapless edge modes, corresponding to density and spin excitations. On the BEC side, one anticipates that the groundstate is a Laughlin state of bosonic molecules, with[19] $\nu_m = 1/2$; this state has only one gapless edge mode. The change in edge mode structure shows that the states on the two sides are topologically distinct; they must be separated by a (quantum) phase transition [223,225,226]. An effective theory has been derived for this phase transition [226], but the nature of the transition remains unclear.

The existence of a phase transition in the three-dimensional case was predicted [223], based on the above two-dimensional argument combined with the observation that the three-dimensional system forms a CDW of layers of $\nu_a = 2$ states at high rotation rate. If the CDW order survives with the same period on passing to the BEC side, each layer must undergo the above topological phase transition; the only alternative is that the CDW does not survive (or changes period), which also signals a phase transition of another kind.

6. Experimental aspects

Throughout the preceding text, we have mentioned existing experimental studies relevant to the theoretical results presented. In this section, we focus only on those aspects of the experiments that relate to the strongly correlated phases at small filling factors. However, there also remain many interesting issues to explore experimentally beyond this strong-correlation regime.

6.1. *Experimental signatures of strongly correlated phases*

Experimental detection of the properties of cold atomic gases is typically performed following the removal of the trapping potentials and expansion of the gas. An important aspect of the physics of rapidly rotating atomic gases is that, provided the interactions are weak enough that the gas is in the LLL limit (20), the expanded gas provides a direct map of the wavefunction prior to expansion: the only effect of expansion is a rotation and rescaling of the coordinates [227]. The use of expansion as a 'wavefunction microscope' makes probing the rotating gas particularly straightforward. This is in contrast to the case of a non-rotating gas where (in the simplest cases) the expanded image is a measure of the velocity distribution in the trap, and spatial structure is recovered only after Fourier transformation.

The most dramatic feature of the strongly correlated phases predicted by theory is that they are incompressible. As a result, the density distribution in a trapped system will show characteristic 'wedding cake' structures [125], with regions in which the two-dimensional particle density is pinned to values $\nu^* n_v$ where ν^* are the filling factors at which the groundstate is incompressible. This density distribution differs markedly from the expected density distribution of the vortex lattice phase which is compressible and, hence, follows a Thomas–Fermi distribution [41,43]. An extreme case is the Laughlin state, $\nu = 1/2$, for which the average particle density is constant out to the radius $R \sim 2\sqrt{N}\ell$.

An interesting feature of particles in the two-dimensional LLL is that the condensate fraction of the many-body phases can be determined from measurements of the expectation value of the particle density [228]. In this way, and by repeated measurements to construct the expectation value of the density, one could directly distinguish between a condensed state (such as the vortex lattice) and any strongly correlated phase for which the condensate fraction vanishes.

In order to detect the nature of the correlated phase, it was proposed that the particle distributions in single-shot measurements of the expanded wavefunction be used to directly measure the density–density correlation functions of the states in the trap [227]. This method, also referred to as measurements of 'noise correlations' [229], is particularly powerful in the present case, where the scaling of the wavefunction allows direct measurements of spatial correlations in the gas. The statistics of the density fluctuations can be used to measure the compressibility of the fluid, and to distinguish between different strongly correlated phases [227]. Noise correlations are also expected to show signatures of strongly correlated phases of bosons on rotating lattices [31,152]

Further information on the nature of the incompressible phases can be deduced by studying the properties of their excitations.

The clearest indication of the formation of an incompressible liquid phase in semiconductor systems is the appearance of a (fractionally) quantized Hall resistance [23]. This is a consequence of the pinning of the quasi-particles by disorder and the dissipationless flow of the incompressible liquid past these localized states. Proposals have been made [31,157] for how analogous transport measurements might be performed in rotating Bose gases on optical lattices.

Quantum Hall states, while gapped in the bulk, carry gapless edge excitations. These are collective modes (waves of particle density) on the surface of the incompressible fluid. The form of these excitations is fixed by the nature of the bulk phase [105].

Direct detection of the spectrum of edge excitations [230] could allow identification of the bulk incompressible state [106].

A direct measurement of fractional statistics of the quasiparticle excitations of the incompressible states would be a very dramatic confirmation of theoretical expectations. Indeed, even in conventional electronic FQHE systems, which are very well understood and much explored experimentally, an (accepted) experimental measurement of the fractional exchange statistics is still lacking. An ambitious scheme for measuring the semion statistics of the quasiparticle excitations of the Laughlin state of rotating bosons has been proposed in [231].

6.2. *Strongly correlated phases: experimental status and outlook*

The reader is referred to [4] for a recent authoritative review of experiments on rotating atomic gases. Here we describe the current experimental status in connection with the strongly correlated phases which are predicted to occur at low filling factors, and discuss the outlook for future experimental work in this area.

To date, the highest vortex densities in rotating atomic Bose gases have been achieved by the group of Eric Cornell. In these experiments, the mean interaction energy $\mu \sim g\bar{n}$ is sufficiently small that the gases are in or close to the two-dimensional LLL regime, $\mu \lesssim 2\hbar\Omega_\perp, \hbar\omega_\parallel$. However, the smallest filling factor reported is $\nu \simeq 500$ (see [90]). This is deep in the regime $\nu > \nu_c$ where one expects the groundstate to be a vortex lattice [22,49,50], and indeed this is what is observed. Reducing the filling factor further (reducing N at fixed N_v) leads to a gas that is so dilute that collisions are too infrequent for thermalization on the lifetime of the gas.

Clearly further special efforts are require in order to reach the regime $\nu \lesssim 6$ where one expects quantum fluctuations of vortices to destabilize the lattice. There appear to be two main difficulties in reaching this regime, arising from weak interactions and from heating.

Weak interactions. In the two-dimensional LLL, the typical interaction energy that stabilizes the strongly correlated phases is small. The relevant energy scale is the pseudo-potential V_0, Equation (30). To gain some physical intuition for the origin of this energy scale, it is useful to note that it sets the chemical potential (the mean interaction energy) for a rotating gas at a filling factor $\nu \sim 1$. The centrifugal limit (18) sets a maximum rotation rate $\Omega = \omega_\perp$, and hence a maximum vortex density (10) $n_v = 2M\omega_\perp/h$. For $\nu = 1$ the maximum two-dimensional particle density is $n_{2d} = n_v = 2M\omega_\perp/h$ and so the maximum three-dimensional density is of the order of $\bar{n} \sim 2M\omega_\perp/(ha_\parallel)$. The chemical potential associated with this density is

$$\mu \sim g\bar{n} \sim \frac{\hbar^2 a_s}{M} \frac{1}{a_\perp^2 a_\parallel} \sim \frac{a_s}{a_\parallel} \hbar\omega_\perp, \tag{122}$$

which recovers V_0 (30) up to a numerical factor.

This energy scale sets the size of the incompressibility gap of the strongly correlated phases. It therefore sets the required temperature scales in order to observe these phases. In typical experiments in magnetic traps, $\hbar\omega_\perp \sim 5$ nK, while $a_s/a_\parallel \sim 0.01$, leading to gaps that are small fractions of a nano-Kelvin, much smaller than the temperatures that can currently be reached in such an experiment.

Equation (122) highlights ways in which to overcome this difficulty.

- Increase a_s. This can be achieved by using a Feshbach resonance to enter a strongly interacting regime [232]. For bosons three-body losses can be large close to a Feshbach resonance, which may limit the usefulness of this approach. Losses are much smaller for Fermi gases close to an *s*-wave Feshbach resonance [233]. The FQHE regime for rotating fermions in the BCS–BEC crossover is therefore a very interesting situation to consider. It may be easier to achieve the strong-correlation regime ($\nu \sim 1$) for a strongly interacting two-component Fermi gas (close to the unitary limit) than for a typical Bose gas [234].
- Decrease $a_{\|}$. The introduction of an optical lattice, with wavevector parallel to the rotation axis can slice the condensate up into many parallel layers with a much stronger subband confinement ($a_{||}^{\text{layer}} < d_{\|}$); see Figure 14. This can lead to a significant increase in the interaction energy scale [125]. It is important that the subband confinement retains rotational symmetry, to prevent loss of angular momentum or heating (see below).
- Increase $\omega_{\perp}$. A tighter harmonic confinement would allow an increased vortex density and, hence, stronger interactions at $\nu \sim 1$. Much tighter traps can be formed by using atom chip traps formed on surface microstructures [235], allowing transverse trapping frequencies of the order of 100 kHz. (Such systems are highly anisotropic, $\omega_{\|} \ll \omega_{\perp}$, so could potentially be used to study the three-dimensional LLL regime (34).) Very tight confinement can also be achieved in the wells of an optical lattice. This might allow studies of rotating clusters of small numbers of atoms. There are interesting proposals [236,237] for how clusters of small numbers of particles might be transferred adiabatically from a non-rotating state into the strongly correlated Laughlin state.
- Optical lattice systems. The energy scales that set the correlation energies in optical lattices are large. Physical rotation of the optical lattice [26,133] involves the same centrifugal limit (18), again limiting the vortex density to the values leading to (122). This method will therefore likely also need to be supplemented with tight harmonic confinement in order to achieve a large interaction energy at $\nu \sim 1$. However, the proposed schemes for imprinting Peierls phases onto the inter-site tunnelling matrix elements [28,29,136] appear to allow field configurations that mimic uniform rotation without a centrifugal limit. If flux densities of the order of one flux per site can be generated, these systems could show strongly correlated states with a large energy scale (see Section 3).

Heating. An atomic gas that has come to equilibrium at a rotation rate Ω is at rest in the rotating frame of reference. For example, in the vortex lattice phase the positions of the vortices are at rest in the rotating frame. In the laboratory frame, the fluid a distance $r_{\perp}$ from the rotation axis is moving at a velocity of $\Omega r_{\perp}$. As a result, the rotating gas will experience any non-axisymmetric perturbation that is static in the laboratory frame (e.g. a trap that is not circularly symmetric, or any scattered light from optical traps) as a time-dependent potential in the rotating frame. This can lead to excitation, or heating, of the rotating gas.

It is instructive to estimate the importance of such excitations on an incompressible liquid state, by applying a form of Landau criterion. For an incompressible liquid state, the collective excitations (in the bulk) have a gap, Δ, that is of the order of the interaction

energy, V_0, or of the order of the cyclotron energy, $2\hbar\omega_\perp$, whichever is the smaller[20]. Therefore, the maximum possible gap (achievable for $V_0 \sim \hbar\omega_\perp$) is $\Delta \sim \hbar\omega_\perp$. The edge of a rotating cloud of radius R moves with a linear velocity of $v = \Omega R$, which is close to $v \sim \omega_\perp R$ for a system with a large number of vortices (92). Owing to this motion, in this edge region the collective modes with wavevectors $q \gtrsim \Delta/(\hbar v) \sim 1/R$ have negative energy in the laboratory frame. These excitations can therefore be spontaneously generated by any perturbation that is static in the laboratory frame and has Fourier components on the relevant scale, $q \gtrsim 1/R$. This sets a strict requirement on the potential: any static perturbation in the laboratory frame that has a wavelength less than of the order of the radius of the cloud can efficiently generate collective modes of the rotating gas (i.e. cause heating).

The use of geometric phases to simulate rotation (or a uniform magnetic field), either in a lattice-based system [28,29,136] or in the continuum [238], has the advantage that the gas remains at rest in the laboratory frame. This removes the relative motion of the gas with respect to possible perturbations at rest in the laboratory frame, and eliminates these as sources of heating. Recent experimental work has introduced a vector potential [239] of vanishing curl using two-photon-induced geometric phases, setting the stage for extensions to vector potentials with non-zero curl.

7. Summary

Rapidly rotating degenerate atomic gases offer the possibility to explore the physics of quantized vortices and vortex lattices in novel parameter regimes. In this review we have described some of the novel equilibrium properties that can appear: for rotating spinless and multi-component Bose gases; for Bose gases on rotating lattices; and for rotating Fermi gases. Interesting new physics can emerge both within the realm where mean-field theories are applicable (as is dramatically illustrated by the novel vortex lattice phases in Figures 4, 15 and 16), and within regimes where mean-field theory fails (as evidenced by the theoretical predictions of some very exotic strongly correlated phases). While theoretical studies have helped to clarify some of the expected properties of these systems, our understanding is still very much limited. It is hoped that these theoretical predictions will motivate and inform future experimental investigations of these novel phenomena. At the very least, these theoretical studies show that very interesting aspects of many-body quantum physics are at play in rotating degenerate atomic gases; this is an area where future theory and experiment are likely to uncover dramatic new phenomena.

Acknowledgements

I have benefitted very much from working closely with many people on this and related topics: Nick Read, Stavros Komineas, Ed Rezayi, Steve Simon, Kareljan Schoutens, Miguel Cazalilla, Duncan Haldane, Gunnar Möller and, in particular, Nicola Wilkin and Mike Gunn who introduced me to the subject and who have been continued sources of help and advice. I also acknowledge useful discussions with many others, including Misha Baranov, Gordon Baym, Eric Cornell, Jean Dalibard, Eugene Demler, David Feder, Sandy Fetter, Victor Gurarie, Jason Ho, Jainendra Jain, Thierry Jolicoeur, Wolfgang Ketterle, Maciej Lewenstein, Chris Pethick and Nicholas Regnault. Finally, I am grateful to Sandy Fetter, Gunnar Möller and Kareljan Schoutens for helpful comments on a draft version of this manuscript.

Notes

1. The connection between a rotating neutral fluid and a charged fluid in a magnetic field is clarified later.
2. Bose–Einstein condensation has been measured by neutron scattering, yielding a condensate fraction at low temperatures of about 9% (see [5]).
3. For the strong inequalities in (20) to hold, the factor of two in this expression is clearly unimportant. We leave this factor in this formula merely as a reminder that the lowest-energy single-particle excitation out of the lowest Landau level (LLL) has energy $2\hbar\omega_\perp$. In practice, one expects the physics derived by theoretical studies in the regime (20) to be at least qualitatively accurate even in experiments in which these inequalities are not well satisfied.
4. The validity of the restriction of single-particle states to the two-dimensional LLL has been explored in [37]. The numerical results are interpreted to indicate disagreement with the condition (20) for restriction to the LLL, for the case of incompressible states at fixed filling factor $\nu = N/N_\mathrm{v}$, Equation (66). However, the criterion applied, the shift of the rotation frequency Ω, appears to overlook the dependence of Ω on N_v, e.g. (92) for $N_\mathrm{v} \gg 1$. An analysis based on (92) together with the assumption that $\mu \sim g\bar{n}$ with a correction due to Landau-level mixing $\delta\mu \sim (g\bar{n})^2/\hbar\omega_\perp$ that is small ($\delta\mu \ll \mu$) leads to the conclusion that the quantity g_max defined in [37] should vary as $g_\mathrm{max} \sim N_\mathrm{v}^2/N$. Thus, $g_\mathrm{max} \propto 1/N$ at fixed N_v and $g_\mathrm{max} \propto N$ at fixed ν, in rough agreement with the numerical results [37].
5. When the exact groundstate is known (as for the Laughlin state at $L = N(N-1)$), discussions reduce to considerations of the properties of this state.
6. This is easily checked by constructing the Euler–Lagrange equations for (70).
7. These are the guiding-centre coordinates of a particle in a single Landau level.
8. The exact relation $N_\mathrm{v} = 2N - 2$ should be interpreted as $N_\mathrm{v} = N/\nu - \mathcal{S}$ where $\mathcal{S}$ is the 'shift' of the state on the sphere, see Appendix B.
9. As written the states (79) are not eigenstates of total angular momentum. They form an over-complete basis for the zero-energy states with $L > N(N-1)$.
10. See Note 2.1 regarding the units in [100,101].
11. Such geometries have been studied in the groups of E. Cornell and J. Dalibard.
12. Within mean-field theory the results are identical for the quasi-two-dimensional and three-dimensional LLL regimes.
13. The more general form is $\nu = 2k/(2kq+3)$ with q an even/odd integer for bosons/fermions [182].
14. Since the components are different hyperfine states of the same atomic species, the mass M is the same for all components.
15. The more general forms are $\nu = 3k/(3kq+4)$ for $\mathrm{SU}(4)|_k$ and $\nu = k/(kq+1)$ for $\mathrm{SO}(5)|_k$ with q an even/odd integer for bosons/fermions [197].
16. One exception is the trivial statement that $\nu = 1$ is a fully filled Landau level.
17. Note that, in the BCS limit, this is a much lower rotation rate than that required to put one flux quantum through one Cooper pair, which would be $\hbar\Omega \gtrsim \Delta$.
18. This transition cannot be captured within the theory in the narrow resonance limit [220], as the bosonic molecules are non-interacting so the Laughlin state does not appear.
19. The relation $\nu_\mathrm{m} = \nu_\mathrm{a}/4$ follows from the fact that there are half as many molecules as atoms, and the vortex density for a molecule is twice that for an atom [119].
20. The lowest-energy gap is proportional to V_0 in the two-dimensional LLL, $V_0 \ll \hbar\omega_\perp$. For $V_0 \gg \hbar\omega_\perp$, there will be mixing of Landau levels and the lowest-energy gap will not grow beyond the cyclotron gap $2\hbar\omega_\perp$.

References

[1] R.J. Donnelly, *Quantized Vortices in Helium II*, Cambridge University Press, Cambridge, 1991.
[2] E.A. Cornell and C.E. Wieman, Rev. Mod. Phys. 74 (2002), pp. 875–893.
[3] W. Ketterle, Rev. Mod. Phys. 74 (2002), pp. 1131–1151.
[4] I. Bloch, J. Dalibard, and W. Zwerger, Rev. Mod. Phys. 80 (2008), p. 885.

[5] P.E. Sokol, in *Bose-Einstein Condensation*, A. Griffin, D.W. Snoke, and S. Stringari, eds., Cambridge University Press, Cambridge, 1995, p. 51.
[6] A.J. Leggett, Rev. Mod. Phys. 73 (2001), pp. 307–356.
[7] H.E. Hall and W.F. Vinen, Proc. Roy. Soc. A 238 (1956), pp. 204–214.
[8] N.R. Cooper, *Les Houches Lecture Notes*, 2008, (Unpublished).
[9] L.J. Campbell and R.M. Ziff, Phys. Rev. B 20 (1979), pp. 1886–1902.
[10] E.J. Yarmchuk, M.J.V. Gordon, and R.E. Packard, Phys. Rev. Lett. 43 (1979), pp. 214–217.
[11] E.J. Yarmchuk and R.E. Packard, J. Low Temp. Phys. 46 (1982), pp. 479–515.
[12] K.W. Madison, F. Chevy, W. Wohlleben, and J. Dalibard, Phys. Rev. Lett. 84 (2000), pp. 806–809.
[13] J.R. Abo-Shaeer, C. Raman, J.M. Vogels, and W. Ketterle, Science 292 (2001), p. 476.
[14] E. Hodby, G. Hechenblaikner, S.A. Hopkins, O.M. Marago, and C.J. Foot, Phys. Rev. Lett. 88 (2002), p. 010405.
[15] D.L. Feder, A.A. Svidzinsky, A.L. Fetter, and C.W. Clark, Phys. Rev. Lett. 86 (2001), pp. 564–567.
[16] F. Dalfovo and S. Stringari, Phys. Rev. A 63 (2000), p. 011601.
[17] K.W. Madison, F. Chevy, V. Bretin, and J. Dalibard, Phys. Rev. Lett. 86 (2001), pp. 4443–4446.
[18] C. Lobo, A. Sinatra, and Y. Castin, Phys. Rev. Lett. 92 (2004), p. 020403.
[19] I. Coddington, P. Engels, V. Schweikhard, and E.A. Cornell, Phys. Rev. Lett. 91 (2003), p. 100402.
[20] V. Schweikhard, I. Coddington, P. Engels, V.P. Mogendorff, and E.A. Cornell, Phys. Rev. Lett. 92 (2004), p. 040404.
[21] N.K. Wilkin, J.M.F. Gunn, and R.A. Smith, Phys. Rev. Lett. 80 (1998), p. 2265.
[22] N.R. Cooper, N.K. Wilkin, and J.M.F. Gunn, Phys. Rev. Lett. 87 (2001), p. 120405.
[23] R.E. Prange and S.M. Girvin (eds.), *The Quantum Hall Effect*, 2nd ed., Springer, Berlin, 1990.
[24] S.D. Sarma and A. Pinczuk (eds.), *Perspectives in Quantum Hall Effects: Novel Quantum Liquids in Low-Dimensional Semiconductor Structures*, Wiley, New York, 1997.
[25] S. Tung, V. Schweikhard, and E.A. Cornell, Phys. Rev. Lett. 97 (2006), p. 240402.
[26] M. Hafezi, A.S. Sørensen, E. Demler, and M.D. Lukin, Phys. Rev. A 76 (2007), p. 023613.
[27] D. Jaksch and P. Zoller, New J. Phys. 5 (2003), p. 56.
[28] E.J. Mueller, Phys. Rev. A 70 (2004), p. 041603.
[29] A.S. Sørensen, E. Demler, and M.D. Lukin, Phys. Rev. Lett. 94 (2005), p. 086803.
[30] R.N. Palmer and D. Jaksch, Phys. Rev. Lett. 96 (2006), p. 180407.
[31] R.N. Palmer, A. Klein, and D. Jaksch, Phys. Rev. A 78 (2008), p. 013609.
[32] A.L. Fetter, Rotating trapped Bose-Einstein condensates, Preprint arXiv:0801.2952 (2008).
[33] L.D. Landau and E.M. Lifshitz, *Statistical Physics Part 1*, Vol. 5, Butterworth Heinemann, Oxford, 1981, Section 26.
[34] J. Fröhlich, *Les Houches Lecture Notes*, Elsevier, Amsterdam, 1994.
[35] V. Fock, Z. Phys. 47 (1928), p. 446.
[36] C.G. Darwin, Proc. Cambridge Philos. Soc. 27 (1930), p. 86.
[37] A.G. Morris and D.L. Feder, Phys. Rev. A 74 (2006), p. 033605.
[38] T.L. Ho, Phys. Rev. Lett. 87 (2001), p. 060403.
[39] Z. Tesanovic, Phys. Rev. B 44 (1991), pp. 12635–12638.
[40] D.A. Butts and D.S. Rokhsar, Nature 397 (1999), pp. 327–329.
[41] N.R. Cooper, S. Komineas, and N. Read, Phys. Rev. A 70 (2004), p. 033604.
[42] A. Aftalion, X. Blanc, and J. Dalibard, Phys. Rev. A 71 (2005), p. 023611.
[43] G. Watanabe, G. Baym, and C.J. Pethick, Phys. Rev. Lett. 93 (2004), p. 190401.
[44] A. Abrikosov, Zh. Eksp. Teor. Fiz. 32 (1957), p. 1442.
[45] W.H. Kleiner, L.M. Roth, and S.H. Autler, Phys. Rev. 133 (1964), pp. A1226–A1227.
[46] U.R. Fischer and G. Baym, Phys. Rev. Lett. 90 (2003), p. 140402.
[47] M. Cozzini, S. Stringari, and C. Tozzo, Phys. Rev. A 73 (2006), p. 023615.

[48] I. Coddington, P.C. Haljan, P. Engels, V. Schweikhard, S. Tung, and E.A. Cornell, Phys. Rev. A 70 (2004), p. 063607.
[49] J. Sinova, C.B. Hanna, and A.H. MacDonald, Phys. Rev. Lett. 89 (2002), p. 030403.
[50] G. Baym, Phys. Rev. A 69 (2004), p. 043618.
[51] V. Schweikhard, I. Coddington, P. Engels, S. Tung, and E.A. Cornell, Phys. Rev. Lett. 93 (2004), p. 210403.
[52] E.B. Sonin, Phys. Rev. A 72 (2005), p. 021606.
[53] A.L. Fetter, Phys. Rev. A 75 (2007), p. 013620.
[54] M. Linn, M. Niemeyer, and A.L. Fetter, Phys. Rev. A 64 (2001), p. 023602.
[55] M.O. Oktel, Phys. Rev. A 69 (2004), p. 023618.
[56] S. Sinha and G.V. Shlyapnikov, Phys. Rev. Lett. 94 (2005), p. 150401.
[57] P. Sánchez-Lotero and J.J. Palacios, Phys. Rev. A 72 (2005), p. 043613.
[58] M. Baranov, L. Dobrek, K. Goral, L. Santos, and M. Lewenstein, Phys. Scr. T 102 (2002), p. 74.
[59] A. Griesmaier, J. Werner, S. Hensler, J. Stuhler, and T. Pfau, Phys. Rev. Lett. 94 (2005), p. 160401.
[60] T. Lahaye, T. Koch, B. Frählich, M. Fattori, J. Metz, A. Griesmaier, S. Giovanazzi, and T. Pfau, Nature 448 (2007), p. 672.
[61] K.K. Ni, S. Ospelkaus, M.H.G. de Miranda, A. Pe'er, B. Neyenhuis, J.J. Zirbel, S. Kotochigova, P.S. Julienne, D.S. Jin and J. Ye, A high phase-space-density gas of polar molecules, Preprint arXiv:0808.2963 (2008).
[62] N.R. Cooper, E.H. Rezayi, and S.H. Simon, Phys. Rev. Lett. 95 (2005), p. 200402.
[63] J. Zhang and H. Zhai, Phys. Rev. Lett. 95 (2005), p. 200403.
[64] A.A. Koulakov, M.M. Fogler, and B.I. Shklovskii, Phys. Rev. Lett. 76 (1996), pp. 499–502.
[65] R. Moessner and J.T. Chalker, Phys. Rev. B 54 (1996), pp. 5006–5015.
[66] Hurley, M. M. and Singer, S. J. J. Phys. Chem., 96 (1992), pp. 1938–1950.
[67] S. Komineas and N.R. Cooper, Phys. Rev. A 75 (2007), p. 023623.
[68] R.A. Smith and N.K. Wilkin, Phys. Rev. A 62 (2000), p. 061602.
[69] G.F. Bertsch and T. Papenbrock, Phys. Rev. Lett. 83 (1999), pp. 5412–5414.
[70] M.S. Hussein and O.K. Vorov, Phys. Rev. A 65 (2002), p. 035603.
[71] O.K. Vorov, M.S. Hussein, and P.V. Isacker, Phys. Rev. Lett. 90 (2003), p. 200402.
[72] A.D. Jackson and G.M. Kavoulakis, Phys. Rev. Lett. 85 (2000), pp. 2854–2856.
[73] E.H. Lieb and R. Seiringer, Commun. Math. Phys. 264 (2006), pp. 505–537.
[74] A.D. Jackson, G.M. Kavoulakis, B. Mottelson, and S.M. Reimann, Phys. Rev. Lett. 86 (2001), pp. 945–949.
[75] P.W. Anderson, Chapter 2, *Basic notions of condensed matter physics*, in *Frontiers in Physics*, Vol. 55, Benjamin Cummings, New York, 1984.
[76] N.R. Cooper, Vortex Liquids and Vortex Lattices in Weakly Interacting Bose Gases, Proceedings of CMMP 2000 (2000), SSp.P2.29.
[77] M. Ueda and T. Nakajima, Phys. Rev. A 73 (2006), p. 043603.
[78] D. Dagnino, N. Barberán, K. Osterloh, A. Riera, and M. Lewenstein, Phys. Rev. A 76 (2007), p. 013625.
[79] M.I. Parke, N.K. Wilkin, J.M.F. Gunn, and A. Bourne, Phys. Rev. Lett. 101 (2008), p. 110401.
[80] I. Romanovsky, C. Yannouleas, and U. Landman, Phys. Rev. A 78 (2008), p. 011606.
[81] R.B. Laughlin, Phys. Rev. Lett. 50 (1983), pp. 1395–1398.
[82] N.K. Wilkin and J.M.F. Gunn, Phys. Rev. Lett. 84 (2000), pp. 6–9.
[83] N.R. Cooper and N.K. Wilkin, Phys. Rev. B 60 (1999), pp. R16279–R16282.
[84] J.K. Jain, Phys. Rev. Lett. 63 (1989), pp. 199–202.
[85] O. Heinonen, *Composite Fermions: A Unified View of the Quantum Hall Regime*, World Scientific, Singapore, 1998.
[86] J.K. Jain and T. Kawamura, Europhys. Lett. 29 (1995), pp. 321–326.
[87] N. Barberán, M. Lewenstein, K. Osterloh, and D. Dagnino, Phys. Rev. A 73 (2006), p. 063623.

[88] I. Romanovsky, C. Yannouleas, and U. Landman, Phys. Rev. Lett. 93 (2004), p. 230405.
[89] L.O. Baksmaty, C. Yannouleas, and U. Landman, Phys. Rev. A 75 (2007), p. 023620.
[90] V. Schweikhard, I. Coddington, P. Engels, V.P. Mogendorff, and E.A. Cornell, Phys. Rev. Lett. 92 (2004), p. 040404.
[91] A.L. Fetter, Phys. Rev. 162 (1967), pp. 143–153.
[92] F.D.M. Haldane and Y.S. Wu, Phys. Rev. Lett. 55 (1985), pp. 2887–2890.
[93] A. Rozhkov and D. Stroud, Phys. Rev. B 54 (1996), pp. R12697–R12700.
[94] V. Tkachenko, Zh. Eksp. Teor. Fiz. 49 (1965), p. 1875 [Sov. Phys. JETP 22, 1282 (1966)].
[95] V. Tkachenko, Zh. Eksp. Teor. Fiz. 50 (1966), p. 1573 [Sov. Phys. JETP 23, 1049 (1966)].
[96] V. Tkachenko, Zh. Eksp. Teor. Fiz. 56 (1969), p. 1763 [Sov. Phys. JETP 29, 245 (1969)].
[97] N.R. Cooper and E.H. Rezayi, Phys. Rev. A 75 (2007), p. 013627.
[98] S.M. Girvin and A.H. MacDonald, Phys. Rev. Lett. 58 (1987), pp. 1252–1255.
[99] N. Read, Phys. Rev. Lett. 62 (1989), pp. 86–89.
[100] N. Regnault and T. Jolicoeur, Phys. Rev. Lett. 91 (2003), p. 030402.
[101] N. Regnault and T. Jolicoeur, Phys. Rev. B 69 (2004), p. 235309.
[102] S. Viefers, T.H. Hansson, and S.M. Reimann, Phys. Rev. A 62 (2000), p. 053604.
[103] B.I. Halperin, Phys. Rev. Lett. 52 (1984), pp. 1583–1586.
[104] C.C. Chang, N. Regnault, T. Jolicoeur, and J.K. Jain, Phys. Rev. A 72 (2005), p. 013611.
[105] X.G. Wen, Adv. Phys. 44 (1995), p. 405.
[106] M.A. Cazalilla, Phys. Rev. A 67 (2003), p. 063613.
[107] M.A. Cazalilla, N. Barberán, and N.R. Cooper, Phys. Rev. B 71 (2005), p. 121303.
[108] E.H. Rezayi, N. Read, and N.R. Cooper, Phys. Rev. Lett. 95 (2005), p. 160404.
[109] N. Regnault and T. Jolicoeur, Phys. Rev. B 76 (2007), p. 235324.
[110] C. Nayak, S.H. Simon, A. Stern, M. Freedman, and S.D. Sarma, Rev. Mod. Phys. 80 (2008), p. 1083.
[111] G. Moore and N. Read, Nucl. Phys. B 360 (1991), pp. 362–396.
[112] N. Read and E.H. Rezayi, Phys. Rev. B 59 (1999), pp. 8084–8092.
[113] E.H. Rezayi, N. Read, Non-Abelian quantized Hall states of electrons at filling factors 12/5 and 13/5 in the first excited Landau level, Preprint arXiv:0608346 (2006).
[114] A. Cappelli, L.S. Georgiev, and I.T. Todorov, Nucl. Phys. B 559 (2001), p. 499.
[115] N.K. Wilkin and J.M.F. Gunn, Phys. Rev. Lett. 84 (2000), pp. 6–9.
[116] M. Oshikawa, Y.B. Kim, K. Shtengel, C. Nayak, and S. Tewari, Ann. Phys. 322 (2007), p. 1477.
[117] B. Chung and T. Jolicoeur, Phys. Rev. A 77 (2008), p. 043608.
[118] N. Regnault and T. Jolicoeur, Mod. Phys. Lett. B 51 (2004), p. 1003.
[119] N.R. Cooper, Phys. Rev. Lett. 92 (2004), p. 220405.
[120] H. Seki and K. Ino, Phys. Rev. A 77 (2008), p. 063602.
[121] N.R. Cooper, E.H. Rezayi, and S.H. Simon, Solid State Commun. 140 (2006), p. 61.
[122] B.I. Halperin, P.A. Lee, and N. Read, Phys. Rev. B 47 (1993), pp. 7312–7343.
[123] M.A. Baranov, H. Fehrmann, and M. Lewenstein, Phys. Rev. Lett. 100 (2008), p. 200402.
[124] A. Aftalion, X. Blanc, and F. Nier, Phys. Rev. A 73 (2006), p. 011601.
[125] N.R. Cooper, F.J.M. van Lankvelt, J.W. Reijnders, and K. Schoutens, Phys. Rev. A 72 (2005), p. 063622.
[126] M. Snoek and H.T.C. Stoof, Phys. Rev. Lett. 96 (2006), p. 230402.
[127] M. Snoek and H.T.C. Stoof, Phys. Rev. A 74 (2006), p. 033615.
[128] J.P. Martikainen and H.T.C. Stoof, Phys. Rev. Lett. 91 (2003), p. 240403.
[129] A.T. Fiory, A.F. Hebard, and S. Somekh, Appl. Phys. Lett. 32 (1978), pp. 73–75.
[130] C. Reichhardt, C.J. Olson, and F. Nori, Phys. Rev. B 57 (1998), pp. 7937–7943.
[131] W.V. Pogosov, A.L. Rakhmanov, and V.V. Moshchalkov, Phys. Rev. B 67 (2003), p. 014532.
[132] C. Reichhardt, C.J. Olson, and F. Nori, Phys. Rev. Lett. 78 (1997), pp. 2648–2651.

[133] S. Tung, V. Schweikhard, and E.A. Cornell, Phys. Rev. Lett. 97 (2006), p. 240402.
[134] D. Jaksch, C. Bruder, J.I. Cirac, C.W. Gardiner, and P. Zoller, Phys. Rev. Lett. 81 (1998), pp. 3108–3111.
[135] M. Greiner, O. Mandel, T. Esslinger, T.W. Hansch, and I. Bloch, Nature 415 (2001), pp. 39–44.
[136] D. Jaksch and P. Zoller, New J. Phys. 5 (2003), p. 56.
[137] K. Osterloh, M. Baig, L. Santos, P. Zoller, and M. Lewenstein, Phys. Rev. Lett. 95 (2005), p. 010403.
[138] J.W. Reijnders and R.A. Duine, Phys. Rev. Lett. 93 (2004), p. 060401.
[139] J.W. Reijnders and R.A. Duine, Phys. Rev. A 71 (2005), p. 063607.
[140] H. Pu, L.O. Baksmaty, S. Yi, and N.P. Bigelow, Phys. Rev. Lett. 94 (2005), p. 190401.
[141] T. Sato, T. Ishiyama, and T. Nikuni, Phys. Rev. A 76 (2007), p. 053628.
[142] M. Polini, R. Fazio, A.H. MacDonald, and M.P. Tosi, Phys. Rev. Lett. 95 (2005), p. 010401.
[143] K. Kasamatsu, J. Low Temp. Phys. 50 (2008), pp. 593–598.
[144] S. Teitel and C. Jayaprakash, Phys. Rev. Lett. 51 (1983), pp. 1999–2002.
[145] T.C. Halsey, Phys. Rev. B 31 (1985), pp. 5728–5745.
[146] J.P. Straley and G.M. Barnett, Phys. Rev. B 48 (1993), pp. 3309–3315.
[147] P.G. Harper, Proc. Phys. Soc. A 68 (1955), pp. 874–878.
[148] D.R. Hofstadter, Phys. Rev. B 14 (1976), pp. 2239–2249.
[149] C. Wu, H.D. Chen, J.P. Hu, and S.C. Zhang, Phys. Rev. A 69 (2004), p. 043609.
[150] M.O. Oktel, M. Niţă, and B. Tanatar, Phys. Rev. B 75 (2007), p. 045133.
[151] D.S. Goldbaum and E.J. Mueller, Phys. Rev. A 77 (2008), p. 033629.
[152] P. Vignolo, R. Fazio, and M.P. Tosi, Phys. Rev. A 76 (2007), p. 023616.
[153] A.A. Burkov and E. Demler, Phys. Rev. Lett. 96 (2006), p. 180406.
[154] M. Hafezi, A.S. Sørensen, M.D. Lukin, and E. Demler, Europhys. Lett. 81 (2008), p. 10005.
[155] R. Bhat, M.J. Holland, and L.D. Carr, Phys. Rev. Lett. 96 (2006), p. 060405.
[156] R. Bhat, B.M. Peden, B.T. Seaman, M. Krämer, L.D. Carr, and M.J. Holland, Phys. Rev. A 74 (2006), p. 063606.
[157] R. Bhat, M. Krämer, J. Cooper, and M.J. Holland, Phys. Rev. A 76 (2007), p. 043601.
[158] B.I. Halperin, Helv. Phys. Acta 56 (1983), pp. 75–102.
[159] T.L. Ho and V.B. Shenoy, Phys. Rev. Lett. 77 (1996), pp. 3276–3270.
[160] B.D. Esry, C.H. Greene, J.P. Burke Jr, and J.L. Bohn, Phys. Rev. Lett. 78 (1997), pp. 3594–3597.
[161] K. Kasamatsu, M. Tsubota, and M. Ueda, Phys. Rev. A 71 (2005), p. 043611.
[162] E.G.M. van Kempen, S.J.J.M.F. Kokkelmans, D.J. Heinzen, and B.J. Verhaar, Phys. Rev. Lett. 88 (2002), p. 093201.
[163] D.M. Harber, H.J. Lewandowski, J.M. McGuirk, and E.A. Cornell, Phys. Rev. A 66 (2002), p. 053616.
[164] P. Ao and S.T. Chui, Phys. Rev. A 58 (1998), pp. 4836–4840.
[165] C.J. Myatt, E.A. Burt, R.W. Ghrist, E.A. Cornell, and C.E. Wieman, Phys. Rev. Lett. 78 (1997), pp. 586–589.
[166] H.J. Miesner, D.M. Stamper-Kurn, J. Stenger, S. Inouye, A.P. Chikkatur, and W. Ketterle, Phys. Rev. Lett. 82 (1999), pp. 2228–2231.
[167] G. Modugno, M. Modugno, F. Riboli, G. Roati, and M. Inguscio, Phys. Rev. Lett. 89 (2002), p. 190404.
[168] G. Thalhammer, G. Barontini, L.D. Sarlo, J. Catani, F. Minardi, and M. Inguscio, Phys. Rev. Lett. 100 (2008), p. 210402.
[169] S.B. Papp, J.M. Pino, and C.E. Wieman, Phys. Rev. Lett. 101 (2008), p. 040402.
[170] M.R. Matthews, B.P. Anderson, P.C. Haljan, D.S. Hall, C.E. Wieman, and E.A. Cornell, Phys. Rev. Lett. 83 (1999), pp. 2498–2501.
[171] E.J. Mueller, Phys. Rev. A 69 (2004), p. 033606.

[172] S.T. Chui, V.N. Ryzhov, and E.E. Tareyeva, Phys. Rev. A 63 (2001), p. 023605.
[173] D.M. Jezek, P. Capuzzi, and H.M. Cataldo, Phys. Rev. A 64 (2001), p. 023605.
[174] U. Leonhardt and G. Volovik, JETP Lett. 72 (2000), p. 46.
[175] S. Bargi, J. Christensson, G.M. Kavoulakis, and S.M. Reimann, Phys. Rev. Lett. 98 (2007), p. 130403.
[176] J.W. Reijnders, F.J.M. van Lankvelt, K. Schoutens, and N. Read, Phys. Rev. A 69 (2004), p. 023612.
[177] E.J. Mueller and T.L. Ho, Phys. Rev. Lett. 88 (2002), p. 180403.
[178] K. Kasamatsu, M. Tsubota, and M. Ueda, Phys. Rev. Lett. 91 (2003), p. 150406.
[179] S.J. Woo, S. Choi, L.O. Baksmaty, and N.P. Bigelow, Phys. Rev. A 75 (2007), p. 031604.
[180] M. Keçeli and M.O. Oktel, Phys. Rev. A 73 (2006), p. 023611.
[181] V. Schweikhard, I. Coddington, P. Engels, S. Tung, and E.A. Cornell, Phys. Rev. Lett. 93 (2004), p. 210403.
[182] E. Ardonne and K. Schoutens, Phys. Rev. Lett. 82 (1999), pp. 5096–5099.
[183] R. Barnett, G. Refael, M.A. Porter, and H.P. Büchler, New Journal of Physics 10 (2008), p. 043030.
[184] S.J. Woo, Q.H. Park, and N.P. Bigelow, Phys. Rev. Lett. 100 (2008), p. 120403.
[185] T. Ohmi and K. Machida, J. Phys. Soc. Jpn. 67 (2008), pp. 1822–1825.
[186] T.L. Ho, Phys. Rev. Lett. 81 (1998), pp. 742–745.
[187] F. Zhou, Phys. Rev. Lett. 87 (2001), p. 080401.
[188] M.D. Barrett, J.A. Sauer, and M.S. Chapman, Phys. Rev. Lett. 87 (2001), p. 010404.
[189] D.M. Stamper-Kurn, M.R. Andrews, A.P. Chikkatur, S. Inouye, H.J. Miesner, J. Stenger, and W. Ketterle, Phys. Rev. Lett. 80 (1998), pp. 2027–2030.
[190] J. Stenger, S. Inouye, D.M. Stamper-Kurn, H.J. Miesner, A.P. Chikkatur, and W. Ketterle, Nature 396 (1998), pp. 345–348.
[191] S.K. Yip, Phys. Rev. Lett. 83 (1999), pp. 4677–4681.
[192] T. Mizushima, K. Machida, and T. Kita, Phys. Rev. Lett. 89 (2002), p. 030401.
[193] J.P. Martikainen, A. Collin, and K.A. Suominen, Phys. Rev. A 66 (2002), p. 053604.
[194] T. Kita, T. Mizushima, and K. Machida, Phys. Rev. A 66 (2002), p. 061601.
[195] T.L. Ho and E.J. Mueller, Phys. Rev. Lett. 89 (2002), p. 050401.
[196] B. Paredes, P. Zoller, and J.I. Cirac, Phys. Rev. A 66 (2002), p. 033609.
[197] J.W. Reijnders, F.J.M. Lankveltvan, K. Schoutens, and N. Read, Phys. Rev. Lett. 89 (2002), p. 120401.
[198] B. DeMarco and D.S. Jin, Science 285 (1999), pp. 1703–1706.
[199] C.A. Regal, C. Ticknor, J.L. Bohn, and D.S. Jin, Phys. Rev. Lett. 90 (2003), p. 053201.
[200] T.L. Ho and C.V. Ciobanu, Phys. Rev. Lett. 85 (2000), pp. 4648–4651.
[201] M.A. Baranov, K. Osterloh, and M. Lewenstein, Phys. Rev. Lett. 94 (2005), p. 070404.
[202] K. Osterloh, N. Barberán, and M. Lewenstein, Phys. Rev. Lett. 99 (2007), p. 160403.
[203] K. Günter, T. Stöferle, H. Moritz, M. Köhl, and T. Esslinger, Phys. Rev. Lett. 95 (2005), p. 230401.
[204] J.P. Gaebler, J.T. Stewart, J.L. Bohn, and D.S. Jin, Phys. Rev. Lett. 98 (2007), p. 200403.
[205] J. Zhang, E.G.M. Kempenvan, T. Bourdel, L. Khaykovich, J. Cubizolles, F. Chevy, M. Teichmann, L. Tarruell, S.J.J.M.F. Kokkelmans, and C. Salomon, Phys. Rev. A 70 (2004), p. 030702.
[206] C.H. Schunck, M.W. Zwierlein, C.A. Stan, S.M.F. Raupach, W. Ketterle, A. Simoni, E. Tiesinga, C.J. Williams, and P.S. Julienne, Phys. Rev. A 71 (2005), p. 045601.
[207] Y. Inada, M. Horikoshi, S. Nakajima, M. Kuwata-Gonokami, M. Ueda, and T. Mukaiyama, Phys. Rev. Lett. 101 (2008), p. 100401.
[208] V. Gurarie and L. Radzihovsky, Ann. Phys. 322 (2007), p. 2.
[209] N. Regnault and T. Jolicoeur, Phys. Rev. B 70 (2004), p. 241307.
[210] F.D.M. Haldane, Phys. Rev. Lett. 51 (1983), pp. 605–608.

[211] J. Levinsen, N.R. Cooper, and V. Gurarie, Phys. Rev. Lett. 99 (2007), p. 210402.
[212] W. Ketterle and M. Zwierlein, *Making, probing and understanding ultracold Fermi gases*, in *Ultracold Fermi Gases*, M. Inguscio, W. Ketterle, and C. Salomon, eds., IOS Press, Amsterdam, 2008.
[213] R. Grimm, in *Ultracold Fermi gases in the BEC–BCS crossover: a Review from the Innsbruck perspective*, M. Inguscio, W. Ketterle, and C. Salomon, eds., IOS Press, Amsterdam, 2008.
[214] M.W. Zwierlein, A. Schirotzek, C.H. Schunck, and W. Ketterle, Science 311 (2006), pp. 492–496.
[215] G.B. Partridge, W. Li, R.I. Kamar, Y.A. Liao, and R.G. Hulet, Science 311 (2006), pp. 503–505.
[216] M.W. Zwierlein, J.R. Abo-Shaeer, A. Schirotzek, C.H. Schunck, and W. Ketterle, Nature 435 (2005), p. 1047.
[217] P. Gorkov, Zh. Eksp. Teor. Phys. 36 (1959), p. 1918 [JETP 9 1364 (1959)].
[218] P. Gorkov, Zh. Eksp. Teor. Phys. 37 (1959), p. 833 [JETP 10 593 (1960)].
[219] N.R. Werthamer, E. Helfand, and P.C. Hohenberg, Phys. Rev. 147 (1966), pp. 295–302.
[220] M.Y. Veillette, D.E. Sheehy, L. Radzihovsky, and V. Gurarie, Phys. Rev. Lett. 97 (2006), p. 250401.
[221] A.V. Andreev, V. Gurarie, and L. Radzihovsky, Phys. Rev. Lett. 93 (2004), p. 130402.
[222] H. Zhai and T.L. Ho, Phys. Rev. Lett. 97 (2006), p. 180414.
[223] G. Möller and N.R. Cooper, Phys. Rev. Lett. 99 (2007), p. 190409.
[224] M. Rasolt and Z. Tešanović, Rev. Mod. Phys. 64 (1992), pp. 709–754.
[225] F.D.M. Haldane, E.H. Rezayi, KITP conference, and private communication (2004).
[226] K. Yang and H. Zhai, Phys. Rev. Lett. 100 (2008), p. 030404.
[227] N. Read and N.R. Cooper, Phys. Rev. A 68 (2003), p. 035601.
[228] J. Sinova, C.B. Hanna, and A.H. MacDonald, Phys. Rev. Lett. 90 (2003), p. 120401.
[229] E. Altman, E. Demler, and M.D. Lukin, Phys. Rev. A 70 (2004), p. 013603.
[230] L.O. Baksmaty, S.J. Woo, M. Banks, S. Choi, and N.P. Bigelow, Phys. Rev. A 72 (2005), p. 063615.
[231] B. Paredes, P. Fedichev, J.I. Cirac, and P. Zoller, Phys. Rev. Lett. 87 (2001), p. 010402.
[232] S.B. Papp, J.M. Pino, R.J. Wild, S. Ronen, C.E. Wieman, D.S. Jin, and E.A. Cornell, Phys. Rev. Lett. 101 (2008), p. 135301.
[233] D.S. Petrov, C. Salomon, and G.V. Shlyapnikov, Phys. Rev. Lett. 93 (2004), p. 090404.
[234] M. Antezza, M. Cozzini, and S. Stringari, Phys. Rev. A 75 (2007), p. 053609.
[235] R. Folman, P. Krüger, J. Schmiedmayer, J. Denschlag, and C. Henkel, Adv. At. Mol. Opt. Phys. 48 (2002), p. 263.
[236] M. Popp, B. Paredes, and J.I. Cirac, Phys. Rev. A 70 (2004), p. 053612.
[237] S.K. Baur, K.R.A. Hazzard, E.J. Mueller, Stirring trapped atoms into fractional quantum Hall puddles, Preprint arXiv:0806.1517 (2008).
[238] G. Juzeliūnas, J. Ruseckas, P. Öhberg, and M. Fleischhauer, Phys. Rev. A 73 (2006), p. 025602.
[239] Y.J. Lin, R.L. Compton, A.R. Perry, W.D. Phillips, J.V. Porto, I.B. Spielman, A Bose–Einstein condensate in a uniform light-induced vector potential, Preprint arXiv:0809.2976 (2008).
[240] A.L. Fetter and J.D. Walecka, Quantum Theory of Many-Particle Systems, Dover Publications, 2003.
[241] N. d'Ambrumenil and R. Morf, Phys. Rev. B 40 (1989), pp. 6108–6119.
[242] F.D.M. Haldane, Phys. Rev. Lett. 55 (1985), pp. 2095–2098.
[243] G. Fano, F. Ortolani, and E. Colombo, Phys. Rev. B 34 (1986), pp. 2670–2680.
[244] D. Yoshioka, B.I. Halperin, and P.A. Lee, Phys. Rev. Lett. 50 (1983), pp. 1219–1222.

Appendix A: Haldane pseudo-potentials

Within the space of two-dimensional LLL states, any two-body interaction that is rotationally-symmetric in the two-dimensional plane can be conveniently parameterized by its

'Haldane pseudo-potentials' [210]. Owing to the rotational symmetry, the interaction conserves the relative angular momentum of two particles. Thus, its effects are determined by the expectation value of the two-body potential in the two-particle wavefunction

$$\Psi_{m_c,m}(\boldsymbol{r}_1,\boldsymbol{r}_2) \propto (\zeta_1+\zeta_2)^{m_c}(\zeta_1-\zeta_2)^m e^{-|\zeta_1|^2/4} e^{-|\zeta_2|^2/4} e^{-z_1^2/2a_\parallel^2} e^{-z_2^2/2a_\parallel^2} \tag{A1}$$

$$V_m = \int\int V(\boldsymbol{r}_1-\boldsymbol{r}_2)|\Psi_{m_c,m}(\boldsymbol{r}_1,\boldsymbol{r}_2)|^2\, d^3\boldsymbol{r}_1\, d^3\boldsymbol{r}_2, \tag{A2}$$

where m and m_c are the relative and centre-of-mass angular momenta. For spinless bosonic (fermionic) particles, m must be even (odd) so only the subset of even (odd) Haldane pseudo-potentials of the interaction are important. For contact interactions (13), the only non-zero pseudo-potential is

$$V_0 = \frac{4\pi\hbar^2 a_s}{M}\int d^3\boldsymbol{r}\, \frac{1}{(\pi a_\perp^2)^2} e^{-2(x^2+y^2)/a_\perp^2} \frac{1}{(\pi a_\parallel^2)} e^{-2z^2/a_\parallel^2} = \sqrt{\frac{2}{\pi}}\frac{\hbar^2 a_s}{a_\perp^2 a_\parallel}. \tag{A3}$$

This is the only energy scale entering the low-energy physics of a rapidly rotating Bose gas in the two-dimensional LLL regime.

For the three-dimensional LLL regime (34), an approximation often made [38] is that the particle density in the z direction is set by the Thomas–Fermi distribution. (See Section 2.6 for a discussion of this approximation.) One can view this as a change in the subband wavefunction in the z direction, $\varphi(z)$. In the Thomas–Fermi approximation, the normalized particle density in the z direction is taken to be

$$|\varphi_{\rm TF}(z)|^2 = \frac{3}{4W_z}\left(1-\frac{z^2}{W_z^2}\right), \quad (|z| \le W_z), \tag{A4}$$

in which the extension along the z-axis, W_z, is set by the chemical potential, $\mu = (1/2)M\omega_\parallel^2 W_z^2$. The only influence of the subband wavefunction in the z-direction $\varphi(z)$ is to introduce a numerical factor to the Haldane pseudo-potentials, which for contact interactions is $\int {\rm d}z|\varphi(z)|^4$. Using the Thomas–Fermi form for the particle density in the z direction leads to

$$V_0^{\rm TF} = \frac{6}{5}\frac{\hbar^2 a_s}{M a_\perp^2 W_z}. \tag{A5}$$

Appendix B: Numerical techniques

Determining the groundstate of a rapidly rotating atomic gas in a harmonic well poses an essentially strongly interacting, non-perturbative theoretical problem. In the absence of interactions, the many-particle states at high angular momentum are degenerate, see Section 2.1. Interactions lift this degeneracy and select a groundstate. To understand the properties of the groundstate (and the low-lying excitations) it has proved very useful to make use of exact diagonalization studies.

The restriction of single-particle states to the two-dimensional LLL (21) limits the size of the Hilbert space. This makes exact diagonalization feasible for systems that can be large enough to observe clear signatures of strongly correlated many-particle states. Numerical studies have been performed in several different geometries, described in detail below. In each case, the strategy is the use of the 'configuration interaction' method.

- One chooses a finite number of (orthonormal) single-particle basis states, $\phi_\alpha(\boldsymbol{r})$, with $\alpha = 1, 2, \ldots, M$ which span the two-dimensional LLL for the geometry considered. For example, in the uniform plane, these are the two-dimensional LLL wavefunctions of (21) with α labelling the angular momentum $m = 0, 1, \ldots, M-1$, where M sets the

cut-off in total angular momentum. The wavefunctions in other geometries are discussed below. The interaction Hamiltonian may then be written in a second-quantized form as [240]:

$$\hat{V} = \frac{1}{2} \sum_{\alpha,\beta,\gamma,\delta=1}^{M} V_{\alpha\beta\gamma\delta} \hat{a}_\alpha^\dagger \hat{a}_\beta^\dagger \hat{a}_\gamma \hat{a}_\delta, \tag{B1}$$

where $\hat{a}^{(\dagger)}$ are the field operators for particles (which could be bosons or fermions) in the single-particle state $\phi_\alpha(\boldsymbol{r})$. The matrix elements are

$$V_{\alpha\beta\gamma\delta} \equiv \langle \alpha\beta | \hat{V} | \delta\gamma \rangle = \int d^3\boldsymbol{r} \int d^3\boldsymbol{r}' \phi_\alpha^*(\boldsymbol{r}) \phi_\beta'^*(\boldsymbol{r}') \phi_\gamma(\boldsymbol{r}') \phi_\delta(\boldsymbol{r})\ V(\boldsymbol{r} - \boldsymbol{r}') \tag{B2}$$

where $V(\boldsymbol{r})$ is the two-body interaction potential.

- One generates a complete set of (orthogonal) many-particle basis states for a system of N particles occupying the single-particle basis $\phi_\alpha(\boldsymbol{r})$, with $\alpha = 1, 2, \ldots, M$. These states are conveniently taken to be the Fock states, represented by the occupation numbers of the M orbitals, $|n_1, n_2, \ldots, n_M\rangle$. (The Fock states are symmetric/antisymmetric under particle exchange for the case of spinless bosons/fermions.) For bosons, the total number of such many-particle states is

$$\frac{(N+M-1)!}{N!(M-1)!} \overset{N,M\to\infty}{\longrightarrow} e^{\gamma N}, \tag{B3}$$

where the limit $N \to \infty$ is taken with fixed $\nu = N/M$, which sets the value γ. The number of basis states can be reduced by the use of symmetries, which depend on the geometry (see below). Nevertheless, the general feature that the number of basis states grows exponentially with system size survives, and sets the ultimate limitation to exact diagonalization studies.

- Within the (symmetry reduced) many-particle basis, one constructs the matrix elements of the Hamiltonian (B1). This is typically a very sparse matrix. Efficient numerical solution is possible for a small number of eigenvalues/eigenvectors using the Lanczos method. This allows the diagonalization of systems with of order 10^7 basis states on a modern desktop PC.

The different geometries that have been used in such studies are the 'disc', 'sphere' and 'torus' geometries, and are described in detail in Appendices B.1, B.2 and B.3, respectively. They each have their own benefits and/or drawbacks.

- *Disc*. This is appropriate for the direct simulation of experimental systems, in which particles are confined in a harmonic well. It allows studies of the effects of inhomogeneity, including edge structures. Limitations arise in the study of correlated phases which can appear at large angular momentum. The inhomogeneity makes it difficult to observe emergent bulk phases. For a finite-size system, it is unclear how to define the number of vortices N_v, so the filling factor (66) is not defined accurately.
- *Sphere*. This is useful for studying bulk incompressible liquid phases. The uniformity of the geometry reduces the finite size effects associated with numerical studies of the inhomogeneous system on a disc. The number of particles N and vortices N_v are fixed integers, allowing a well-defined filling factor ν to be studied, via

$$N_\mathrm{v} = \frac{1}{\nu} N - \mathcal{S}. \tag{B4}$$

The offset $\mathcal{S}$ is referred to as the "shift", which is a characteristic of a given incompressible liquid phase [241]. Owing to this offset (B4), different competing incompressible liquid states at a given filling factor can be studied independently on the sphere if they have different shifts. This is an advantage if the shift of the groundstate is known: consistent extrapolation to the thermodynamic limit along a sequence with that shift is strong

evidence for this phase describing the thermodynamic limit. However, it is a disadvantage if the possible groundstates (and their shifts) are unknown. The sphere is not convenient for the study of crystalline states.

- *Torus*. This is useful for studying bulk incompressible liquid phases, and bulk crystalline phases (states with broken translational invariance). Finite size effects are reduced by the periodic boundary conditions. The number of particles N and vortices N_v are integers, allowing a well-defined filling factor ν to be studied

$$\nu = \frac{N}{N_v}. \tag{B5}$$

Since there is no shift, all possible groundstates in the thermodynamic limit can compete within the same finite-size calculation. This geometry is therefore useful if the nature of the phase in the thermodynamic limit is unknown. For crystalline phases, the possibility to vary the geometry (aspect ratio) of the torus is a powerful way to investigate the optimal translational symmetry of the crystal. Certain incompressible liquid states are characterized by a groundstate degeneracy on the torus [116]; the appearance of this non-trivial degeneracy in the exact spectrum is strong evidence for the groundstate being in this topological phase. It is somewhat harder to implement calculations on the torus than on the disc or sphere, especially when full advantage is made of the translational symmetries [242].

In the following, we provide specific details for the different geometries that are required for the implementation of exact diagonalization studies.

B.1. *Disc*

The orthononormal single particle basis states in the two-dimensional LLL are

$$\psi_m(r) = \frac{1}{\sqrt{2\pi 2^m m!}\ell}\left(\frac{x+iy}{\ell}\right)^m e^{-(x^2+y^2)/4\ell^2}\ \frac{1}{(\pi a_\parallel^2)^{1/4}} e^{-z^2/2a_\parallel^2} \tag{B6}$$

with $m = 0, 1, \ldots$.

For contact interactions (13), the matrix elements of the Hamiltonian are

$$V_{m_1,m_2,m_3,m_4} = V_0 \frac{(m_1+m_4)!}{2^{m_1+m_2}} \delta_{m_1+m_2,m_3+m_4}, \tag{B7}$$

where V_0 is the Haldane pseudo-potential (30).

For a set of N particles, in orbitals m_i, the total angular momentum

$$L = \sum_{i=1}^{N} m_i$$

is conserved by the interactions. The many-particle Hilbert space can therefore be split into subspaces of fixed L and N. There is an additional symmetry reflecting the independence of the interaction energy on the centre-of-mass coordinate of the particle. This symmetry can be used to further reduce the size of the Hilbert space, but this is not commonly implemented.

B.2. *Sphere*

A monopole of $N_v \equiv 2S$ (N_v an integer) flux quantum is chosen to be positioned at the centre of a sphere, and to have uniform flux density over the surface [210]. The radius of the sphere is set by the condition that the total flux is $2S = 4\pi R^2 n_v$, i.e. $R = \sqrt{S}\ell$ where ℓ is the conventional magnetic length (24). The lowest-energy single particle states, analogous to the LLL states, consist of $2S+1$

degenerate levels. Using a gauge choice that is symmetric about the polar axis, the single-particle wavefunctions on the sphere may be written [243]

$$\phi_m(\theta,\phi) = \left[\frac{2S+1}{4\pi}\binom{2S}{S+m}\right]^{1/2} u^{S+m} v^{S-m} \tag{B8}$$

for $m = -S, -S+1, \ldots, S$, where $u \equiv \cos(\theta/2)e^{i\phi/2}$, $v \equiv \sin(\theta/2)e^{-i\phi/2}$ and (θ,ϕ) are the polar angles on the sphere.

The matrix elements of the contact interaction (13) are

$$V_{m_1,m_2,m_3,m_4} = V_0 \frac{[(2S+1)!]^2(2S+m_1+m_2)!(2S-m_1-m_2)!}{S(4S+1)!\sqrt{\prod_{i=1}^4 (S+m_i)!(S-m_i)!}} \delta_{m_1+m_2,m_3+m_4}, \tag{B9}$$

where we have chosen a two-dimensional contact interaction of strength $g_{2\mathrm{d}} = g/(\sqrt{2\pi}a_\parallel)$ to take account of the quasi-two-dimensional motion along the rotation axis.

These interactions (and any rotationally invariant interaction on the sphere) preserve the z-component of the angular momentum

$$L_z = \sum_{i=1}^{N} m_i. \tag{B10}$$

This can be easily imposed to reduce the size of the many-body basis. Rotational invariance also conserves the *total* angular momentum. The Hilbert space can therefore be further reduced to the many-particle basis states of definite $\hat{L}^2$. In practice, it is difficult to construct a basis of fixed $\hat{L}^2$, so this is not commonly used.

B.3. *Torus*

The 'torus' geometry is defined by a unit cell on the plane on which opposite faces are identified to impose periodic boundary conditions. It is specified by two (linearly independent) basis vectors $\boldsymbol{a}$, $\boldsymbol{b}$ in the plane. We focus on the simplest case of a rectangular unit cell, with basis vectors $a\hat{\boldsymbol{x}}$ and $b\hat{\boldsymbol{y}}$, with $\hat{\boldsymbol{x}}$, $\hat{\boldsymbol{y}}$ orthonormal. A consistent quantum theory on the periodic geometry requires that an integer number of flux quanta N_v pierce the unit cell, with $N_\mathrm{v} = abn_\mathrm{v} = ab/(2\pi\ell^2)$ an integer. To construct single particle states it is convenient to use the Landau gauge, with a vector potential directed along $\hat{\boldsymbol{y}}$. Then the linear momentum along y is conserved and spans the N_v states in the two-dimensional LLL. Expressing the linear momentum along $\hat{\boldsymbol{y}}$ in units of $2\pi/b$, it can take the integer values $m = 0, 1, \ldots, N_\mathrm{v}-1$. The single particle states in the two-dimensional LLL are [244]

$$\psi_m(\boldsymbol{r}) = \frac{\exp(-z^2/2a_\parallel^2)}{(\pi a_\parallel^2)^{1/4}} \left(\frac{1}{b\pi^{1/2}\ell}\right)^{1/2} \sum_{p=-\infty}^{\infty} \exp\left[i\frac{(X_m+pa)y}{\ell^2} - \frac{(X_m+pa-x)^2}{2\ell^2}\right] \tag{B11}$$

where $X_m \equiv 2\pi\ell^2 m/b$.

The matrix elements of the contact interaction are

$$V_{m_1,m_2,m_3,m_4} = V_0\sqrt{\frac{8}{\pi}}\frac{\ell}{b} \sum_{p,q=-\infty}^{\infty} e^{-\frac{(X_{m_1}-X_{m_3}+pa)^2}{2\ell^2} - \frac{(X_{m_2}-X_{m_3}+qa)^2}{2\ell^2}} \delta^{N_\mathrm{v}}_{m_1+m_2,m_3+m_4} \tag{B12}$$

where $\delta^{N_\mathrm{v}}_{i,j} = 1$ if $i-j = 0 \bmod N_\mathrm{v}$ and zero otherwise.

The total momentum in the $\hat{\boldsymbol{y}}$ direction

$$K_y = \sum_i m_i \tag{B13}$$

is conserved modulo N_v. This provides a convenient way in which to reduce the size of the many-body basis size (by a factor of the order of N_v). Owing to the symmetry under magnetic translations

along $\hat{\boldsymbol{x}}$, a second conserved momentum K_x can be constructed [242]. At a filling factor $N/N_\mathrm{v} = p/q$ (with p and q co-prime), with number of particles $N = p\bar{N}$ and number of flux $N_\mathrm{v} = q\bar{N}$, the momenta (K_x, K_y) take $\bar{N}^2$ distinct states in a (rectangular) Brillouin zone. Construction of many-particle basis states that are eigenstates of both K_x and K_y allows a significant further reduction in the overall size of the Hilbert space. At particular points in the Brillouin zone there exist additional point-group symmetries.